DETERMINING THE STRUCTURAL AND FUNCTIONAL CHARACTERISTICS OF ENAMELIN IN ENAMEL FORMATION

by

Yuhe Lu

A dissertation submitted in partial fulfillment
of the requirements for the degree of
Doctor of Philosophy
(Oral Health Sciences)
in The University of Michigan
2010

Doctoral Committee:

Professor Jan Ching Chun Hu, Co-Chair
Professor James P. Simmer, Co-Chair
Professor Renny T. Franceschi
Professor Jun-lin Guan
Professor Paul H. Krebsbach

DEDICATION

This dissertation is dedicated to my parents, for their unconditional love and support; and to my husband, for his love, care, encouragement and criticism.

ACKNOWLEDGEMENTS

I would like to thank everyone who has given me this opportunity to start and finish my doctoral studies. First, I want to thank my graduate mentors, Drs. Jan Hu and James Simmer for their training and support. They gave me very solid training and greatest support. They are the best scientists that I learned so much, and need so much more to learn from. I would also like to thank my committee members, Dr. Jun-lin Guan, Dr. Renny Franceschi and Dr. Paul Krebsbach for being always helpful and supportive.

Special thanks are due to all the members of the Hu-Simmer lab for their generous help in the past four years, especially Dr. Yuanyuan Hu, who gave me unlimited support on all kinds of technical problems, shared ideas and experiences with me. She helped me with the Scanning Electron Microscopy, micro CT, and in the real-time PCR analyses in Chapters 3, 4, and 5. Also special thanks are due to Dr. Yasuo Yamakoshi, who gave me help and support on protein preparation and western blot experiment in Chapter 3. I also enjoyed working and collaborating with Dr. Yong-hee Chun and Dr. Yilei Cui.

I would like to thank Dr. Charlotte Mistretta, who is the program director of our Oral Health Sciences program who gave me strongest support and encouragement over the past six years.

Final thanks are due to my friends in Ann Arbor who have accompanied me on my journey in science and in life.

Appendix A is reprinted from *Journal of Biological Chemistry*, Volume 238, Yasuo Yamakoshi, Yuhe Lu, Jan C.-C. Hu, Jung-Wook Kim, Takanori Iwata, Kazuyuki

Kobayashi, Takatoshi Nagano, Fumiko Yamakoshi, Yuanyuan Hu, Makoto Fukae, and James P. Simmer. Porcine Dentin Sialophosphoprotein-length polymorphism, glycosylation, phosphorylation, and stability. pg.14835-14844, Copyright (2008). This paper was written by Dr. James Simmer. I amplified and cloned the porcine Dpp coding region from multiple pigs and prepared the primers and plasmid templates for DNA sequencing to identify polymorphisms in porcine dentin sialophosphoprotein. My work contributed to Fig A.4 C, Fig A.5, and Fig A.8.

Appendix B is a manuscript that already has been submitted and accepted from *Journal of Dental Research*, Yong-Hee P. Chun, Yuhe Lu, Yuanyuan Hu, Paul H. Krebsbach, Yoshihiko Yamada, Jan C-C. Hu, and James P. Simmer. Transgenic Rescue of Enamel Phenotype in *Ambn* Null Mice. This paper was written by Dr. James Simmer. I fabricated the transgene construct that was used to establish the ameloblastin transgenic mice lines that were used in this paper.

TABLE OF CONTENTS

LIST OF TABLES

Table:

LIST OF FIGURES

Figure：

LIST OF APPENDICES

ABSTRACT

Enamelin (*Enam*) is essential for proper dental enamel formation. In *Enam* null mice the mineralization front associated with the secretory surface of the ameloblast membrane fails to initiate and elongate enamel mineral ribbons, so no true enamel forms. The mineralization front is a complex of enamel proteins that cannot be reconstituted *in vitro*. The main purpose of this dissertation was to develop an *in vivo* assay to study the structural and functional characteristics of enamelin in enamel formation by establishing a range of enamelin transgene expression that recovers the enamel phenotype of *Enam* knockout mice. A mouse expression vector was constructed using 4.6 kb of 5' amelogenin gene up to the translation initiation codon, the 3.8 kb *Enam* cDNA, and 1.1 kb of amelogenin 3' noncoding sequence. This construct was assembled and used to generate enamelin transgenic mice. The expression level of *Enam* gene in different transgenic mice lines varies from very little to as high as around 5 times as the amount of endogenous gene expression. Using these transgenic mice to breed with *Enam* knockout mice, we found that appropriate transgene expression level can fully recover the defective phenotype of *Enam* knockout mice. In one transgenic mouse line, which has a moderate expression level, the transgene successfully rescued the defective phenotype of *Enam*

knockout mice. The enamel thickness and microstructure of enamel is the same as wild-type mouse in this transgene expressed in knockout background mice. Other transgenic mouse lines have a normal enamel thickness and normal decussation pattern when the transgene is expressed in heterozygous background. The teeth appear yellowish and smooth, which is similar to that of the wild-type mouse. We also found in moderate to high expression level enamelin transgenic mouse lines, the enamel started to have defective phenotypes: with moderate expression level, the teeth show protrusive structure on the surface of enamel; with high transgene expression, the enamel layer is almost lost. This is the first time in the literature that described the effect of over-expression of enamelin in developing enamel.

Chapter I

INTRODUCTION

Problem Statement

A tooth is comprised of three mineralized tissues: enamel, dentin, and cementum, and is connected to a fourth mineralized tissue, bone, by the periodontal ligament. Due to its high mineral content and organized structure, enamel has exceptional functional properties and is the hardest substance in the human body (Margolis et al., 2006). Dental enamel formation (amelogenesis) is under genetic control and is the result of highly orchestrated extracellular processes that regulate the initiation, growth, and organization of forming mineral crystals (Margolis et al., 2006; Nanci, 2003).

Amelogenesis can be subdivided into several stages: presecretory, secretory, transition and maturation stages. During the secretory stage, ameloblasts elaborate and organize the entire enamel thickness, resulting in the formation of a highly ordered tissue. During the maturation stage, ameloblasts modulate between smooth and ruffle-ended phases and transport the ions required for the mineral deposition (Nanci, 2003). The three major enamel matrix proteins secreted in the secretory stage are amelogenin,

ameloblastin and enamelin. Enamelin is the largest and least abundant enamel matrix protein. It makes up about 1-5% of total enamel matrix protein (Fukae et al., 1996; Hu et al., 2001b). It was originally characterized when it was isolated from unerupted pig teeth (Fukae and Tanabe, 1987a). Porcine enamelin is a glycoprotein with a molecular weight of 186 kDa (Hu et al., 1997b). Human enamelin gene (*ENAM*) is localized on chromosome 4 (4q13.3) near ameloblastin (*AMBN*), which is a region linked to inherited enamel defects known as *amelogenesis imperfecta* (Hu et al., 2001b; Karrman et al., 1997). *Enam* is a tooth-specific gene and is expressed predominantly by the enamel organ, and at very low levels in odontoblasts (Hu et al., 1998; Hu et al., 2001b; Nagano et al., 2003). Studies of enamelin null ($Enam^{-/-}$) mice show a dose effect: both heterozygous and homozygous mice have defective enamel with the null mice showing a more severe phenotype. The incisors of enamelin null mice appear chalky-white and rough, while the teeth of wild-type mice are yellow and smooth. In heterozygous mice, only lower incisors are affected. This suggests that enamelin plays a role in the process of enamel matrix mineralization. Although it is clear that enamelin plays a critical role in amelogenesis, the exact mechanism of how it functions remains unclear. Enamel mineralization is a complex process. While ameloblasts retreat from dentin and secret enamel proteins into the enamel matrix, enamel crystals grow in length. The mineralization front is along the secretory surface of the ameloblast plasma membrane. The mineralization front is critical in amelogenesis and has never been reconstituted *in vitro*.

The goal of this study is to establish an *in vivo* animal model to study the structural and functional characteristics of enamelin in enamel formation. The strategy is to generate an enamelin transgene that will be expressed by ameloblasts at the same time that wild-type enamelin is normally expressed. It is expected that ameloblasts in different transgenic mice will express the enamelin transgene at different levels depending upon the copy number and chromosomal insertion site of the transgene. It is hoped that a range of transgenic enamelin expression levels can be identified that recovers the normal enamel phenotype in the *Enam* null background. Then subsequent studies can express enamelin transgenes containing site-directed mutations within the range of wild-type *Enam* transgene expression that previously recovered the phenotype in *Enam* null mice. Deviations from the normal enamel phenotype can then be ascribed to the change introduced by the mutation, rather than being due to differences in the *Enam* expression level. Therefore, if a range of wild-type enamelin transgene expression that fully recovers the enamel phenotype can be determined, this system will be a valuable tool to study the function of specific regions of the enamelin protein *in vivo*. Such an *in vivo* model system could be used to define protein-protein interaction domains or ion interaction domains and other structure-function relationships.

Goal

To develop an *in vivo* assay to study the structural and functional characteristics of *Enam* in enamel formation by establishing a range of enamelin transgene expression that recovers the enamel phenotype of enamelin knockout mice.

Hypothesis

Enamelin plays a crucial role in dental enamel formation. The enamelin null mice showed no mineralization at the mineralization front during the secretory stage. The specific function of enamelin and its correlation with enamel mineralization is unclear. We hypothesize that by establishing transgenic mice expressing full-length enamelin, and breeding these enamelin transgenic mice with enamelin null mice, we can discover a range of enamelin transgenic expression that recovers the enamel phenotype in null mice. By characterizing the enamel phenotypes of enamelin transgenic mice we will achieve a better understanding of enamelin function while establishing an *in vivo* animal system to study the structural and functional characteristics of enamelin in the process of enamel formation.

Specific Aims

The central hypothesis will be tested by addressing the following specific aims:

Specific Aim 1: Establish enamelin transgenic mice and determine enamelin expression levels in transgenic mice. The mouse enamelin cDNA sequence will be flanked by the 5' amelogenin promoter and 3' amelogenin untranslated region. This

construct will be used to generate enamelin transgenic mice. In these transgenic mice, we expect that enamelin will be expressed specifically by the enamel organ epithelium (EOE) during the secretory stage of enamel formation. Founders of these transgenic mice will be mated with wild-type C57BL/6 mice. Subsequent generations of offspring will be sacrificed on day 5, molars and incisors will be collected and analyzed separately. Real-time PCR and Western blotting will be performed to determine the expression levels of the enamelin transgene in developing teeth.

Specific Aim 2: Cross breed enamelin transgenic mice with enamelin null mice and characterize the phenotype of the offspring. Enamelin transgenic mice ($Enam^{tg;+/+}$) from different transgenic founders will be crossed with enamelin knockout mice ($Enam^{-/-}$). Wild-type mice and mice having the parental genotypes will be characterized along with offspring having the following genotypes: 1) $Enam^{tg;+/-}$, 2) $Enam^{tg;-/-}$, and 3) $Enam^{+/-}$. Histological, radiographic and scanning electron microscopic (SEM) evaluations will be conducted to compare enamel formed in mice with these genetic backgrounds to see whether the transgene can rescue the phenotype of the null mice. Day 5 first molars of the F2 offspring will be collected to check enamelin expression, at the protein level by Western-blotting and at the mRNA level by real-time PCR.

Specific Aim 3: Characterize the enamel phenotype of $Enam^{+/+}$ mice expressing the *Enam* transgene ($Enam^{tg;+/+}$). Founders of the transgenic mice will be mated with wild-type C57BL/6 mice. Transgene-positive offspring of enamelin transgenic

mice will be sacrificed at 7 weeks. Oral photographs and scanning electron microscopy (SEM) will be performed to characterize the enamel phenotype specifically with respect to enamel prism decussation and the total thickness of the enamel layer.

Significance and Background

Unlike other mineralized tissues, mature enamel is composed of over 95% (by weight) apatite crystals and has a unique hierarchical structure. Due to its high mineral content and organized structure, enamel has exceptional functional properties and is the hardest substance in the human body (Margolis et al., 2006). Dental enamel is made up of mineral crystals which are ionic solids comprised mainly of calcium (Ca^{2+}), phosphate (PO_4^{3-}), and hydroxyl (OH^-) ions. The observed configuration is primarily calcium hydroxyapatite, which has the chemical formula $Ca_{10}(PO_4)_6(OH)_2$. Ions such as carbonate (CO_3^{2-}), hydrogen phosphate (HPO_4^{2-}), and fluoride (F^-) can substitute irons in hydroxyapatite (HAP) and locally change the crystal properties (Nanci, 2003). Dental enamel formation (amelogenesis) is under genetic control and is the result of highly orchestrated extracellular processes that regulate the initiation, growth, and organization of forming mineral crystals (Margolis et al., 2006; Nanci, 2003).

Enamel matrix proteins and dental enamel formation. Amelogenesis can be subdivided into several stages: presecretory, secretory, transition and maturation

stages. Ameloblasts are the cells that secrete matrix proteins and are responsible for creating and maintaining an extracellular environment favorable for mineral deposition. During the presecretory stage, differentiating ameloblasts acquire their phenotype, change polarity (of their nuclei), develop an extensive protein synthesis apparatus, and prepare to secrete the organic matrix of enamel. During the secretory stage, ameloblasts elaborate and organize the entire enamel thickness, resulting in the formation of a highly ordered tissue. During a short transition stage, ameloblasts become shorter and wider and reorganize their intracellular structures. A new basal lamina is established and maintains a strong connection between the enamel layer and maturation stage ameloblasts. During the maturation stage, ameloblasts modulate and transport the ions required for the deposition of mineral (Nanci, 2003). The three major enamel matrix proteins secreted in the secretory stage are amelogenin, ameloblastin and enamelin. Amelogenin and its cleavage products make up over 90% of the enamel matrix (Fincham et al., 1999b; Termine et al., 1980). They are mostly 20 to 25 kDa in size, and hydrophobic (Margolis et al., 2006). Amelogenin null mice show a phenotype similar to human *amelogenesis imperfecta*, with a thin surface layer of mineral lacking a typical rod pattern (Gibson et al., 2001). Ameloblastin is another major protein in the secretory stage enamel matrix. Over-expression of ameloblastin in mice significantly changes enamel crystal habit and enamel rod morphology, also in a fashion resembling *amelogenesis imperfecta* (Paine et al., 2003). In ameloblastin knockout mice, ameloblasts seem to de-differentiate soon after the onset of secretory enamel deposition, resulting in nearly no enamel formation (Fukumoto et al., 2004).

Neurotrophic factor neurotrophin 4 (NT-4) induces ameloblastin expression *in vitro* and may regulate proliferation and differentiation of the dental epithelium and promote production of the enamel matrix (Yoshizaki et al., 2008). *Enam* null mice show a failure to mineralize enamel, suggesting a critical function of enamelin in mineralization (Hu et al., 2008). Secreted enamel matrix proteins are cleaved by two proteinases that are also secreted in the enamel matrix. *MMP-20*, or enamelysin, is expressed during secretory stage. *Mmp20* null mice show a severely abnormal enamel phenotype with altered rod patterns and hypoplastic (thin) enamel. Amelogenin full-length protein was not proteolytically cleaved in *Mmp20* null mice. This suggests proper processing of enamel matrix proteins is important during enamel formation (Beniash et al., 2006; Caterina et al., 2002). Kallikrein 4 *(Klk4*) is the second enamel matrix proteinase. Klk4 is a serine proteinase and synthesized and secreted during the maturation stage (Hu et al., 2002; Simmer et al., 1998). It is believed to be responsible for the complete breakdown of enamel proteins (Simmer and Hu, 2002). The enamel layer in the *Klk4* null mouse was normal in thickness and contained decussating enamel rods, but was rapidly abraded following weaning, despite the mice being maintained on soft chow. In the *Klk4* null mice, individual enamel crystallites of erupted teeth failed to grow together, interlock, and function as a unit. Instead, individual crystallites seemed to spill out of the enamel when fractured. These results demonstrated that *Klk4* is essential for the removal of enamel proteins and the proper maturation of enamel crystals (Simmer et al., 2009). Enamel matrix proteins and their proteolytic cleavage fragments play an important role in the process of enamel

formation. Their structural and functional characteristics are still far from being understood and need to be further studied.

Enamelin and its function in enamel formation. Human enamelin (*ENAM*) consists of 9 exons and 8 introns and encodes a protein of 1103 amino acids and a signal peptide of 39 amino acids. It is a tooth-specific gene and is expressed predominantly by enamel organ, and at a low level in odontoblasts (Hu et al., 1998; Hu et al., 2001b; Nagano et al., 2003). Studies of enamelin null ($Enam^{-/-}$) mice show a dose effect: both heterozygous and homozygous mice have defective enamel with the null mice showing a more severe phenotype. Histological sections of unerupted developing enamel in *Enam* null mice show a failure to mineralize the enamel layer at the secretory surface of the ameloblast, leaving the enamel matrix unmineralized (Hu et al., 2008) (Fig 1.1). Histological sections of unerupted, un-decalcified molars after von Kossa staining show mineralization of alveolar bone, dentin, and enamel in the various genotypes, as indicated (Fig 1.1). Whereas well-developed and mineralized enamel (*e*) and dentin (*d*) are present in both wild-type ($Enam^{+/+}$) (Fig 1.1 D) and heterozygous ($Enam^{+/-}$) (Fig 1.1 E) mice, only small, punctate foci of mineralization are observed in the enamel layer of *Enam* null mice ($Enam^{-/-}$) (Fig 1.1 *F*). These foci localize near the dentino-enamel junction (DEJ), despite there being a thick accumulation of organic material in the enamel layer, presumably amelogenin and other enamel matrix constituents. This suggests that enamelin plays a critical role in the process of enamel matrix mineralization, especially at the mineralization front.

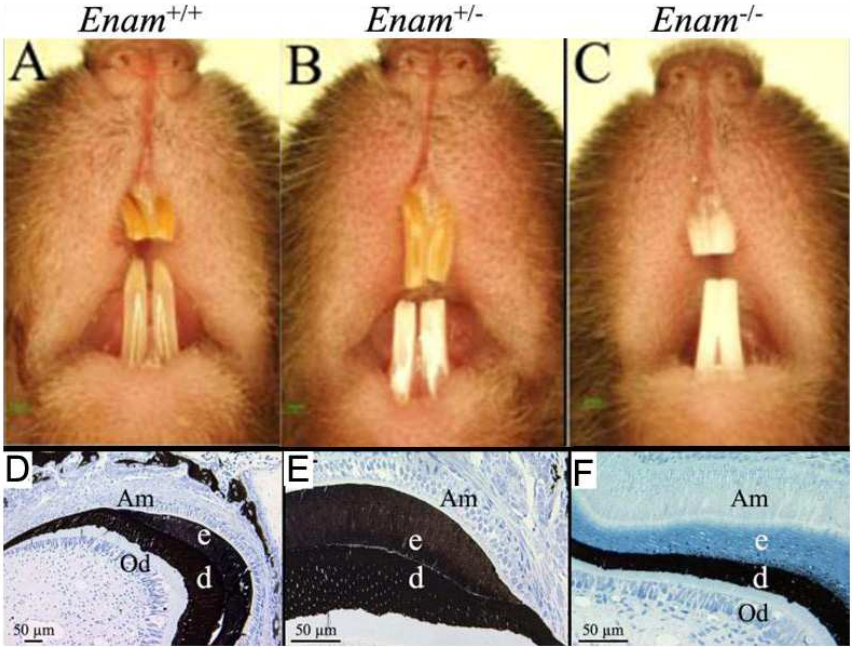

Fig 1.1: Phenotype of enamelin knockout mice. Oral photograph of enamelin wild-type (*Enam*$^{+/+}$) (A), enamelin heterozygous (*Enam*$^{+/-}$) (B) and enamelin knockout (*Enam*$^{-/-}$) (C) mice are shown. Von Kossa staining for 1 week old incisors sections for enamelin wild-type (*Enam*$^{+/+}$) (D), enamelin heterozygous (*Enam*$^{+/-}$) (E) and enamelin knockout (*Enam*$^{-/-}$) (F) mice are also shown. Od, odontoblast; Am, ameloblast; e, enamel; d, dentin. (Hu JC *et al.* J Biol Chem. 2008)

Enamelin and *Amelogenesis Imperfecta*. The importance of the enamelin in enamel formation was first demonstrated when defects in *ENAM* mutations were found to cause autosomal dominant *amelogenesis imperfecta*. *Amelogenesis imperfecta* (AI) is a group of inherited disorders that are clinically heterogeneous and exhibit tooth enamel defects without systemic manifestations (Stephanopoulos et al., 2005; Witkop, 1988). Both the primary and permanent dentitions are affected (Aldred and Crawford, 1995). The major clinical manifestations are enamel hypoplasia (enamel is thin but seemingly well mineralized), hypomineralization (subdivided into hypomaturation

and hypocalcification), or a combined phenotype, which is seen in most cases (Aldred and Crawford, 1995; Stephanopoulos et al., 2005). *Amelogenesis imperfecta* can be subdivided according to its pattern of inheritance: autosomal-dominant, autosomal-recessive, or X-linked. *AmelX* mutations cause X-linked *amelogenesis imperfecta* (Aldred et al., 2003; Stephanopoulos et al., 2005). The first mutation in *ENAM* was reported in 2001. It was a single nucleotide change, g.6395G>A, at the splice donor site of intron 8, probably caused the skipping of exon 8, resulting in an in-frame deletion of the amino acid sequence encoded by this exon. The phenotype of the affected individual is thin and smooth hypoplastic enamel, with a diagnosis of autosomal-dominant *amelogenesis imperfecta* (ADAI) (Fig 1.2) (Rajpar et al., 2001).

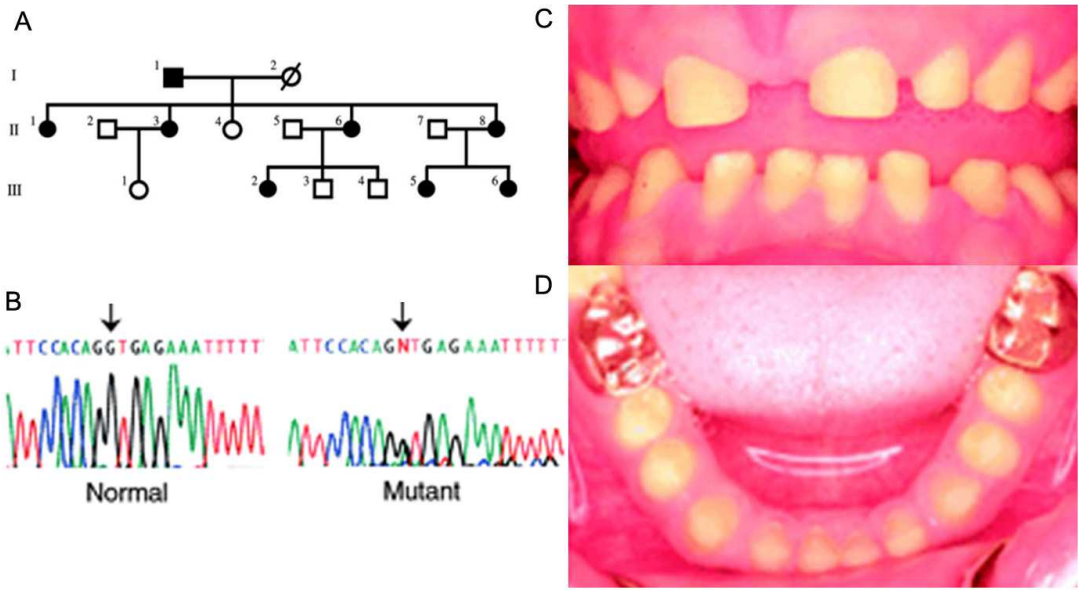

Fig 1.2: Mutation of enamelin gene cause *Amelogenesis Imperfecta* (AI). (A), Pedigree of one AI family; filled symbols denote affected individuals. (B), Sequencing of DNA from individual Ⅱ.1 reveals the presence of the mutation nt841+1 (G→A) (arrowed), which is not present in a control sample. (C and D), Photographs of individual Ⅱ.8 showing the small, smooth, yellow teeth that result from the enamel hypoplasia. (Rajpar *et al*. Hum Mol Gen. 2001)

The second *ENAM* mutation causing ADAI was g.2382A>T. It was a single base substitution in exon 5, resulting in a change of lysine to a stop codon, which truncated the protein of only 55 amino acids (Mardh et al., 2002). The third mutation was g.8344delG. It is also an ADAI and caused by a single G-deletion within a series of 7 G residues at the exon9-intron boundary of *ENAM*. This mutation alters the reading frame and causes a premature stop codon in the 5' region of exon 10 (Kida et al., 2002). This same mutation was later found in several other families with generalized and severe thinning of the enamel (Hart et al., 2003a; Kim et al., 2005b; Pavlic et al., 2007). The fourth *ENAM* was a 2-bp insertion mutation that resulted in a premature stop codon in exon 10 (g.13185_13186insAG) (Hart et al., 2003b). This mutation was also found in several other families (Kang et al., 2009; Ozdemir et al., 2005; Pavlic et al., 2007; Chan et al., 2010). A fifth *ENAM* mutation was found in 2005, it was g.4806A>G. This mutation altered the intron 6 splice acceptor site, which potentially results in two defective splicing outcomes. Inclusion of intron 6 would cause a premature stop codon, while the skipping of exon 7 would delete a portion of the protein (Kim et al., 2005b). Two more mutations were also found in 2005 in one study. One is g.12663C>A, a single substitution in exon 10 that leads to a truncated protein. This mutation causes ADAI. The second mutation results in an in-frame insertion of 7

amino acids in exon 10 (g.12946_12947insAGTCAGTACCAGTACTGTGTC), and was claimed to lead to an autosomal-recessive *amelogenesis imperfecta* (ARAI) (Ozdemir et al., 2005). One mutation was found in 2007 that causes ADAI. It was a c.G817T, generating a change of arginine to methionine in position 179 of the protein (Gutierrez et al., 2007). Two more mutations were found in 2009. One is a single T deletion in exon 10 (g.14917delT, c.2991delT), which is predicted to result in a frame shift with a premature termination codon (p.L998fsX1062) (Kang et al., 2009). The second mutation found in 2009 was a novel missense mutation (g.12573C>T) that substitutes leucine for a phosphorylated serine (p.S216L) (Chan et al., 2010). As summarized in Table 1.1, the phenotype of these ten *ENAM* mutations varies from localized pitting, smooth thin enamel, to generalized thin hypoplastic enamel. These mutations of *ENAM* and their correlation with *amelogenesis imperfecta* demonstrate strongly that enamelin plays an important role in amelogenesis in human.

The inheritance pattern of enamel defects associated with *ENAM* mutations blurred after characterization of three kindreds with severe generalized enamel hypoplasia inherited in an autosomal recessive pattern (Hart et al., 2003b). All three probands were homozygous for p.P422fsX448. Most interestingly, all persons that were heterozygous for this mutation had localized hypoplastic enamel pitting. These defects were originally thought to be too minor to classify as AI, but in the light of these and later genetic analyses, they are clearly an enamel phenotype caused by a defective single allele of *ENAM*. In another AI kindred with severe generalized enamel hypoplasia the proband was a compound heterozygote, with the p.P422fsX448 defect

in one *ENAM* allele paired with a novel in-frame insertion of 7 amino acids (p.V340_M341insSQYQYCV) in the other (Ozdemir et al., 2005). In addition, simple heterozygotes with either of these defective *ENAM* alleles paired with a wild-type allele displayed mild localized hypoplasia mainly consisting of well-circumscribed enamel pits. Characterization of other simple heterozygotes with the p.P422fsX448 defect showed the enamel phenotype could range from chalky white enamel with only mild local hypoplastic alterations to local hypoplastic AI (Pavlic et al., 2007). Simple heterozyotes for another *ENAM* frame shift mutation (p.L998fsX1062) showed similar differences in severity (Kang et al., 2009). One affected person had chalky white enamel with localized pitting while another had prominent horizontal bands of hypoplastic enamel affecting primarily the cervical third of the crowns. In another study, individuals with the mutation p.S216L in one *ENAM* allele paired with a wild-type allele had chalky-white enamel with surface roughness or highly polished enamel with some localized surface pitting (Chan et al, 2010). Researchers in this field start to believe now that all inherited enamel defects, including minor pitting and surface roughness, be included under the designation *amelogenesis imperfecta*. Excluding minor phenotypes would sometimes require diagnosing siblings with the same *ENAM* mutation as having and not having AI when one enamel phenotype is only moderately more severe than the other. If we accept that minor inherited enamel defects are AI, *ENAM* defects can be said to have an autosomal dominant pattern of inheritance. Penetrance is variable, as some individuals heterozygous for the p.P422fsX448 mutation showed no detectable enamel phenotype, not even pitting (Kang et al., 2009).

Expressivity is also variable as persons heterozygous for the p.P422fsX448 mutation can exhibit chalky enamel with minor pitting or more severe horizontal grooves of enamel hypoplasia.

Table 1.1: Enamelin mutation and *Amelogenesis Imperfecta*

location	Protein	Gene	Diagnosis	References
Exon 5	p.K53X	g:2382A>T	Local Hypoplastic	Mårdh *et al* (2002)
Intron 6	p.M71-Q157del	g.4806A>C	Hypoplastic	Kim *et al* (2005)
Intron 8	p.A158-Q178del	g.6395G>A	Smooth Hypoplastic	Rajpar et al (2001)
Exon 9	p.R179M	c.G817T	Smooth Hypoplastic	Gutierrez et al (2007)
Intron 9	p.N197fsX277	g.8344delG	Pitted/smooth Hypoplastic	Kida *et al* (2002) Hart *et al* (2003a) Kim *et al* (2005) Pavlic *et al* (2007)
Exon 10	p.S216L	g.12573C>T	Pitted	Chan *et al* (2010)
Exon 10	p.S246X	g.12663C>A	Hypoplastic	Ozdemir *et al* (2005)
Exon 10	p.V340-M341insSQYQYCV		Hypoplastic	Ozdemir *et al* (2005)
Exon 10	p.P422fsX448 in both alleles	g.13185/6insAG	Hypoplastic	Hart *et al* (2003b) Ozdemir *et al* (2005) Pavlic *et al* (2007) Kang *et al* (2009) Chan *et al* (2010)
Exon 10	p.L998fsX1062	g.14917delT	Hypoplastic	Kang *et al* (2009)

An interesting observation from the above mentioned reports as well as repots of *AMELX* mutations is that the clinical presentation of those cases share similar enamel defects. For example, patients with *amelogenisis imperfecta* caused by *ENAM* and *AMELX* mutations generally have thin and hypoplastic enamel. A possible

explanation for this observation is that both of those genes produce proteins in secretory stage enamel formation that are important in proper enamel formation. The functions of those proteins may be similar in facilitating crystal elongation thus in their absence enamel doesn't reach its full thickness. Another possibility is that those gene products may function differently, however, they interact together to regulate enamel crystal formation. Thus in the absence of either one of them, the defective enamel phenotypes are similar.

Biochemistry and proteolytic cleavage of enamelin. Porcine enamelin cDNA was cloned in 1997, this was the first enamelin gene sequence reported (Hu et al., 1997b). Before this, studies of enamelin were all at the protein level. The porcine animal model is used to extract proteins from developing unerupted teeth because of its high quantity of protein and easy availability. Full-length enamelin protein has 1142 amino acids, with the first 38 being the signal peptide. The secreted intact protein is 186 kDa (residues 39-1142), and the large enamelin cleavage products (155-kDa, 142 kDa, 89 kDa) were shown to accumulate only near the enamel surface, not in the matrix. All of these cleavage products contain the original N-terminus, since the enamelin protein is processed by successive cleavages from its C-terminus. Among these fragments, the 89 kDa protein was studied in detail. It extends from Met39 to Trp665 (Hu et al., 1997b; Hu and Yamakoshi, 2003; Hu et al., 2005). Using antibody raised from this 89 kDa enamel cleavage protein, and as well as antibodies against amelogenin, amelogenin C-terminus and ameloblastin 13-17 kDa protein, immunohistochemistry

showed these different enamel matrix protein cleavage products have different localization patterns (Hu and Yamakoshi, 2003; Uchida et al., 1991b) (Fig. 1.3).

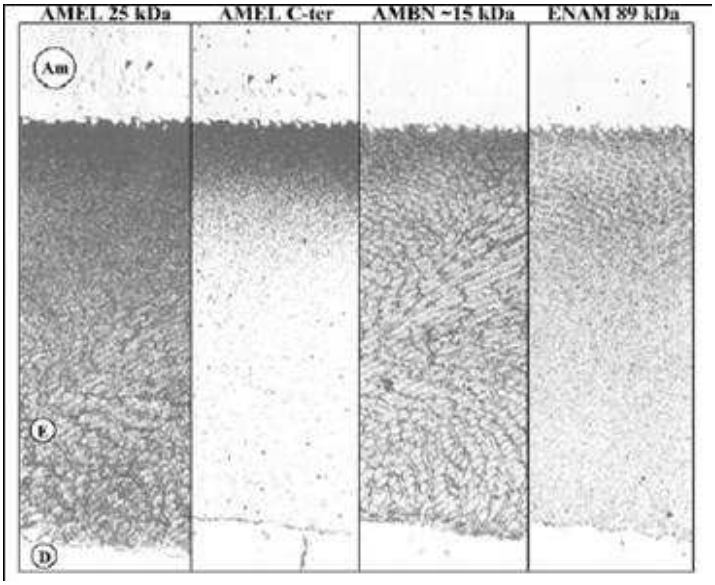

Fig 1.3: Variation of enamel matrix protein localization. Immunohistochemistry of the porcine secretory-stage enamel showing immunolocalization of enamel proteins using light microscopy. The four antibodies used (from left to right) were a polyclonal antibody raised against intact (25 kDa) amelogenin, an anti-peptide antibody specific for the amelogenin C-terminus, polyclonal antibodies raised against 13 to 17 kDa ameloblastin cleavage products, and polyclonal antibodies raised against the 89 kDa enamelin. The amelogenin C-terminal antibody, indicative of the intact protein, was restricted to the surface enamel. The ameloblastin antibody produced a honeycomb pattern over the entire thickness of the immature enamel. The enamelin antibody generated a reverse honeycomb pattern. (Uchida *et al.* Histochemistry. 1991)

Amelogenin cleavage products accumulate throughout the whole thickness of the enamel matrix, while the intact protein (containing the C-terminus) is present only on

the surface. Ameloblastin cleavage products localize in the sheath of enamel rods producing a “honeycomb pattern”. The distribution pattern of enamelin 89 kDa has a “reverse-honeycomb pattern” and localizes among the enamel rods. This observation strongly suggests that the proteolytic cleavage products of enamel proteins are not simply degradation products. They are functional polypeptides, and their functions are possibly different from those of their intact proteins (Hu and Yamakoshi, 2003). Other smaller cleavage products of secreted enamelin include 25 kDa, 34 kDa and 32 kDa fragments. Among these, the 32 kDa (residue 174-279) fragment was intensively studied. It is a hydrophilic and acidic fragment with two phosphorylated serines (Ser191 and Ser216) and three glycosylated asparagines (Asn245, Asn252, and Asn264) (Yamakoshi, 1995). Immunohistochemistry using antibody against the 32 kDa enamelin specifically stained the enamel rods (Uchida et al., 1991a). The 32 kDa enamelin and amelogenin proteins might cooperate to promote the nucleation of apatite crystals *in vitro* (Bouropoulos and Moradian-Oldak, 2004). This further indicates the crystal binding function of this fragment.

References

Aldred MJ, Crawford PJ (1995). Amelogenesis imperfecta--towards a new classification. *Oral Dis* 1(1)*:*2-5.

Aldred MJ, Savarirayan R, Crawford PJ (2003). Amelogenesis imperfecta: a classification and catalogue for the 21st century. *Oral Dis* 9(1)*:*19-23.

Beniash E, Skobe Z, Bartlett JD (2006). Formation of the dentino-enamel interface in enamelysin (MMP-20)-deficient mouse incisors. *Eur J Oral Sci* 114 Suppl 1(24-9; discussion 39-41, 379.

Bouropoulos N, Moradian-Oldak J (2004). Induction of apatite by the cooperative effect of amelogenin and the 32-kDa enamelin. *J Dent Res* 83(4)*:*278-82.

Caterina JJ, Skobe Z, Shi J, Ding Y, Simmer JP, Birkedal-Hansen H, et al. (2002). Enamelysin (matrix metalloproteinase 20)-deficient mice display an amelogenesis imperfecta phenotype. *J Biol Chem* 277(51)*:*49598-604.

Chan HC, Mai L, Oikonomopoulou A, Chan HL, Richardson AS, Wang SK, et al.(2010) Altered enamelin phosphorylation site causes amelogenesis imperfecta. *J Dent Res* 89(7)*:*695-9.

Fincham AG, Moradian-Oldak J, Simmer JP (1999). The structural biology of the developing dental enamel matrix. *J Struct Biol* 126(3)*:*270-99.

Chan HC, Mai L, Oikonomopoulou A, Chan HL, Richardson AS, Wang SK, et al. Altered enamelin phosphorylation site causes amelogenesis imperfecta. *J Dent Res* 89(7)*:*695-9.

Fukae M, Tanabe T (1987). Nonamelogenin components of porcine enamel in the protein fraction free from the enamel crystals. *Calcif Tissue Int* 40(5)*:*286-93.

Fukae M, Tanabe T, Murakami C, Dohi N, Uchida T, Shimizu M (1996). Primary structure of the porcine 89-kDa enamelin. *Adv Dent Res* 10(2)*:*111-8.

Fukumoto S, Kiba T, Hall B, Iehara N, Nakamura T, Longenecker G, et al. (2004). Ameloblastin is a cell adhesion molecule required for maintaining the differentiation state of ameloblasts. *J Cell Biol* 167(5)*:*973-83.

Gibson CW, Yuan ZA, Hall B, Longenecker G, Chen E, Thyagarajan T, et al. (2001). Amelogenin-deficient mice display an amelogenesis imperfecta phenotype. *J Biol Chem* 276(34)*:*31871-5.

Gutierrez SJ, Chaves M, Torres DM, Briceno I (2007). Identification of a novel mutation in the enamelin gene in a family with autosomal-dominant amelogenesis imperfecta. *Arch Oral Biol* 52(5)*:*503-6.

Hart PS, Michalec MD, Seow WK, Hart TC, Wright JT (2003a). Identification of the enamelin (g.8344delG) mutation in a new kindred and presentation of a standardized ENAM nomenclature. *Arch Oral Biol* 48(8)*:*589-96.

Hart TC, Hart PS, Gorry MC, Michalec MD, Ryu OH, Uygur C, et al. (2003b). Novel ENAM mutation responsible for autosomal recessive amelogenesis imperfecta and localised enamel defects. *J Med Genet* 40(12)*:*900-6.

Hu CC, Fukae M, Uchida T, Qian Q, Zhang CH, Ryu OH, et al. (1997). Cloning and characterization of porcine enamelin mRNAs. *J Dent Res* 76(11)*:*1720-9.

Hu CC, Simmer JP, Bartlett JD, Qian Q, Zhang C, Ryu OH, et al. (1998). Murine enamelin: cDNA and derived protein sequences. *Connect Tissue Res* 39(1-3)*:*47-61; discussion 63-7.

Hu JC, Zhang CH, Yang Y, Karrman-Mardh C, Forsman-Semb K, Simmer JP (2001). Cloning and characterization of the mouse and human enamelin genes. *J Dent Res* 80(3)*:*898-902.

Hu JC, Sun X, Zhang C, Liu S, Bartlett JD, Simmer JP (2002). Enamelysin and kallikrein-4 mRNA expression in developing mouse molars. *Eur J Oral Sci* 110(4)*:*307-15.

Hu JC, Yamakoshi Y (2003). Enamelin and autosomal-dominant amelogenesis imperfecta. *Crit Rev Oral Biol Med* 14(6)*:*387-98.

Hu JC, Yamakoshi Y, Yamakoshi F, Krebsbach PH, Simmer JP (2005). Proteomics and genetics of dental enamel. *Cells Tissues Organs* 181(3-4)*:*219-31.

Hu JC, Hu Y, Smith CE, McKee MD, Wright JT, Yamakoshi Y, et al. (2008). Enamel defects and ameloblast-specific expression in Enam knockout/lacz knock-in mice. *J Biol Chem* 283(16)*:*10858-71.

Kang HY, Seymen F, Lee SK, Yildirim M, Tuna EB, Patir A, et al. (2009). Candidate gene strategy reveals ENAM mutations. *J Dent Res* 88(3)*:*266-9.

Karrman C, Backman B, Dixon M, Holmgren G, Forsman K (1997). Mapping of the locus for autosomal dominant amelogenesis imperfecta (AIH2) to a 4-Mb YAC contig on chromosome 4q11-q21. *Genomics* 39(2)*:*164-70.

Kida M, Ariga T, Shirakawa T, Oguchi H, Sakiyama Y (2002). Autosomal-dominant hypoplastic form of amelogenesis imperfecta caused by an enamelin gene mutation at the exon-intron boundary. *J Dent Res* 81(11)*:*738-42.

Kim JW, Seymen F, Lin BP, Kiziltan B, Gencay K, Simmer JP, et al. (2005). ENAM mutations in autosomal-dominant amelogenesis imperfecta. *J Dent Res* 84(3)*:*278-82.

Mardh CK, Backman B, Holmgren G, Hu JC, Simmer JP, Forsman-Semb K (2002). A nonsense mutation in the enamelin gene causes local hypoplastic autosomal dominant amelogenesis imperfecta (AIH2). *Hum Mol Genet* 11(9)*:*1069-74.

Margolis HC, Beniash E, Fowler CE (2006). Role of macromolecular assembly of enamel matrix proteins in enamel formation. *J Dent Res* 85(9)*:*775-93.

Nagano T, Oida S, Ando H, Gomi K, Arai T, Fukae M (2003). Relative levels of mRNA encoding enamel proteins in enamel organ epithelia and odontoblasts. *J Dent Res* 82(12)*:*982-6.

Nanci N (2003). Ten Cate's Oral Histology: Development, Structure, and Function. 6th edition).

Ozdemir D, Hart PS, Firatli E, Aren G, Ryu OH, Hart TC (2005). Phenotype of ENAM mutations is dosage-dependent. *J Dent Res* 84(11)*:*1036-41.

Paine ML, Wang HJ, Luo W, Krebsbach PH, Snead ML (2003). A transgenic animal model resembling amelogenesis imperfecta related to ameloblastin over-expression. *J Biol Chem* 278(21)*:*19447-52.

Pavlic A, Petelin M, Battelino T (2007). Phenotype and enamel ultrastructure characteristics in patients with ENAM gene mutations g.13185-13186insAG and 8344delG. *Arch Oral Biol* 52(3)*:*209-17.

Rajpar MH, Harley K, Laing C, Davies RM, Dixon MJ (2001). Mutation of the gene encoding the enamel-specific protein, enamelin, causes autosomal-dominant amelogenesis imperfecta. *Hum Mol Genet* 10(16)*:*1673-7.

Simmer JP, Fukae M, Tanabe T, Yamakoshi Y, Uchida T, Xue J, et al. (1998). Purification, characterization, and cloning of enamel matrix serine proteinase 1. *J Dent Res* 77(2)*:*377-86.

Simmer JP, Hu JC (2002). Expression, structure, and function of enamel proteinases. *Connect Tissue Res* 43(2-3)*:*441-9.

Simmer JP, Hu Y, Lertlam R, Yamakoshi Y, Hu JC (2009). Hypomaturation enamel defects in Klk4 knockout/LacZ knockin mice. *J Biol Chem* 284(28)*:*19110-21.

Stephanopoulos G, Garefalaki ME, Lyroudia K (2005). Genes and related proteins involved in amelogenesis imperfecta. *J Dent Res* 84(12)*:*1117-26.

Termine JD, Belcourt AB, Miyamoto MS, Conn KM (1980). Properties of dissociatively extracted fetal tooth matrix proteins. II. Separation and purification of fetal bovine dentin phosphoprotein. *J Biol Chem* 255(20)*:*9769-72.

Uchida T, Tanabe T, Fukae M, Shimizu M (1991a). Immunocytochemical and immunochemical detection of a 32 kDa nonamelogenin and related proteins in porcine tooth germs. *Arch Histol Cytol* 54(5)*:*527-38.

Uchida T, Tanabe T, Fukae M, Shimizu M, Yamada M, Miake K, et al. (1991b). Immunochemical and immunohistochemical studies, using antisera against porcine 25 kDa amelogenin, 89 kDa enamelin and the 13-17 kDa nonamelogenins, on immature enamel of the pig and rat. *Histochemistry* 96(2)*:*129-38.

Witkop CJ, Jr. (1988). Amelogenesis imperfecta, dentinogenesis imperfecta and dentin dysplasia revisited: problems in classification. *J Oral Pathol* 17(9-10)*:*547-53.

Yamakoshi Y (1995). Carbohydrate moieties of porcine 32 kDa enamelin. *Calcif Tissue Int* 56(4)*:*323-30.

Yoshizaki K, Yamamoto S, Yamada A, Yuasa K, Iwamoto T, Fukumoto E, et al. (2008). Neurotrophic factor neurotrophin-4 regulates ameloblastin expression via full-length TrkB. *J Biol Chem* 283(6)*:*3385-91.

Chapter II

ESTABLISHING ENAMELIN TRANSGENIC MOUSE LINES

Abstract

Enamelin (*Enam*) is essential for proper dental enamel formation. In *Enam* null mice the mineralization front associated with the secretory surface of the ameloblast membrane fails to initiate and elongate enamel mineral ribbons, so no true enamel forms. The mineralization front is a complex of enamel proteins that cannot be reconstituted *in vitro,* so an *in vivo* system is being developed. A mouse ameloblast-specific expression vector was constructed using 4.6 kb of 5' amelogenin gene up to the translation initiation codon, the 3.8 kb *Enam* cDNA, and 1.1 kb of amelogenin 3' non-coding sequence. Rare (8 nucleotide) restriction enzyme recognition sequences were introduced at both ends of the *Enam* cDNA. This construct was assembled and used to generate enamelin transgenic mice. Offspring of the founders were genotyped using PCR to verify integration of the transgene. From thirteen original founders, eight were further derived as they showed stable integration of the expression construct and were fertile.

Introduction

The objectives of this study were to establish enamelin transgenic mice that express a wild-type enamelin transgene in ameloblasts using the amelogenin promoter (this chapter), to determine the transgene expression levels in each founding line (chapter 3), and to characterize the enamel phenotypes of $Enam^{+/+}$, $Enam^{+/-}$, and $Enam^{-/-}$ mice (chapters 4 and 5) expressing the *Enam* transgenes from different founders.

Amelogenin is the most abundant protein in developing enamel (Fincham et al., 1999b). The mouse amelogenin (*AmelX*) 5' transcriptional regulatory region has been successfully used to drive transgenic expression specifically in ameloblasts (Snead et al., 1996; Snead et al., 1998b; Wen et al., 2008b). In this study, we introduced (by PCR amplification) four rare (8 bp) restriction sites at the edges of the mouse *AmelX* 5' and 3' gene regulatory regions, and inserted the 3845 bp *Enam* cDNA sequence between them. The amplification products were cloned and used to construct an *Enam* transgene by serial subcloning. Enamelin transgenic mouse lines were established using this enamelin transgene construct.

Materials and Methods

Establishing the enamelin transgene construct. Genomic DNA from the tail tissue of C57BL/6 mice was isolated with the DNeasy Tissue kit (Qiagen, Valencia, CA) and used as template to amplify 5' and 3' *AmelX* sequences. The mouse enamelin

cDNA (NM_017468.2) was similarly amplified and cloned to add specific restriction enzyme sites. The three fragments of amplification products were ligated into the pCR2.1-TOPO cloning vector (Invitrogen) separately and ligated together as indicated (Fig 2.1) using the introduced restriction enzyme sites. Final enamelin transgene construct sequence is shown in Fig 2.2.

Generation of *Enam* transgenic mice. The 9.6 kb *Enam* transgene was excised from the vector by restriction digestion with *Not*I-*Srf*I purified with a gel extraction kit (Qiagen, Germantown, Md., USA) and microinjected into fertilized C57BL/6 X SJL F2 oocytes and surgically transferred to recipients at the Transgenic Animal Model Core at the University of Michigan. A total of 13 independent lines were generated and mated with C57BL/6 mice.

Genotyping enamelin transgenic mice. One primer set was designed to specifically detect the *Enam* transgene. The forward primer anneals to the amelogenin promoter and a reverse primer that anneals to the enamelin cDNA sequence. This primer set generates a 236 bp amplification product when the genomic DNA is isolated from mice carrying the enamelin transgenic mouse. Genomic DNA from wild-type mice does not amplify. A second primer set anneals to enamelin intron sequences and produces a 324 bp amplification product. This primer set detects only the wild-type enamelin gene. A third primer set anneals to the *lac*Z sequence, which is found only in the enamelin knockout, and produces a 397 bp amplification product Sequence of these three primer sets were shown in Table 2.1. Basically PCR condition is to

maintain the DNA at 94°C for 5 minutes followed by 32 cycles of denaturation at 94°C for 30 seconds, annealing at 58°C for 30 seconds, extension 72°C for 60 seconds and then maintain the reaction at 72°C for 7 minutes to complete final reaction.

Breeding the transgenic founders. The transgenic founders were bred to generate mice carrying the amelogenin-promoter-driven-enamelin-transgene in various genetic backgrounds. The first breeding strategy was to breed the transgenic mouse founders to C57BL/6 wild-type mice. Transgene in wild-type background (*Enam*$^{tg,+/+}$) and wild-type mice (*Enam*$^{+/+}$) will be generated from this strategy (Fig 2.3 left). Genotyping for this breeding strategy is shown in Fig 2.4 (A and B). The second breeding strategy is to breed the transgenic mice to *Enam* null mice for two generations to generate four genotypes: *Enam*$^{tg,-/-}$, *Enam*$^{tg,+/-}$, *Enam*$^{-/-}$ and *Enam*$^{+/-}$. Original transgenic founders or offspring carrying the *Enam* transgene (Tg) were mated with *Enam*$^{-/-}$ mice. F1 offspring positive for the transgene and heterozygous for *Enam* (*Enam*$^{+/-}$) were mated with *Enam*$^{-/-}$ mice, yielding four genotypes: enamelin transgene expressed in null background (*Enam*$^{tg,-/-}$), enamelin transgene expressed in heterozygous background (*Enam*$^{tg,+/-}$), enamelin null mice (*Enam* $^{-/-}$) and enamelin heterozygous mice (*Enam*$^{+/-}$) (Fig 2.3 right). Three primer sets were used to genotype the offspring: "*Enam* tg", "*Enam* 4&5" and "*lac*Z". Genotyping strategy for this breeding scheme is shown in Fig 2.4 (D, E, F and G).

Results

Fabricating the enamelin transgene. The expression construct used to establish enamelin transgenic mice contained three fragments: the amelogenin (*AmelX*) promoter region (4.6 kb), the enamelin full-length cDNA coding region (3.8 kb) and the 3' amelogenin region (1.1 kb). In order to make this gene construct, we performed a series of PCR amplification and subcloning steps. To introduce rare restriction enzyme sites, we designed PCR primers that had the designated restriction sites at the 5' ends (Fig 2.1 B). The *AmelX* promoter (5'*AmelX*, 4655 bp), *Enam* coding region (*Enam*, 3845 bp) and *AmelX* downstream (3'*AmelX*, 1143 bp) sequences were amplified and then ligated into pCR2.1-TOPO (3931 bp) vector. We designated the clones "clone 1" (5'*AmelX*-pCR2.1-TOPO), "clone 2" (*Enam*- pCR2.1-TOPO), and "clone 3" (3'*AmelX*-pCR2.1-TOPO) (Fig 2.1 C).

Clones 1 and 2 were both restricted with *NotI* and *AscI*, and the 4.6 kb *AmelX* promoter from clone 1 was ligated to the 5' side of the *Enam* coding sequence in Clone 2 to generate Clone 4 so that *AmelX* promoter sequence and *Enam* cDNA sequence were ligated together (Fig 2.1 D). Clones 3 and 4 were then restricted with *NotI* and *SgfI*, and the 8.5kb 5'*AmelX-Enam* fusion from clone 4 was ligated to Clone 3 to generate Clone 5, with the *AmelX* promoter-*Enam* cDNA fusion and the *AmelX* 3' sequence ligated together (Fig 2.1 E). Clone 5 is the final gene construct. Clone 5 was restricted with *NotI* and *SrfI* and the *Enam* transgene (9.6 kb) was separated from the cloning vector (3.9 kb) by agarose gel electrophoresis. The *5'AmelX-Enam-3'AmelX* restriction fragment was used to generate transgenic mice. Transcription of the

transgene is predicted to initiate in the 5'*AmelX* region at the start of the amelogenin exon 1, which is non-coding. Intron 1 (1277 bp) of *AmelX* is removed by RNA splicing. Exon 2 contains 10 nucleotides from the amelogenin exon 2, the *AscI* site, followed by the *Enam* translation initiation codon and entire coding sequence (3845 bp) (Fig 2.1 G). The DNA sequence of the transgene construct is shown in Fig 2.2.

Generation of *Enam* transgenic mice. The 9.6 kb *Enam* transgene was excised from the vector by restriction digestion with *NotI-SrfI*, purified with a gel extraction kit, and microinjected into fertilized C57BL/6 X SJL F2 oocytes and then surgically transferred to recipients at the Transgenic Animal Model Core at the University of Michigan. A total of 13 independent lines were generated and mated with C57BL/6 mice. The transgene fragment inserted randomly into genome, so the transgenic lines have different copy numbers and integration sites. The transgene expression levels are therefore expected to differ in the various transgenic lines. A summary of the 13 transgenic mouse founders is shown in Table 2.2.

Breeding the enamelin founders with C57/BL6 mice. These founders were used to breed with C57BL/6 wild-type mice to maintain the transgenic lines (Fig 2.3 left). Offspring of this breeding have two genotypes: enamelin transgenic mouse ($Enam^{tg,+/+}$) and wild-type mouse ($Enam^{+/+}$). "*Enam* tg" primer set is designed for genotyping transgenic mice. This primer set uses a forward primer that anneals to the amelogenin promoter and a reverse primer that anneals to the enamelin cDNA sequence. This primer set only amplifies genomic DNA isolated from mice carrying the enamelin

transgene and produces a 236 bp amplification product. Wild-type mice do not have a PCR product for this primer set. Enamelin transgenic mice also have a positive band for the "*Enam* 4&5" primer set, because the endogenous enamelin gene is still present in the genome of enamelin transgenic mouse; but have no positive bands for "*LacZ*" primer set, because there is no enamelin knockout construct sequence present in the genome of mice with this genotype (Fig 2. B). Wild-type mice have a positive band for "*Enam* 4&5" primers, while the other two primer sets are both negative (Fig 2.4 A). Founders 5, 8 and 13 were infertile. Founders 6 and 9 spawned offspring, but genotyping showed all of their pups were transgene negative, so breeding was terminated. All other founders were able to pass the transgene on to subsequent generations. It was expected that high enamelin transgene expression levels might result in enamel malformations. Oral photographs of offspring from the 8 transgenic lines along with the wild-type are shown in Fig 2.5.

Breeding the enamelin founders with *Enam* null mice. *Enam* transgenic mice were used to breed with *Enam* null mice to generate F1 offspring. *Enam* transgene positive F1 were used to breed with *Enam* null mice again to generate F2 offspring. Four genotype are generated in F2 offspring: $Enam^{tg,\ -/-}$, $Enam^{tg,\ +/-}$, $Enam^{-/-}$ and $Enam^{+/-}$ (Fig 2.3 right). These genotypes were determined using three primer sets: "*Enam* tg", "*Enam* 4&5" and "*lacZ*". "*Enam* tg" has a forward primer anneals to the *AmelX* promoter region and has a reverse primer anneals to 5' of enamelin cDNA sequence; primer "*Enam* 4&5" recognize enamelin intron between exon 4 and 5; primer "*lacZ*"

recognize the *Enam* null construct sequence. *Enam*$^{tg, -/-}$ mice have positive bands for "*Enam* tg" and "*lacZ*" (Fig 2.4 C). *Enam*$^{tg, +/-}$ mice have positive bands for all three primer sets (Fig 2.4 D). *Enam*$^{-/-}$ mice have positive bands for only "*lacZ*" primer (Fig 2.4 E). *Enam*$^{+/-}$ mice have positive bands for both "*Enam* 4&5" and "*lacZ*" primers (Fig 2.4 F).

Discussion

We designed and fabricated a plasmid construct with rare restriction enzyme recognition sites positioned at key places so that desired coding sequences can be expressed specifically in ameloblasts. This construct allows for one-step directional cloning of any coding sequence between the 5' and 3' sequences from *AmelX*, provided that the coding region does not contain the 8-base recognition sequences for the restriction enzymes.

The thirteen *Enam* transgenic founders were bred with wild-type C57BL/6 mouse for the following reasons: 1) to obtain lines with stable transgene expression level (examine which lines can have the transgene stably passed onto the next generations); 2) to maintain the different transgenic mouse lines; 3) to collect secretory stage molars from the offspring of all genotypes from this breeding strategy and examine the enamelin gene expression level of different transgenic mouse lines. Eight different transgenic mouse lines were maintained: lines 1, 2, 3, 4, 7, 10, 11, and 12.

By gross evaluation of the oral-photograph of the incisors, it is evident that offspring of line 3 has obvious enamel defects: their teeth appear chalky and white. Offspring of line 2 and 12 has some roughness on the surface of incisors, with line 2 being more obvious than line 12 (Fig 2.5).

Figures and Legends

A Primers:

1) AmelX5'F(*NotI*) agcggccgcTGCACAAACAGATATTTGGAAT

2) AmelX5'R (*AscI*) tggcgcgccCTTGATGGTTCTGAAATGTAAATC

3) Enam F(*AscI*): tggcgcgccGAAAACATGTTGCTGCTTCAGTG

4) Enam R(*SgfI*): agcgatcgcAGTTGAAGCGATCCCTAAGCC

5) AmelX3'F(*SgfI*): tgcgatcgcCGAAGTGGATACTTTGGTTG

6) AmelX3'R(*SrfI*): agcccgggcCTAAGGATAAGGAATTACTG

B

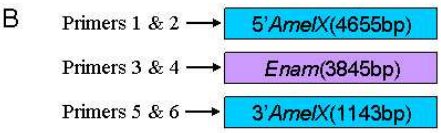

C

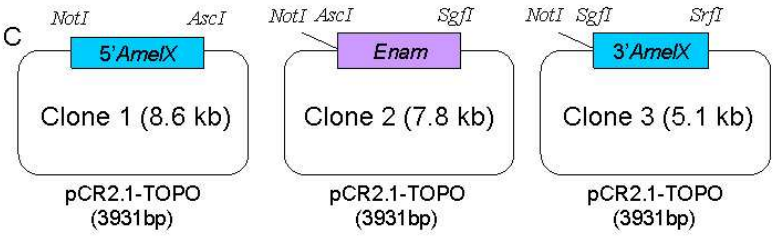

D Clone 1 and 2 were restricted with *NotI* and *AscI*. the 4.6kb *AmelX* promoter from clone 1 was ligated to the 5' side of the *Enam* coding sequence in Clone 2 to generate Clone 4.

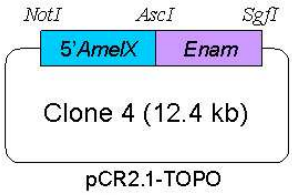

E Clone 3 and 4 were restricted with *NotI* and *SgfI*. the 8.5kb 5'*AmelX-Enam* fusion from clone 4 was ligated to Clone 3 to generate Clone 5.

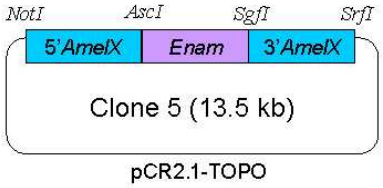

F Clone 5 was restricted with *NotI* and *SrfI* and the *Enam* transgene (9.6kb) was seperated from the clone vector (3.9kb) by electrophoresis. The *5'AmelX-Enam-3'AmelX* restriction fragment was used to generate transgenic mice.

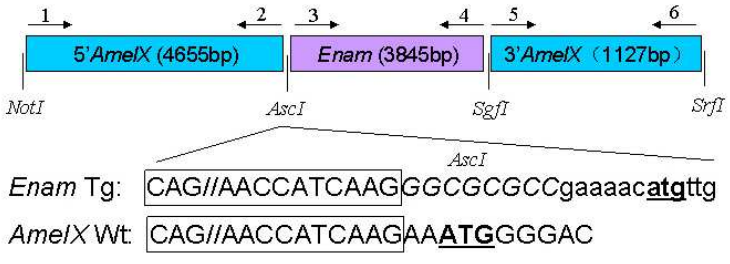

G

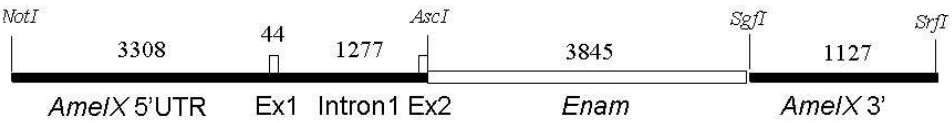

Fig 2.1 Fabricating the enamelin transgene construct. Amplification and cloning of *Enam* transgene (Tg) components. **A:** Sequences of the six PCR primers used to amplify target sequences and to introduce rare (8 base cutter) restriction cut sites. **B:** The *AmelX* promoter (5'*AmelX*, 4655 bp), the *Enam* cDNA (*Enam*, 3845 bp) and *AmelX* downstream (3'*AmelX*, 1143 bp) sequence were amplified from three pair of primers showed in A. **C:** the three amplification products were ligated into pCR2.1-TOPO (3931 bp). Recombinant plasmids having the 5' ends of the PCR products on the *NotI* side of the vector were used to construct the *Enam* transgene. **D:** Strategy to ligate *AmelX* promoter sequence and *Enam* cDNA sequence together. **E:** strategy to ligate *the AmelX* promoter-*Enam* cDNA fusion to *AmelX* 3' sequence. **F and G:** Final gene construct to make enamelin transgenic mice. Sequence of AmelX5'-*Enam* connecting area is shown (*Enam* Tg). Sequence of wild-type *AmelX* gene in same area is also shown as compare (*AmelX* Wt). Transcription initiates in the 5'*AmelX* region at the start of the exon 1, which is non-coding. Intron 1 (1277 bp) of *AmelX* is removed by RNA splicing. The *AscI* site connects 5'*AmelX*, including 10 nucleotides in exon 2, to the *Enam* cDNA sequence (3845 bp). The splice junction at the start of exon 2 is indicated by hash marks in the expanded sequence surrounding the *AscI* site. The *Enam* cDNA sequence is immediately downstream of the *AscI* site and is in lower case. The *AmelX* and *Enam* translation initiation codons are underlined and in bold.

```
   1 AAGGGCGAAT TCCAGCACAC TGGCGGCCGT TACTAGTGGA TCCGAGCTCG GTACCAAGCT
  61 TGGCGTAATC ATGGTCATAG CTGTTTCCTG TGTGAAATTG TTATCCGCTC ACAATTCCAC
 121 ACAACATACG AGCCGGAAGC ATAAAGTGTA AAGCCTGGGG TGCCTAATGA GTGAGCTAAC
 181 TCACATTAAT TGCGTTGCGC TCACTGCCCG CTTTCCAGTC GGGAAACCTG TCGTGCCAGC
 241 TGCATTAATG AATCGGCCAA CGCGCGGGGA GAGGCGGTTT GCGTATTGGG CGCTCTTCCG
 301 CTTCCTCGCT CACTGACTCG CTGCGCTCGG TCGTTCGGCT GCGGCGAGCG GTATCAGCTC
 361 ACTCAAAGGC GGTAATACGG TTATCCACAG AATCAGGGGA TAACGCAGGA AAGAACATGT
 421 GAGCAAAAGG CCAGCAAAAG GCCAGGAACC GTAAAAAGGC CGCGTTGCTG GCGTTTTTCC
 481 ATAGGCTCCG CCCCCCTGAC GAGCATCACA AAAATCGACG CTCAAGTCAG AGGTGGCGAA
 541 ACCCGACAGG ACTATAAAGA TACCAGGCGT TTCCCCCTGG AAGCTCCCTC GTGCGCTCTC
 601 CTGTTCCGAC CCTGCCGCTT ACCGGATACC TGTCCGCCTT TCTCCCTTCG GGAAGCGTGG
 661 CGCTTTCTCA TAGCTCACGC TGTAGGTATC TCAGTTCGGT GTAGGTCGTT CGCTCCAAGC
 721 TGGGCTGTGT GCACGAACCC CCCGTTCAGC CCGACCGCTG CGCCTTATCC GGTAACTATC
 781 GTCTTGAGTC CAACCCGGTA AGACACGACT TATCGCCACT GGCAGCAGCC ACTGGTAACA
 841 GGATTAGCAG AGCGAGGTAT GTAGGCGGTG CTACAGAGTT CTTGAAGTGG TGGCCTAACT
 901 ACGGCTACAC TAGAAGAACA GTATTTGGTA TCTGCGCTCT GCTGAAGCCA GTTACCTTCG
 961 GAAAAAGAGT TGGTAGCTCT TGATCCGGCA AACAAACCAC CGCTGGTAGC GGTGGTTTTT
1021 TTGTTTGCAA GCAGCAGATT ACGCGCAGAA AAAAAGGATC TCAAGAAGAT CCTTTGATCT
1081 TTTCTACGGG GTCTGACGCT CAGTGGAACG AAAACTCACG TTAAGGGATT TTGGTCATGA
1141 GATTATCAAA AAGGATCTTC ACCTAGATCC TTTTAAATTA AAAATGAAGT TTTAAATCAA
1201 TCTAAAGTAT ATATGAGTAA ACTTGGTCTG ACAGTTACCA ATGCTTAATC AGTGAGGCAC
1261 CTATCTCAGC GATCTGTCTA TTTCGTTCAT CCATAGTTGC CTGACTCCCC GTCGTGTAGA
1321 TAACTACGAT ACGGGAGGGC TTACCATCTG GCCCCAGTGC TGCAATGATA CCGCGAGACC
1381 CACGCTCACC GGCTCCAGAT TTATCAGCAA TAAACCAGCC AGCCGGAAGG GCCGAGCGCA
1441 GAAGTGGTCC TGCAACTTTA TCCGCCTCCA TCCAGTCTAT TAATTGTTGC CGGGAAGCTA
1501 GAGTAAGTAG TTCGCCAGTT AATAGTTTGC GCAACGTTGT TGCCATTGCT ACAGGCATCG
1561 TGGTGTCACG CTCGTCGTTT GGTATGGCTT CATTCAGCTC CGGTTCCCAA CGATCAAGGC
1621 GAGTTACATG ATCCCCCATG TTGTGCAAAA AAGCGGTTAG CTCCTTCGGT CCTCCGATCG
1681 TTGTCAGAAG TAAGTTGGCC GCAGTGTTAT CACTCATGGT TATGGCAGCA CTGCATAATT
1741 CTCTTACTGT CATGCCATCC GTAAGATGCT TTTCTGTGAC TGGTGAGTAC TCAACCAAGT
1801 CATTCTGAGA ATAGTGTATG CGGCGACCGA GTTGCTCTTG CCCGGCGTCA ATACGGGATA
1861 ATACCGCGCC ACATAGCAGA ACTTTAAAAG TGCTCATCAT TGGAAAACGT TCTTCGGGGC
1921 GAAAACTCTC AAGGATCTTA CCGCTGTTGA GATCCAGTTC GATGTAACCC ACTCGTGCAC
1981 CCAACTGATC TTCAGCATCT TTTACTTTCA CCAGCGTTTC TGGGTGAGCA AAAACAGGAA
2041 GGCAAAATGC CGCAAAAAAG GGAATAAGGG CGACACGGAA ATGTTGAATA CTCATACTCT
2101 TCCTTTTTCA ATTCAGAAGA ACTCGTCAAG AAGGCGATAG AAGGCGATGC GCTGCGAATC
2161 GGGAGCGGCG ATACCGTAAA GCACGAGGAA GCGGTCAGCC CATTCGCCGC CAAGCTCTTC
2221 AGCAATATCA CGGGTAGCCA ACGCTATGTC CTGATAGCGG TCCGCCACAC CCAGCCGGCC
2281 ACAGTCGATG AATCCAGAAA AGCGGCCATT TTCCACCATG ATATTCGGCA AGCAGGCATC
2341 GCCATGGGTC ACGACGAGAT CCTCGCCGTC GGGCATGCGC GCCTTGAGCC TGGCGAACAG
2401 TTCGGCTGGC GCGAGCCCCT GATGCTCTTC GTCCAGATCA TCCTGATCGA CAAGACCGGC
2461 TTCCATCCGA GTACGTGCTC GCTCGATGCG ATGTTTCGCT TGGTGGTCGA ATGGGCAGGT
2521 AGCCGGATCA AGCGTATGCA GCCGCCGCAT TGCATCAGCC ATGATGGATA CTTTCTCGGC
```

2581 AGGAGCAAGG TGGGATGACA GGAGATCCTG CCCCGGCACT TCGCCCAATA GCAGCCAGTC
2641 CCTTCCCGCT TCAGTGACAA CGTCGAGCAC AGCTGCGCAA GGAACGCCCG TCGTGGCCAG
2701 CCACGATAGC CGCGCTGCCT CGTCCTGCAG TTCATTCAGG GCACCGGACA GGTCGGTCTT
2761 GACAAAAAGA ACCGGGCGCC CCTGCGCTGA CAGCCGGAAC ACGGCGGCAT CAGAGCAGCC
2821 GATTGTCTGT TGTGCCCAGT CATAGCCGAA TAGCCTCTCC ACCCAAGCGG CCGGAGAACC
2881 TGCGTGCAAT CCATCTTGTT CAATCATGCG AAACGATCCT CATCCTGTCT CTTGATCAGA
2941 TCTTGATCCC CTGCGCCATC AGATCCTTGG CGGCAAGAAA GCCATCCAGT TTACTTTGCA
3001 GGGCTTCCCA ACCTTACCAG AGGGCGCCCC AGCTGGCAAT TCCGGTTCGC TTGCTGTCCA
3061 TAAAACCGCC CAGTCTAGCT ATCGCCATGT AAGCCCACTG CAAGCTACCT GCTTTCTCTT
3121 TGCGCTTGCG TTTTCCCTTG TCCAGATAGC CCAGTAGCTG ACATTCATCC GGGGTCAGCA
3181 CCGTTTCTGC GGACTGGCTT TCTACGTGTT CCGCTTCCTT TAGCAGCCCT TGCGCCCTGA
3241 ATTTTGTTAA AATTCGCGTT AAATTTTTGT TAAATCAGCT CATTTTTTAA CCAATAGGCC
3301 GAAATCGGCA AAATCCCTTA TAAATCAAAA GAATAGACCG AGATAGGGTT GAGTGTTGTT
3361 CCAGTTTGGA ACAAGAGTCC ACTATTAAAG AACGTGGACT CCAACGTCAA AGGGCGAAAA
3421 ACCGTCTATC AGGGCGATGG CCCACTACGT GAACCATCAC CCTAATCAAG TTTTTTGGGG
3481 TCGAGGTGCC GTAAAGCACT AAATCGGAAC CCTAAAGGGA GCCCCCGATT TAGAGCTTGA
3541 CGGGGAAAGC CGGCGAACGT GGCGAGAAAG GAAGGGAAGA AAGCGAAAGG AGCGGGCGCT
3601 AGGGCGCTGG CAAGTGTAGC GGTCACGCTG CGCGTAACCA CCACACCCGC CGCGCTTAAT
3661 GCGCCGCTAC AGGGCGCGTC CATTCGCCAT TCAGGCTGCG CAACTGTTGG GAAGGGCGAT
3721 CGGTGCGGGC CTCTTCGCTA TTACGCCAGC TGGCGAAAGG GGGATGTGCT GCAAGGCGAT
3781 TAAGTTGGGT AACGCCAGGG TTTTCCCAGT CACGACGTTG TAAAACGACG GCCAGTGAAT
3841 TGTAATACGA CTCACTATAG GGCGAATTGG GCCCTCTAGA TGCATGCTCG A**GCGGCCGC**T
3901 GCACAAACAG ATATTTGGAA TGAATATATA ACCAAATAAA GACATATTTG GATTTCATAT
3961 CCTTACACTT GTCTCAGAGA TATCACAATA CAGAAAAATA AATTTATGCT TAAAATAGTG
4021 ACTTAAAAAG AACAAAGATA TACTCAACTT CAAAAGGCAA GAGTAAAAAG AATATTCTGG
4081 AAATGTTATT GATTCTGTAA CAAAATAAAT AATTTATTAA TTTATTAAAT AAATAATTTG
4141 TGTTTTCCAA AGCCAACTTA TAAAAATTAA ATAATTACTT GTTGATAAAA TATTAATTGA
4201 AATATTCTTT TTTCTAAAAC CCTTGGTAAT CTTTGTGTAT TGAGAGTAGA ATGAATCAGT
4261 ATGCATGTTA TTGGAATACA GTGTGGTATG AAGCACTACA TGACCAGCAT GCACTGATCA
4321 GTAATTAGCA TTTTCTTTTC CTAATAATTT CTTTATGGTT TAAGCCTTTG AGGTCCTCTC
4381 TCCAAGTACA TAAAACATAT ATAGGTGATG TGAACTATTA TTATCCTATT GTTCTGTGAA
4441 GCACCAAAAT TTTATTTCCT CTATCTAATT GTGTTTTGGT ATATGCTATC TAACATTCCC
4501 ATTCCTGCCT AGCTTCTAGG AATCAGTATT CGGCATTCAA ATTAATATTT ATAGCTTCTT
4561 CTATAGTTGA CTTATTTCAC TTAACAGGAT TTCGCTTTTT AAAACATTTT TATTAGATAT
4621 ATTCTTTATA TACATTTCAA ATGCTATCCC GAAAGTTACC TATACCCTCC CCCTGCCCTG
4681 CTCCCCTACC CACCCATTGC CACTTCTTGG CCCTGGCATT CCCTTGTACT GGGGCATATA
4741 AAGTTTGCAA TACCAAGGGG CCTCTCTTCC CAGTGATGGC CGACTAGCCC ATCTTCTGCA
4801 TATGTTGCAG ACCCTTTCAG CTCCTTGGGT ACTTTCTCTA GCTTCTCCAT TGTGGGCCCT
4861 TTGTTCCATC TTATAGATTA CTGTGAGCAT CAACTTCTGT ATTTGCCAGG CACTGGCATA
4921 GCCTCAAACG AGACAGCTAT ACCAGGGTCC CTTCAGCAAT ATCTTACTGG CATATGCAAT
4981 AGTGTCTGTG TTTGGTGGCT GATTATGGGA TGGATCCCCG GGTGACTGCC TTTTAGTTCC
5041 ATTCTCTTTT TCTGTTGTAA ATGGCATGAT TTCACTCTTC ATTATGATAC ATTGTGTACA
5101 TATACTTTAT TAATCCATTC ATCTGTTGAT AAACATCTAT GCTGCCTCTA TATCATGAGC
5161 ATTATAAATA GTGCCACAAA AACACCTGGA AGTGCAGTTG TATCTTTGAA TTAATGAAAT

5221 TATTTTCTTT GGATATATGC ACAGGTGTGT AAATATGGAT CACAGAAAAG GTCCATTTTC
5281 AGTGTTCTTT CCACCCTTTA CAGACTTTGC TGCTTCTTAT CCCCTTTCAA CTTTACTTCT
5341 GATATATATG TTTCAGCAAT AAACATATTC ACAAATAAAT GCGAACCTTG GACACATTGA
5401 ATTTTTAGAG ACATATTCTG TGTTCACTTT CCTGTGTACA TTTGACTTAT TATGTCCTTT
5461 TACTACTACT CTCCCAAACT GAATGATGTA CCTTTCATAA TGACGTTCAG CTGTCCTTAC
5521 TAATGTATTC TCAAAGATAA TATTAGAACT TAGACCACAT TAGATCTTAC TATTAGCATC
5581 CTTTAAATAC TTGTCACTTT CAGGGGCATA GAGGTGTGGA ATGGTCAATG AAGAGCTTTC
5641 AATTCCCCTG CCTACATCTC TCACCTAATT TTTATACCCA TCTTCTTAGG TAGATTGTAT
5701 TATCATCCCT GTCCTACACA TAAGGAAATT GTGGTGAATC CGGAGTCAGA ATTAACATTG
5761 CCTAAGTTCG ATATTGTCAT GAAAATTATG CATTACACAA TTTAATAATG TTCCTGTATT
5821 ATCAATTTGA AGAATCTGTA GAAAGTATGT ATATATGTAG CTAAAGAAAA GTGTGCATAT
5881 TTATATAAAT GTATAAACTC AGTTTTTCAA AAGATCCAAC TCTATCACCA GTTACTGCAG
5941 TAATTCAGTA TTGACGCAAA ACCTAGTAGT TCCTGTCAAT AATTATAAAT TTATTTCTTA
6001 AATGATGAAA TTGCAGAATA AAGTAAAACC AACCCATGCT TTATTACAGT AAAGAGGTAA
6061 CAATACATGT AAACTGAGTA GCTAAATCAG AGGTCCCTGC AGGTGAACTG ACTTGGTCAA
6121 TGTTGCTTAA ACAAAGCAGA GCCTGCTGAA AACATGGGGC AATTCTTTGA AATGTGAAGG
6181 GAATTTCAGT TTGCAATATA AGAATCTGGC ATTGGTATGG TCTAGAAAAG ACTTGAGCAG
6241 TGGTTCTCCG TCTTTCTAAT GCTGAGACCC TCTAATATGT TTCCCCATGC TGTGGTAACC
6301 CCCAACCATA AAATTATTTT TGTTGTTATG TCATAACTGT AATTTTGCTG CTGATATGAA
6361 ATGTAATGTA AATATCTGTG TTTTCCAATG GTCTTAGGTG ACCTGTGTCA AAGGGTCATT
6421 TGACCTCCCC AACGGGTCAT GACCGACCAA CAGTTTGGGA ACGACTGGAT TAGAGAGAAG
6481 CCAAATAGCT CTGTAGTAAA ATCAGGGTGA TATTTCCTGT AGCACGCTTG TAAGTATTCA
6541 AGTAGATTTT CAAGCACATT GTATGGTATA TGACATTTGT TAACTTTGTC TTTTATGGCA
6601 TTAGAGTAAG TGTTGCTACT GTAATAGTCT TGAGGTCGTG GCTGTTTGCA TGACAGGTGG
6661 TTTTCTAGAC CAGAGTGGTA ATGGAGGACA GAAGGGACAG AGAAAATATC TGTGTCAGAA
6721 GCAGAGAAAG AACACCAGCG ATTGTGGAAT TTTGGGCGAA CTTTGGATTT TTACAAGAAT
6781 GGGGATTCAA TCCATGCAGC TTGATATGAA AAGTCTGGAG AACCTTAAGT GACTGTTTTG
6841 AGTACACTGG AGAAACTTGA CCATTCACTT AAAAAAAAAA AAAAGTAACG TTAATTGCTA
6901 GAACTGAGAC GTCGACAATG GCATAGCACT TTCTTAAAAA TGAATTCAAA TATATCAGCA
6961 TATGCAGTCA ACTAATTTGC TGACTTGAAG ACAGCTTCCC AAACCTATTA TTGCCTGTAA
7021 TGAACGACTA TATGCACTAA TCACAACATG CAGTCTTGAC AGTGCTCACG GCATCTAAAA
7081 AAATCATGAT ACAGGGATTT TTCTTTAGAC TCAACACATT TTTCATTCAG AAACCTGATT
7141 GGCTGTTCAA AGTGCCCTGC ATGATATAAA TTGGGGCACA GAGTTGGAAG AAACCATCGG
7201 ATCAAGCATC CCTGAGCTTC AGACAGAAAC TCACTGAGCA TACACTCAAA GGTATGTGGA
7261 TTTCATTCAT GATTTACCAT CTCCACTGTG GTCATTTCTT TCTCTGAATT TCATGTTTCA
7321 AATGTGTGAA TGAATTGCAC ATTTCTAATT CTTTGTGCCA TCTACACCAT ATGTACTTCT
7381 TTAGTTTTAC TATAATGAAA TTATAGACTT AAATCATTGA AAAGAAGTTT TAACTTTATA
7441 GTACAGTAAT GTATGTACTT CTGTAAATTT TAGGTCAAGC ATTCCAAAGC CTTTTGGGAG
7501 CCAGATTTGA TACAAAAATG TGTATTTGCT TTTTAGTTAA GATGCTGTTT TAACAGGCTG
7561 AGGGCTACTT CTTTACAAAA TCTTGTTAAA TCTTGTGAAT CCTTTTTCTT ATTACCTCAA
7621 CCTTTGGGGG GAAAAGGTTT AGATGTTAGA AATCCTCAAT GTATTTTTCA TAGGTAACAC
7681 CAATGCATTT TACATTCATG TCCTAAATTT ACTTTCAAGG TGTTGTCCAA AACCAATGGC
7741 ATATTTTAGG ATAGGTAGTT CTTGCTTCAT GTTTCAAAGG CCTTAATATG TAGAAGGAAT
7801 ACAGTATAGT TGACAAGCAA GAAGAGGGTG CTACTGGCTT AAGACAGAAC TCTTTACGTA

7861 GAAACCATTC CACAACCCTT AAAGAAGCTT AGAATGGTAG CACTATTCTC TTTCTTTGGA
7921 TTAAGCATGC CTTCTGCTTC AAACCTGGAG TTTAAAGGCA TTATGAGAGA TTCTTGCCTA
7981 AAATTCTACA AGTGGACCTA AACCCACTCT GCCATTAATC CATTCTGTAA AATTATTCAA
8041 TATTTTCTCA AATAATTACT CTATGTATTT AACAGTAGCA ATGCTCAAGT GGGTTATGCC
8101 CCCCAAAAGA AAAACAACAT TTCTATCTTT TCTTGTTACC AAAGTATAAA ACCATGTTCA
8161 TTTGATTATC TCTCCAACTG TTATACTCAA CCCGATTCTT TTAATCAGTT TTATTGTTTC
8221 CATCTAGCTT CTAGGCATCC TTAGGCTGTA TAGCATAGAA AATGGTTTGC AGCATCATTC
8281 TTGTAGATCA CTTTTGGTCC TCTAACTCGT TAACCTTCAG CTTCAGCTTA GTTTTTAAAC
8341 AAATAAACAC ATTGCAATAT TAGTACTCCA GAAGCAATGA TAATTCCATA TGAATGTCAC
8401 TTTACAATAA GGGCCGCACC TTCTTTTTGA TTAGCAAGAC ATTAATGTGG ATTATATACA
8461 TGTATGAAGC ATAATTATAT TCATGCTTTT AAAAGTTTTT AAATGGTTGG TATTGATTTA
8521 CATTTCAGAA CCATCAAG**GG CGCGCC**GAAA AC**ATG**TTGCT GCTTCAGTGC AGAAATCCGA
8581 CTTCTCCTCC AAAGCCATGT GGCCTGGTAC CAAATGTAAA GATGAGTCTC CTTGTTTTCC
8641 TGGGTCTGCT TGGTGTCTCT GCTGCCATGC CATTCCAGAT GCCAATGCCC CGAATGCCTG
8701 GATTTAGCAG TAAAAGTGAA GAGATGATGC GATATAATCA ATTCAACTTC ATGAATGCCC
8761 CACCAATGAT GCCTATGGGC CCATATGGAA ATGGTATGCC AATGCCGCCA CACATGCCTC
8821 CACAGTACCC TCCATACCAG ATGCCCATGT GGCCTCCACC AGTACCCAAT GGATGGCAGC
8881 AACCCCCAAT GCCCAATTTC CCAAGCAAGA CTGATCAAAC CCAGGAGACC GCCAAACCCA
8941 ACCAGACCAA TCCACAAGAG CCACAGCCAC AAAAGCAGCC TTTAAAGGAA CCACCAAATG
9001 AAGCAGCACG GGCCAAAGAT GACGCCCAGC CACCTCAGCC ATTCCCACCA TTTGGCAATG
9061 GACTTTACCC CTATCCACAA CCACCATGGC CAATTCCACA GAGGGGACCA CCAACAGCGT
9121 TTGGACGGCC AAAGTTCAGC AATGAAGAAG GAAATCCTTA CTATGCATTT TTTGGATATC
9181 ACGGCTTTGG GGGTCGTCCT TATTACTCAG AAGAGATGTT TGAAGATTAT GAAAAACCCA
9241 AAGAAAAAGA CCCTCCTAAA CCAGAGGACC CACCTCCAGA TGACCCACCC CCAGAGGCCT
9301 CTACAAACTC AACTGTGCCT GATGCTAATG CCACTCAATC AATTCCTGAA GGCGGAAATG
9361 ACACTAGCCC AATAGGAAAC ACAGGCCCTG GGCCGAACGC TGGGAACAAT CCTACAGTTC
9421 AAAACGGTGT CTTCCCTCCC CCTAAAGTTA ATGTTTCAGG CCAGGGAGTA CCAAAAAGCC
9481 AAATTCCGTG GAGACCAAGT CAGCCAAATA TTTATGAGAA TTATCCTTAC CCAAATTATC
9541 CTTCAGAAAG ACAATGGCAA ACCACTGGTA CCCAGGGGCC TAGACAGAAT GGACCTGGCT
9601 ACCGAAATCC ACAAGTTGAA AGGGGTCCTC AGTGGAATTC CTTTGCTTGG GAAGGCAAAC
9661 AAGCTACTCG TCCAGGAAAC CCAACTTACG GTAAACCTCC CTCTCCTACC TCCGGGGTTA
9721 ATTATGCAGG AAATCCAGTC CATTTCGGAA GAAACCTGCC AGGGCCAAAT AAACCCTTTG
9781 TGGGAGCCAA TCCGGCCTCA AATAAACCCT TTGTGGGAGC CAATCCGGCC TCAAACAAAC
9841 CCTTTGTGGG AGCTAATCCG GCCTCAAACA AACCCTTTGT GGGAGCCAAT CCGGCCTCAA
9901 ATAAACCCTT TGTGGGAGCC AATCCGGCCT CAAATAAACC CTATGTGGGA GCCAATCCGG
9961 CCTCAAACAA ACCCTTTATA GGAGCCAATC CGGCTGCAAA CAAACCATCT ATAGGAACCA
10021 ATCCAGCCGC AAACAAACCA TCTATAGGAA CCAATCCAGC TGCAAATAAA CCCTTTGTGA
10081 GAAACAATGT AGGTGCAAAT AAACCCTTTG TGGGAACCAA TCCCTCCTCA AACCAACCAT
10141 TTCTGAGAAG CAATCAGGCC TCAAATAAAC CATTTATGAG AAGCAATCAG GCCTCAAATA
10201 AACCATTTGT GGGCACCAAT GTGGCCTCAG TGGGTCCTAA ACAGGTCACT GTTAGCCACA
10261 ATATGAAAAC TCAAAATCCA AAAGAAAAGT CACTAGGTCA AAAAGAAAGA ACAGTCACTC
10321 CTACCAAAGA TGCAAGCAAC CCCTGGAGAA GTGCTAAACA ATATGGAATT AACAATCCAA
10381 ACTATAATTT GCCTCGCTCT GAGGGCAGCA TGGTAGGCCC AAATTTTAAT TCCTTTGATC
10441 AACAAGAAAA CTCCTACTTC TCAAAAGGAG CTTCCAAAAG AGTACCAAGT CCTAATATAC

10501 AAATCCAAAG CCAGAATTTG CCCAAAGGAA TTGCTTTAGA GCCAAGAAGA ACCCCATTTC
10561 AATCAGAAAC TAAAAAACCT GAGTTAAAAC ATGGTACACA CCAGCCTGCA TACCCTAAGA
10621 AAATCCCTTC TCCTACAAGA AAACATTTCC CTGCTGAAAG AAATACCTGG AATCGTCAAA
10681 AAATCCTTCC ACCCTTAAAG GAAGACTATG GGAGGCAAGA CGAAAATTTA CGTCATCCGT
10741 CCTATGGCTC TAGAGGAAAT ATTTTTTACC ATGAATATAC CAATCCTTAT CATAATGAAA
10801 AATCACAGTA CATTAAAAGC AATCCATGGG ATAAGAGCTC TCCCAGTACT ATGATGCGGC
10861 CAGAAAACCC ACAGTACACC ATGACTTCTC TAGACCAGAA GGAGACAGAG CAGTACAATG
10921 AAGAGGATCC AATTGATCCA AATGAAGATG AATCTTTTCC AGGACAAAGT AGATGGGGGG
10981 ATGAAGAGAT GAACTTCAAA GGAAACCCAA CAGTTAGGCA GTATGAAGGT GAGCACTACG
11041 CCTCAACCCT AGCGAAGGAA TACCTTCCTT ATTCCTTAAG TAATCCACCA AAACCCAGTG
11101 AAGATTTTCC TTACAGTGAA TTCTATCCCT GGAACCCACA GGAAACGTTT CCAATATATA
11161 ACCCAGGTCC TACTATAGCA CCACCCGTGG ACCCCAGAAG TTATTATGTT AATAATGCCA
11221 TAGGACAAGA AGAAAGCACT CTCTTTCCTT CATGGACCTC CTGGGACCAC AGGAATCAAG
11281 CTGAGAGGCA GAAAGAGAGT GAGCCATATT TTAACAGAAA TGTCTGGGAT CAGTCAATAA
11341 ATTTACACAA ATCTAATATA CCAAACCATC CTTATTCCAC TACATCCCCT GCTAGATTTC
11401 CAAAAGATCC AACATGGTTT GAAGGTGAGA ATTTGAACTA TGATTTGCAA ATTACTAGTT
11461 TAAGTCCACC AGAAAGAGAA CAGTTGGCTT TCCCAGACTT CCTGCCTCAA AGTTACCCAA
11521 CAGGTCAAAA TGAAGCACAC TTATTTCACC AAAGTCAAAG AGGGTCTTGC TGTATTGGTG
11581 GCTCCACAGG ACATAAAGAC AATGTGCTGG CTCTACAAGA CTACACTTCA TCCTATGGTC
11641 TTCCACCAAG GAAGAACCAA GAAACCAGTC CAGTGCATAC AGAAAGCAGT TATATCAAGT
11701 ATGCAAGACC TAACGTTTCC CCAGCAAGCA TCCTACCTAG TCAAAGAAAT ATCTCAGAGA
11761 ACAAACTAAC TGCAGAAAGC CCAAACCCAA GTCCATTTGG AGATGGTGTG CCTACTGTGA
11821 GGAAAAATAC TCCATATTCT GGAAAGAATC AACTAGAGAC AGGAATTGTG GCCTTTTCTG
11881 AAGCCAGCTC TTCTCAGCCA AAAAACACGC CCTGTCTTAA AAGTGACCTT GGAGGAGATC
11941 GGAGGGATGT TCTGAAACAA TTTTTTGAAG GCAGCCAGCT GAGTGAAAGA ACTGCTGGCC
12001 TTACTCCTGA GCAGCTCGTC ATTGGTATTC CTGATAAAGG CTCTGGCCCA GATAGCATAC
12061 AAAGTGAAGT CCAAGGAAAA GAGGGTGAGA TGCAGCAACA AAGGCCACCT ACCATCATGA
12121 AGTTGCCATG CTTTGGCTCC AATTCAAAAT TTCACTCTTC TACCACTGGA CCTCCAATTA
12181 ACAACAGAAG ACCAACCCTA CTTAATGGTG CTCTCTCCAC ACCCACTGAA AGTCCTAACA
12241 CATTGGTTGG GTTAGCTACT AGGGAACAAC TTAAAAGTAT AAACGTAGAT AAACTTAATG
12301 CAGATGAACA CACTACACTC GAATCTTTTC AAGGAACCAG TCCACAGGAC CAAGGCTGCT
12361 TACTGCTTCA GGCT**TAG**GGA TCGCTTCAAC T**GCGATCGC**C GAAGTGGATA CTTTGGTTGT
12421 TTTTAGGAAT AACTCAAGAA CACAATGATT TGTGCCTACA ATCACTTAGT AAATTCTGTA
12481 ACTAAAAATA AGTATCATTA GCAGATAATA AAATGTTTGA AAAATCATTC ATGTCTTTGT
12541 GTTGAATTAA ATTTAAATTT TCCTATCACT TGAGAGAAGA ACTTATAAGT GAATAATATA
12601 GGGACTGGTC ATTTGCTCCT ACAAATTGAC CATTTAGCAG GCAAATCATG ACTATATCTT
12661 CTTAGAGAAC TTTTATATTA TCTGTAATGT TTTCTTAAAA TAGAAATTTG TACATCATAA
12721 ACAATAGCTG AGAAAGTTAA CAGAAATAGT TAAGCATGGA TAGTCACTGA ACCTGAACCA
12781 AATGAAGGCA AGTTTAGAAG AAATATTCTT TACATTGAAA AAGATAAACT TTAAGGAATG
12841 TTTATATTCT AAATCAAATT AAGACTTGGA ACTTTAGCTT TATTCTTCAC ACCACATCAG
12901 TAACCAAAAT CTGGTCTTTT GATCTCATTC TATAGAAAAA TATTTTGAGT GAAATTATGT
12961 GATATATATG GTAATTCACT GAAATTTAAA TTATTAAAAT AATTATTTTT CCTAAGAAAA
13021 TTAATAACGG AGCCTCAAAC AGAGAATTGC AGTGATTTTA TACACAAGTC ATTTCTTTCA
13081 CCTCATAATC TTTAAGCTGA TTAAGTCTAC CACATGGTCT TCAAAACGCT AACAGATGCG

```
13141 TAAAATGGAC TCAAAACAAG TTTTCTTTCC CACTCATATT TATATTTGAA TCATTTTTCC
13201 TCTTACACCC ACACAAAATT GTAAACAGTC TTTGCAGGAT TTATGTTACA CAGCACCCAC
13261 AGTAACTTTA TTCCAGTACC TTCATGATTA AGGTCTCTCT TAATCATTTT CTGGAATGAA
13321 TAAACATAGC TTTCTCTGAG AAGATATCAA TATGCAAACA AATTAGTTGA TTTTAAAGAA
13381 CTAAAATGCA GTAATAAAGG TAAAAATAAA GCATTTAATG AATTAGCATA GGCCACTTCT
13441 AATCAACTGA GTAAATATTT CTCAAGCACT CACTAGACTG GGTATTACTG TATGTGATAG
13501 TGAAAACAGT AATTCCTTAT CCTTAGGCCC GGGC
```

Fig 2.2 DNA sequence of the *Enam* transgene construct. *Enam* transgene construct starting with pCR2.1-TOPO vector. Restriction sites used during construction are in bold and underlined. The *Enam* translation initiation and termination codons are in bold. 1-3899 is vector sequence ending at the *NotI* (GCGGCCGC) site; 3900-8538 is from the *AmelX* 5' transcription regulatory (promoter) region (4639 bp) ending at the introduced *AscI* (GGCGCGCC) site; 8547-12391 is *Enam* cDNA sequence (3845 bp) ending at the introduced *SgfI* (GCGATCGC) site; 12400-13527 is from the *AmelX* 3' region (1127 bp), which contains multiple transcription termination signals and ends at the introduced *SrfI* (GCCCGGGC) site.

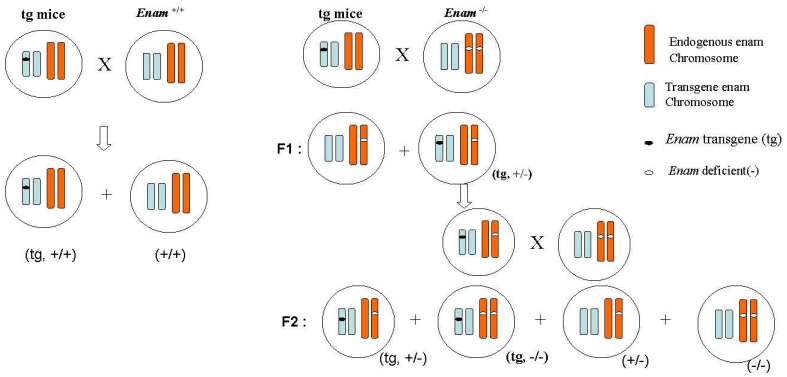

Fig 2.3 Breeding strategy. Two breeding strategy is used for enamelin transgenic mice. Left: *Enam* transgenic mice were used to breed with C57/BL6 wild-type mice to generate transgenic mice ($Enam^{tg,+/+}$) or wild-type mice ($Enam^{+/+}$); Right: *Enam* transgenic mice were used to breed with *Enam* null mice to generate F1 offspring. *Enam* transgene positive F1 ($Enam^{tg,+/-}$) were used to breed with *Enam* null mice again to generate F2 offspring. Four genotypes were generated: $Enam^{tg,-/-}$, $Enam^{tg,+/-}$, $Enam^{-/-}$ and $Enam^{+/-}$.

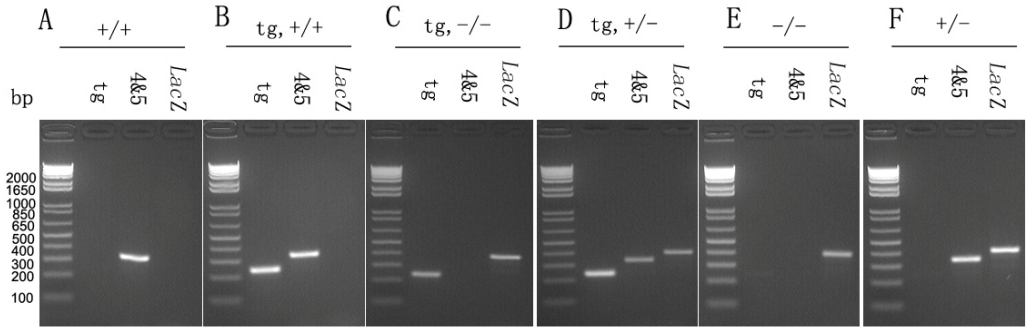

Fig 2.4. Genotyping strategy. Genotyping result using the three primer sets ("*Enam* tg", "*Enam* 4&5", "*LacZ*). Genotypes includes wild-type (A), transgene expressed in wild-type background (B), transgene expressed in null background (C), transgene expressed in heterozygous background (D), homozygous knockout mice (E) and heterozygous knockout mice (F).

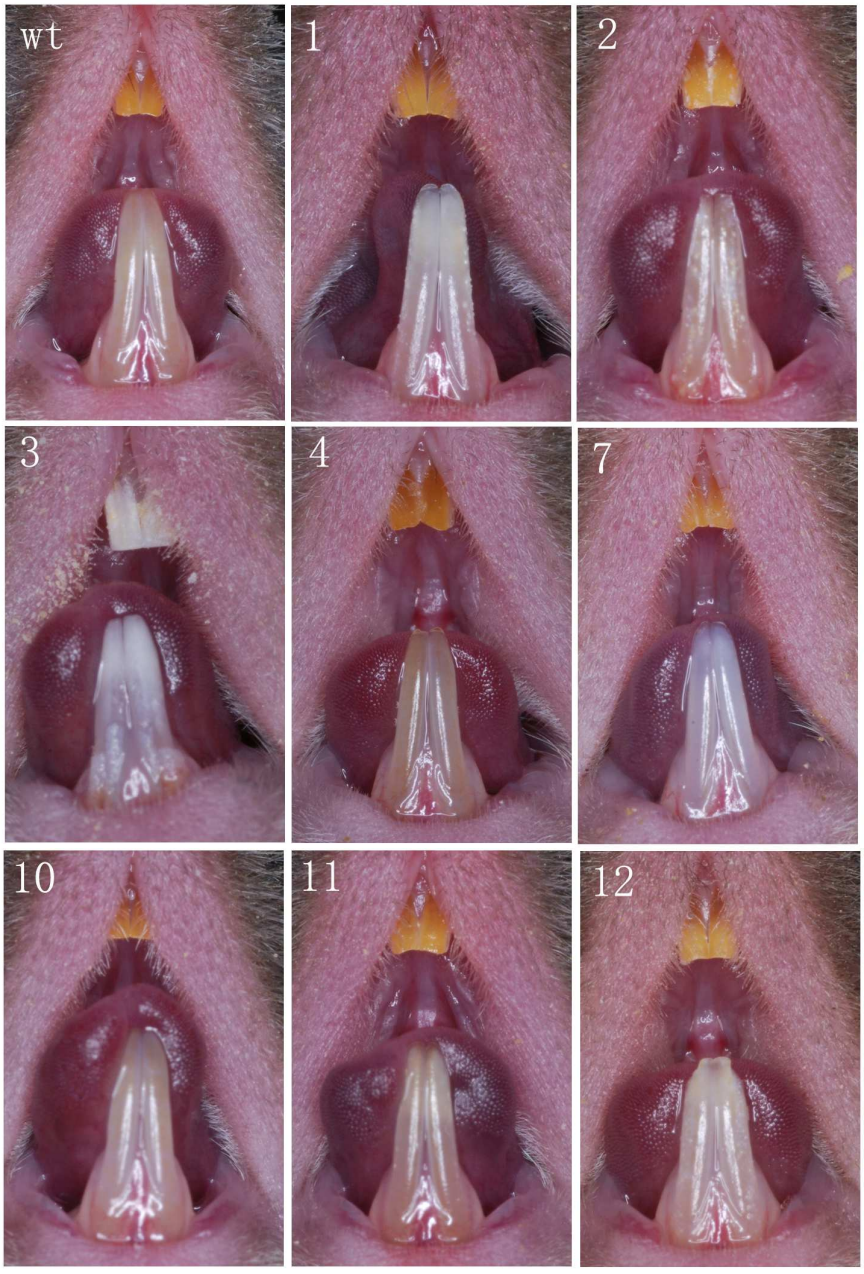

Fig 2.5 Oral photograph of enamelin transgenic mice. Intraoral photographs enamelin transgenic mice are shown. Offspring of transgenic founder were cross bred with C57BL/6 wild-type mouse. Pictures shown are from founder 1, 2, 3, 4, 7, 8, 10, 11 and 12 as noted on the upper left corner of each picture. Wild-type mouse intraoral picture is also shown (wt). Pictures shown of line 3, 4, 7, 8 are from F1 generation of transgenic mouse cross bred with C57BL6 wild-type mouse, while pictures of line 1, 2, 10, 11, 12 are from F2 generation.

Table 2.1 Primer sequences for genotyping

Primers	Sequences	Product size (bp)	Anticipated outcomes (positive in genotypes)
Enam tg F	GCCGCACCTTCTTTTTGAT	236	tg,+/+; tg,+/-; tg,-/-
Enam tg R	CAGACCCAGGAAAACAAGGA		
Enam4&5 F	GCCCAAAGCACAGTCATTTT	324	tg,+/+; tg,+/-; tg,-/-; +/+; +/-
*Enam*4&5 R	TAGGACCTGGCACGTGTCTC		
LacZ F	AAGTTTTGGGATTTGGCTCA	397	tg,+/-; tg,-/-; +/-; -/-
LacZ R	GACAGTATCGGCCTCAGGAA		

Table 2.2 Enamelin transgenic mouse original founder information

Toe cut#	Original ear tag #	Gender	DOB	Positive Transgene Transmission?
1	470	m	3/8-3/9/08	Yes
2	473	f	3/8-3/9/08	Yes
3	481	f	3/8-3/9/08	Yes
4	488	m	3/8-3/9/08	Yes
5	500	f	3/8-3/9/08	No, never give birth
6	504	m	3/8-3/9/08	No, checked six litters, all pups were transgene negative.
7	506	m	3/8-3/9/08	Yes
8	508	f	3/8-3/9/08	Yes, but poor breeding
9	513	f	3/8-3/9/08	No, produced one litter, all pups were transgene negative. Then founder dead.
10	517	f	3/8-3/9/08	Yes
11	526	f	3/8-3/9/08	Yes
12	532	m	3/8-3/9/08	Yes
13	547	f	3/8-3/9/08	Yes, but no adult offspring available. Stop producing collected one litter Day five teeth.

References

Aldred MJ, Crawford PJ (1995). Amelogenesis imperfecta--towards a new classification. *Oral Dis* 1(1)*:*2-5.

Beniash E, Skobe Z, Bartlett JD (2006). Formation of the dentino-enamel interface in enamelysin (MMP-20)-deficient mouse incisors. *Eur J Oral Sci* 114 Suppl 1(24-9; discussion 39-41, 379.

Caterina JJ, Skobe Z, Shi J, Ding Y, Simmer JP, Birkedal-Hansen H, et al. (2002). Enamelysin (matrix metalloproteinase 20)-deficient mice display an amelogenesis imperfecta phenotype. *J Biol Chem* 277(51)*:*49598-604.

Fincham AG, Moradian-Oldak J, Simmer JP (1999). The structural biology of the developing dental enamel matrix. *J Struct Biol* 126(3)*:*270-99.

Fukae M, Tanabe T (1987). Nonamelogenin components of porcine enamel in the protein fraction free from the enamel crystals. *Calcif Tissue Int* 40(5)*:*286-93.

Fukae M, Tanabe T, Murakami C, Dohi N, Uchida T, Shimizu M (1996). Primary structure of the porcine 89-kDa enamelin. *Adv Dent Res* 10(2)*:*111-8.

Fukumoto S, Kiba T, Hall B, Iehara N, Nakamura T, Longenecker G, et al. (2004). Ameloblastin is a cell adhesion molecule required for maintaining the differentiation state of ameloblasts. *J Cell Biol* 167(5)*:*973-83.

Gibson CW, Yuan ZA, Hall B, Longenecker G, Chen E, Thyagarajan T, et al. (2001). Amelogenin-deficient mice display an amelogenesis imperfecta phenotype. *J Biol Chem* 276(34)*:*31871-5.

Hu JC, Zhang CH, Yang Y, Karrman-Mardh C, Forsman-Semb K, Simmer JP (2001). Cloning and characterization of the mouse and human enamelin genes. *J Dent Res* 80(3)*:*898-902.

Hu JC, Sun X, Zhang C, Liu S, Bartlett JD, Simmer JP (2002). Enamelysin and kallikrein-4 mRNA expression in developing mouse molars. *Eur J Oral Sci* 110(4)*:*307-15.

Hu JC, Hu Y, Smith CE, McKee MD, Wright JT, Yamakoshi Y, et al. (2008). Enamel defects and ameloblast-specific expression in Enam knockout/lacz knock-in mice. *J Biol Chem* 283(16)*:*10858-71.

Mamo S, Gal AB, Bodo S, Dinnyes A (2007). Quantitative evaluation and selection of reference genes in mouse oocytes and embryos cultured in vivo and in vitro. *BMC Dev Biol* 7(14.

Margolis HC, Beniash E, Fowler CE (2006). Role of macromolecular assembly of enamel matrix proteins in enamel formation. *J Dent Res* 85(9)*:*775-93.

Paine ML, Wang HJ, Luo W, Krebsbach PH, Snead ML (2003). A transgenic animal model resembling amelogenesis imperfecta related to ameloblastin over-expression. *J Biol Chem* 278(21)*:*19447-52.

Simmer JP, Fukae M, Tanabe T, Yamakoshi Y, Uchida T, Xue J, et al. (1998). Purification, characterization, and cloning of enamel matrix serine proteinase 1. *J Dent Res* 77(2)*:*377-86.

Simmer JP, Hu JC (2002). Expression, structure, and function of enamel proteinases. *Connect Tissue Res* 43(2-3)*:*441-9.

Simmer JP, Hu Y, Lertlam R, Yamakoshi Y, Hu JC (2009). Hypomaturation enamel defects in Klk4 knockout/LacZ knockin mice. *J Biol Chem* 284(28)*:*19110-21.

Snead ML, Paine ML, Chen LS, Luo BY, Zhou DH, Lei YP, et al. (1996). The murine amelogenin promoter: developmentally regulated expression in transgenic animals. *Connect Tissue Res* 35(1-4)*:*41-7.

Snead ML, Paine ML, Luo W, Zhu DH, Yoshida B, Lei YP, et al. (1998). Transgene animal model for protein expression and accumulation into forming enamel. *Connect Tissue Res* 38(1-4)*:*279-86; discussion 295-303.

Stephanopoulos G, Garefalaki ME, Lyroudia K (2005). Genes and related proteins involved in amelogenesis imperfecta. *J Dent Res* 84(12)*:*1117-26.

Termine JD, Belcourt AB, Miyamoto MS, Conn KM (1980). Properties of dissociatively extracted fetal tooth matrix proteins. II. Separation and purification of fetal bovine dentin phosphoprotein. *J Biol Chem* 255(20)*:*9769-72.

Wen X, Zou Y, Luo W, Goldberg M, Moats R, Conti PS, et al. (2008). Biglycan over-expression on tooth enamel formation in transgenic mice. *Anat Rec (Hoboken)* 291(10)*:*1246-53.

Witkop CJ, Jr. (1988). Amelogenesis imperfecta, dentinogenesis imperfecta and dentin dysplasia revisited: problems in classification. *J Oral Pathol* 17(9-10)*:*547-53.

Chapter III

ENAM TRANSGENE EXPRESSION IN DEVELOPING TEETH

Abstract

After generating *Enam* transgenic mice and breeding the founders, the first priority was to determine the expression levels of the *Enam* transgene in developing teeth. It was expected that the amelogenin promoter would dictate ameloblast-specific expression, but integration site and copy number would strongly influence expression levels. Our strategy was to first determine expression levels by real-time PCR. We designed three primer pairs with the following specificities: 1) detects total *Enam* expression (from the transgene and native *Enam* genes) 2) detects expression of the *Enam* transgene only, and 3) detects expression from the native (endogenous) *Enam* genes only. Next we estimated total *Enam* expression levels by Western blot analyses.

Materials and Methods

Primer design. The first priority was to design primers that could specifically detect different mRNA. Historically, amplification products in the 100 to 150 bp range have proven suitable for semi-quantitative applications. The software application Primer3 on the Web was used to help select primers that would not anneal to themselves or to each other to minimize primer-dimer artifacts. Specificity for the endogenous *Enam* mRNA was achieved by having one primer anneal to the *Enam* coding region and the second primer anneal to a region outside the *Enam* coding region that is only found on the native mRNA. Specificity for the *Enam* transgene was achieved by having one primer anneal to the 5' amelogenin-specific sequence and the 3' primer anneal to the *Enam* coding region. Specificity for both the *Enam* transgene and the native *Enam* genes used both primers from the *Enam* coding region. The idea of primer design is showed in Fig 3.1. The sequences of these three primer pairs along with a Gapdh primer pair used to normalize results to the amount of cDNA template, the PCR conditions, and the lengths of the amplification products are shown in Table 3.1.

Isolation of day 5 first molars. Litters of mice were sacrificed at post-natal day 5. These mice were the product of an $Enam^{+/+}$ x $Enam^{tg,+/+}$ cross, or an $Enam^{-/-}$ x $Enam^{tg,+/-}$ cross as described in Chapter 2. The pups were sacrificed on day five and the four first molars surgically extracted. The ameloblasts of mouse first molars are all in the secretory stage. The two molars from one side were used to isolate RNA for reverse transcription-polymerase chain reaction (RT-PCR). The two molars from the

other side were stripped of soft tissue, and the hard tissue was used to extract proteins for Western blot analyses.

Real-time PCR (rtPCR). Real-time PCR was performed on selected litters from *Enam*$^{+/+}$ x *Enam*$^{tg,+/+}$ or *Enam*$^{-/-}$ x *Enam*$^{tg,+/-}$ crosses (Table 3.2). Each mouse was genotyped as described in Chapter 2. Animals were terminated on post-natal day 5, one first upper and one first lower molar were used to isolate mRNA (RNeasy Mini kit, QIAGEN Sciences, USA Cat. No.74104). RNase-Free DNase (Qiagen Cat. No. 79254) was used during RNA isolation to remove genomic DNA. RNA was reverse-transcripted to cDNA using SuperScript® First-Strand Synthesis System for RT-PCR (Invitrogen, Cat. No. 11904-018). PCR reaction reagent used is iQ^{TM} SYBR GREEN SUPERMIX (Bio-Rad Laboratories, Hercules, CA, USA. Cat. No. 170-8882). The 96-well plates and translucent tape that cover the plates were obtained from Bio-Rad (PCR plates, Low 96-well Clear, Cat. No. MLL9601; Optical tape, Cat No. 2239444, Bio-Rad Laboratories, Hercules, CA). Real-time PCR primer sequences are summarized in Table 3.1 (ordered from Invitrogen). Gapdh, the housekeeping gene, was used as internal control. Basically the PCR condition is to maintain the DNA at 95 ℃ for 3 minutes followed by 50 cycles of denaturation at 95 ℃ for 15 seconds, annealing at 60 ℃ for 25 seconds, extension at 72 ℃ for 35 seconds and then maintain the reaction at 95 ℃ for 1 minutes, then at 55 ℃ for 1 minutes followed by 68 cycles of graduate temperature increase reaction starting at 68 ℃ with 0.5 ℃ increasing each time for 10 seconds each cycle to complete final reaction. The

mechanism of real-time PCR experiment used is based on SYBR green as a dye that binds to double stranded DNA, but not single-stranded DNA. Standard curves were generated by diluting the cDNA products of the RT-PCR reactions 10-fold and 100 fold, then performing rtPCR using 1x, 0.1x, and 0.01x concentrations of cDNA as template. The point at which each PCR reaction reached a threshold level was plotted. The correlation coefficient (r^2) value of the standard curves was above 0.99 to be considered as a valid experiment. The rtPCR reactions were run in triplicate using the cDNA generated from each mouse in the litters. When multiple members of the litter had the same genotype, the rtPCR results were averaged. Statistical analyses were performed based upon the triplicate rtPCR runs, and the multiple runs performed when multiple littermates had the same genotype.

Isolation of proteins. The hard tissues from a maxillary and a mandibular first molars were incubated in 800 uL 1 % formic acid (ACROS ORGANICS, New Jersey, Code 147930010) at 4 °C for around 30 hours, centrifuged briefly to remove residual insoluble material, freeze at -80 °C for more than 4 hours, lyophilized overnight. 200 uL of 1x sample buffer (diluted from NuPage LDS sample buffer 4x, Invitrogen, Cat No. NP0007) were added to each sample do dissolve the proteins. 2% 2-mecaptoethanol (Bio-Rad Laboratories, Hercules, CA, Cat No. 161-0710) were added to each sample before load it on SDS-PAGE.

SDS-PAGE and Western blot Analysis. SDS-PAGE and Western blotting was performed on selected litters from *Enam*$^{+/+}$ x *Enam*$^{tg,+/+}$ or *Enam*$^{-/-}$ x *Enam*$^{tg,+/-}$ crosses (Table 3.3). Protein was isolated from the combined mineralized tissues of one maxillary and one mandibular first molar (PN5). When protein was obtained from multiple littermates with the same genotype, the tooth proteins were isolated separately but mixed prior to loading on gels. The amount loaded in each lane was the same fraction of tooth protein per tooth. 5uL sample were loaded to SDS-PAGE (NuPage 4-12% Bis-Tris Gel, Invitrogen, Carlsbad, CA. Cat No. NP0322BOX), transferred to a membrane, and *Enam* bands were visualized by Western blotting using rabbit anti-mouse antibody recognizing enamelin peptide starting from residue 223. The mouse enamelin 223 antibody is used to incubate the membrane at dilution of 1:1000 in 5% milk overnight. Secondary antibody for enamelin antibody experiment is a horseradish peroxidase-linked antibody (from donkey) anti-rabbit IgG (GE Healthcare UK limited, Little Chalfont Bucking Hamshine HP7 9NA UK., Cat. NA934V). Secondary antibody is incubated at dilution of 1:5000 for 3 hours. Amersham ECL Plus Western Blotting Detection System (GE Healthcare UK limited, Little Chalfont Bucking Hamshine HP7 9NA UK., Cat. No. RPN2132) was use to incubate for 5 minutes to visualize the membrane and develop the film. From each transgenic mouse line, offspring of same litter were used to load on one gel to compare the protein expression level among various genotypes from the same transgenic line.

Results

Real-time PCR using the primer set that amplified both the *Enam* transgene and the native *Enam* genes were conducted on $Enam^{+/+}$ and $Enam^{tg,+/+}$ littermates, which permitted normalizing the results to wild-type levels of *Enam* expression (Fig 3.2). By subtracting the value of the wild-type *Enam* expression from the value of the *Enam* transgene plus wild-type levels, we were able to obtain the level of *Enam* transgene expression relative to the *Enam* wild-type expression levels. Transgene expression levels were: line 2 (47%), and line 3 (485%), line 4 (1%), line 10 (11%), line 11 (22%), line 12 (31%) (Fig 3.3).

Real-time PCR using the primer set that amplified only the *Enam* transgene was also conducted on $Enam^{+/+}$ and $Enam^{tg,+/+}$ littermates, but could not be normalized to wild-type expression (as the native *Enam* transcripts were not amplified). Therefore we normalized the results of the reactions with the transgene expression of line 12, which had been determined to express the *Enam* transgene at 31% of normal wild-type *Enam* expression. The results are shown in Figure 3.4. For comparison to the real-time PCR results from the first primer set, the transgene expression levels normalized first to line 12 and then multiplied by 0.31 to adjust to the wild-type levels are: line 2 (40%), and line 3 (542%), line 4 (9%), line 10 (5%), line 11 (7%) and line 12 (31%). (Table 3.4) As shown in Table 3.5, the real-time PCR result using these two primer sets ("*Enam* F/R" and "*Enam* tg F/R") are consistent with each other.

The percentages of transgene expression level using these two primer sets are very close in each transgenic line.

Real-time PCR using the primer set that amplified both the *Enam* transgene and the native *Enam* genes were conducted on $Enam^{+/-}$, $Enam^{tg,+/-}$, $Enam^{-/-}$, and $Enam^{tg,-/-}$ littermates. As a wild-type mouse was not generated in the cross that produced these genotypes, data for wild-type mice were from the breeding of founder 12 (the line for which data is available from all genotypes and real-time PCR primer sets). The real-time PCR results for lines 1, 7, 10, and 12 were shown in Fig 3.5. When transgene expressed in null background (tg, -/-), the enamelin expression from these four lines are 154% (line 1, Fig 3.5 A), 9% (line 10, Fig 3.5 B), 13% (line 7, Fig 3.5C) and 96% (line 12, Fig 3.5D).

To compare the enamelin transgene expression level in different transgenic mice lines on three genetic backgrounds, i.e., on wild-type background, on heterozygous background and on null background, we summarized the real-time PCR results in Table 3.6. The averaged transgene expression level (as a percentage relative to gene expression level of the wild-type mice) in each transgenic lines are 140% (line 1), 47% (line 2), 485% (line 3), 1% (line 4), 14% (line 7), 8% (line 10), 22% (line 11) and 59.3% (line 12).

Real-time PCR using the primer set that amplified only the endogenous *Enam* transgene was also conducted on $Enam^{+/+}$ and $Enam^{tg,+/+}$ littermates from the higher expressing transgenic founder lines (2, 3, and 12) (Fig 3.6). Expression of

endogenous *Enam* was slightly decreased when by *Enam* transgene expression level getting higher.

We used a rabbit anti-mouse antibody recognizing the enamelin peptide starting from residue 223 to check enamelin transgene expression level on protein level. As showed in Fig 3.7, transgenic mouse lines 7, 10 and 11 showed low transgene expression levels, that were almost undetectable when expressed in null background; while transgenic lines 1, 2 and 12 showed higher transgene expression levels. These results are basically consistent with the real-time PCR results, which measured transgene expression at the mRNA level.

Discussion

Transgene expression levels relative to wild-type *Enam* expression calculated from the total *Enam* and *Enam* transgene-specific primers in the wild-type background were: line 4 (1%; 9%), line 10 (11%; 5%), line 11 (22%; 7%), line 12 (31%), line 2 (47%; 40%), and line 3 (485%; 542%). The results from the two primer sets are consistent and support the conclusion that *Enam* transgene expression levels relative to wild-type in lines 4, 10, and 11 are very low, lines 2 and 12 are moderate, and line 3 is very high.

Transgene expression levels in the six different genetic backgrounds using real-time PCR experiment showed some inconsistency. As showed in table 3.6, when transgene expressed in wild-type background, the transgene expression is lower than expressed

in null or heterozygous background. For example, for line 12, it showed 31% above wild-type enamelin expression on wild-type background, but when it expressed in null background, it showed 91% as the amount of wild-type enamelin expression. One possible explanation is that ameloblasts may have a feedback regulation system and try to maintain a certain level of enamelin expression for the proper enamel formation. When transgene and endogenous gene are both present, the ameloblasts try to express less enamelin than the transgene present alone. Another explanation is that if we use more animals in each group in the experiments, the result may show less inconsistency.

Figures and Legends

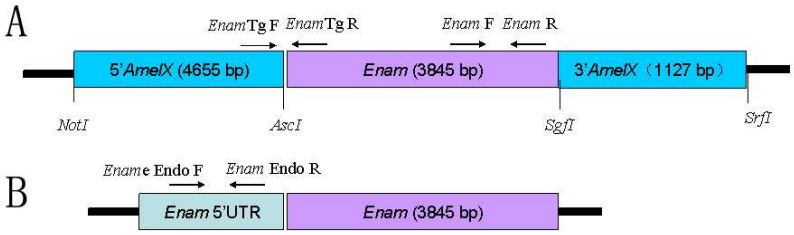

Fig 3.1 Real-time PCR primer design for checking *Enam* transgene expression level. A: Real-time PCR primer design. "*Enam* Tg F" and "*Enam* Tg R" primers amplify only the *Enam* transgene mRNA. "*Enam* F" and "*Enam* R" primers detect both endogenous enamelin and enamelin transgene mRNA. B: "*Enam* Endo F" and "*Enam* Endo R" anneals to the 5' untranslated region of *Enam* cDNA. Gapdh primers are to normalize enamelin expression levels.

Total *Enam* gene expression on wild-type background by realtime PCR (by primer1, each expression normalized by GAPDH then compared with wid-type mice)

	wt	line2	line3	line4	line10	line11	line12
average	1.00	1.47	5.85	1.01	1.11	1.22	1.31
std	0.11	0.15	1.06	0.06	0.27	0.13	0.19

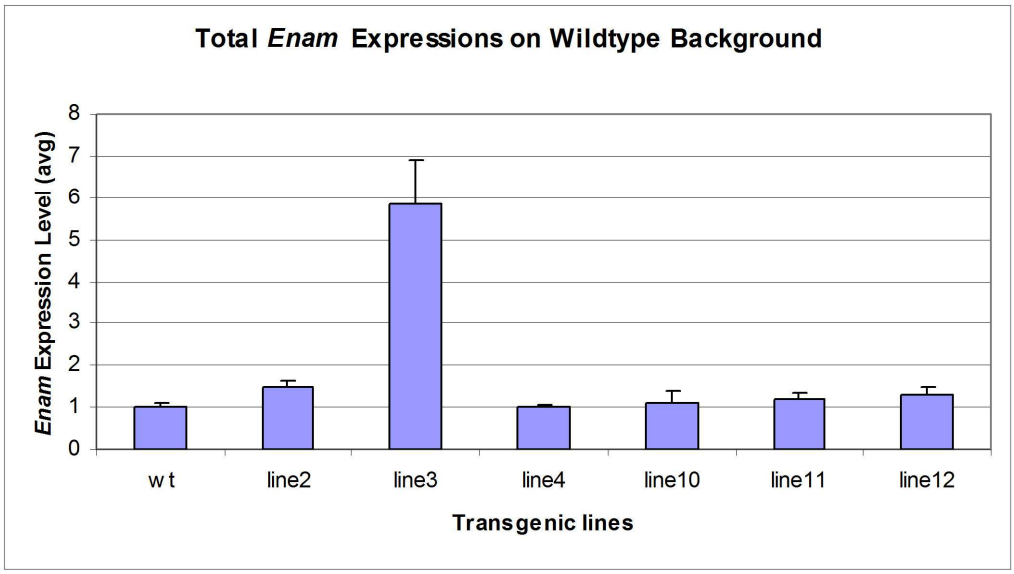

Fig 3.2 Total *Enam* gene expression on wild-type background by Real-time PCR. Real-time PCR was used to check mRNA expression level among transgenic lines. Day 5 first molars were extracted from offspring of Enamelin transgenic mice breeding with C57BL/6 wild-type mice. From each transgenic line, littermates were divided into two groups: transgene positive (tg) group and transgene negative (wt) group. One upper and one lower first molar from each animal were used to isolate mRNA. cDNA was obtained by reverse transcription from mRNA. *Enam* primer detects both endogenous enamelin and transgenic enamelin. "*Enam* tg" primer detects only enamelin from transgene. Each transgenic line has 3-5 transgenic mice and 3-5 wild-type mice. All wild-type animals from each line were averaged as the final "wt" group. Lines 2, 3, 10, 4, 11 are F3 generation of transgenic mouse bred with C57BL/6 mice, while line 12 is F4 generation of the same breeding strategy. Primer used is "*Enam*" primer ("primer 1" in table 3.2) which recognizes both endogenous and transgenic enamelin gene.

Derived *Enam* transgene expression on wild-type background by realtime PCR (by primer 1, each line normalized by GAPDH, compared with wild-type mice and minused the wide type mice expression level)

	wt	line2	line3	line4	line10	line11	line12
avg-wt	0	0.47	4.85	0.01	0.11	0.22	0.31
std	0.11	0.15	1.06	0.06	0.27	0.13	0.19

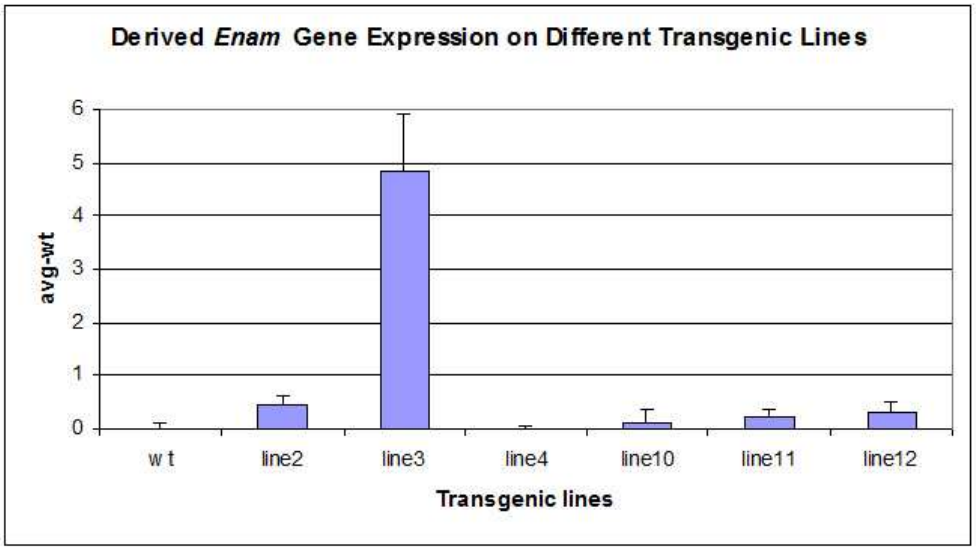

Fig 3.3 Derived *Enam* gene expression on wild-type background by real-time PCR. Material and methods are same as Fig 3.3, but expression level of every group were used to subtract wild-type group expression level to see how much more enamelin gene is expressed in different transgenic mouse lines than wild-type mice.

Relative *Enam* Transgene Expression Level at Different Lines by realtime PCR
(by primer set 2, and the GAPDH normaized *enam* expression levels werer divided by line 12 expression level)

	wt	line 2	line 3	line 4	line 10	line 11	line 12
avg	0	1.32	17.47	0.29	0.15	0.24	1.00
std	0	0.14	3.30	0.05	0.07	0.06	0.20

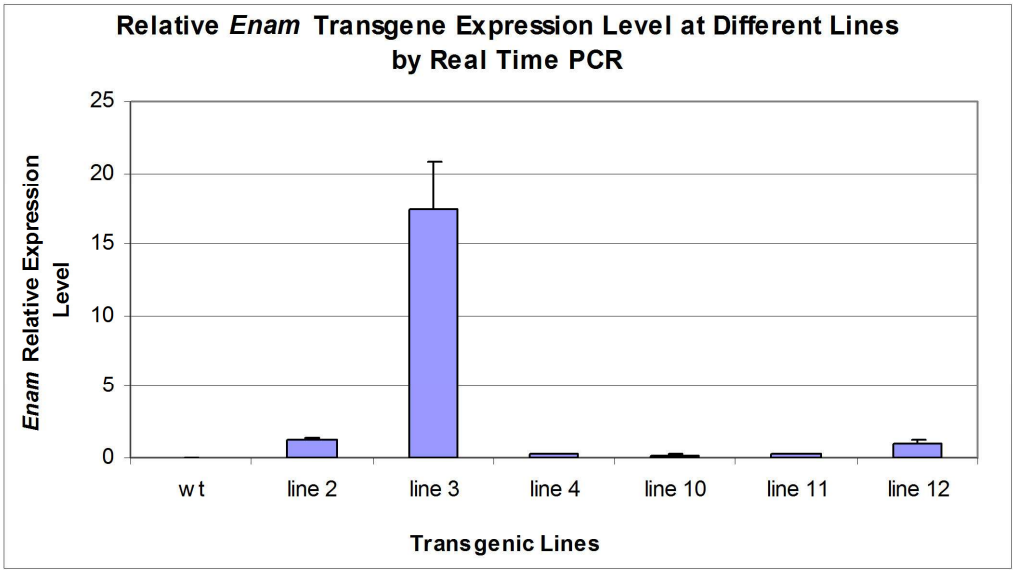

Fig 3.4 Relative *Enam* transgene gene expression level in different lines by real-time PCR. Real-time PCR was used to check mRNA expression level among transgenic lines. Day 5 first molars were extracted from offspring of Enamelin transgenic mice breeding with C57BL/6 wild-type mice. From each transgenic line, littermates were divided into two groups: transgene positive (tg) group and transgene negative (wt) group. One upper and one lower first molar from each animal were used to isolate mRNA. cDNA was obtained by reverse transcription from mRNA. *Enam* primer detects both endogenous enamelin and transgenic enamelin. "*Enam* tg" primer detects only enamelin from transgene. Each transgenic line has 3-5 transgenic mice and 3-5 wild-type mice. All wild-type animals from each line were averaged as the final "wt" group. Lines 2, 3, 10, 4, 11 are F3 generation of transgenic mouse bred with C57BL/6 mice, while line 12 is F4 generation of the same breeding strategy. Primer used is "*Enam* tg" primer ("primer 2" in table 3.2) which recognize only enamelin transgene, not endogenous enamelin gene. Expression level in each group were first subtract wild-type expression levels and then divided by the expression level of line 12 to compare the result of primer 2 ("*Enam* tg" primer, this figure) with primer 1 ("*Enam*" primer, Fig 3.3).

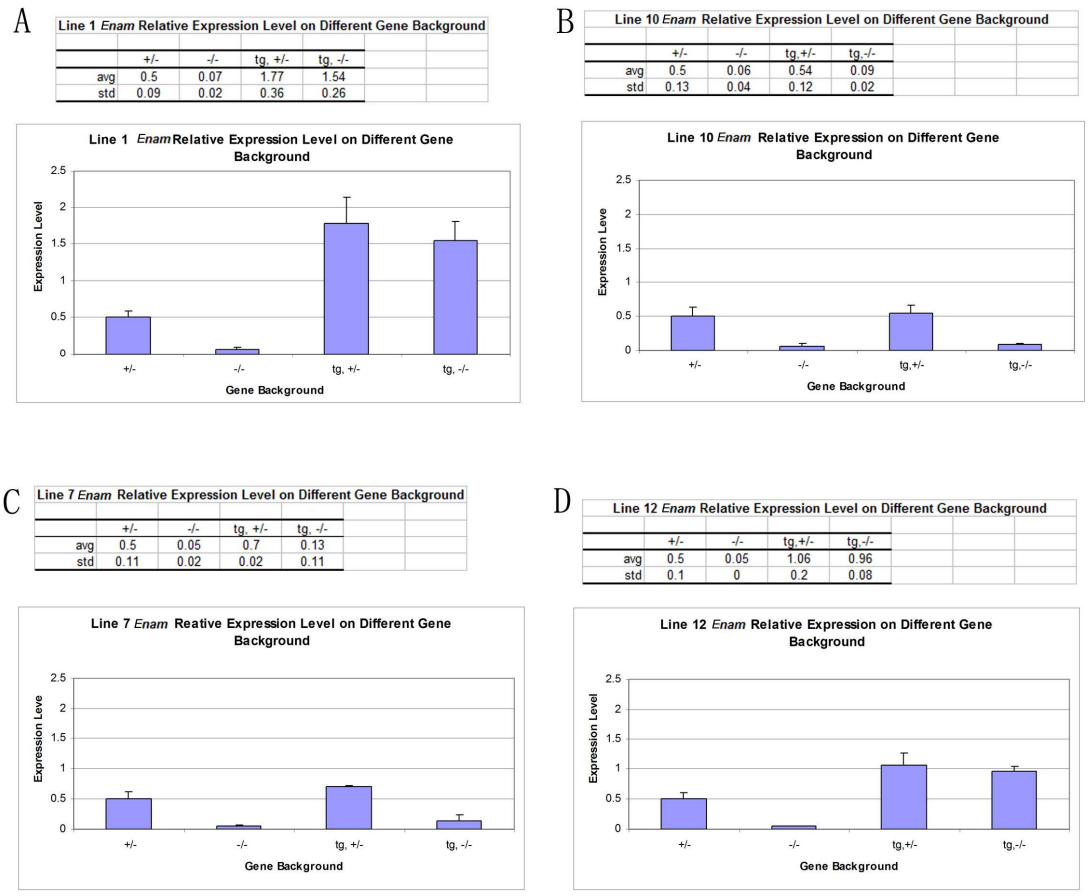

Fig. 3.5 *Enam* transgene expression levels at the mRNA level. *Enam* expression levels of F2 offspring were tested by real-time PCR. One upper and one lower day 5 first molar from each mouse were combined and used to isolate mRNA. Day 5 wild-type mouse samples from the same position were used as control. Gapdh, a housekeeping gene, was used as control. Three animals from each genotype group were used for each transgenic line. Average expression level in each group were divided by the average wild-type expression level to estimate the relative transgene expression level expressed as percentage of wild-type counterparts in line 1 (A), line 10 (B) , line 1(C) and line 12 (D). In each line, genotypes were *Enam* wild-type (wt), $Enam^{tg, -/-}$, $Enam^{tg, +/-}$, $Enam^{-/-}$ and $Enam^{+/-}$ as noted.

Endogenous *Enam* expression level at different transgenic Line				
	WT	line 2	line 3	line12
evg	1	0.85	0.61	1.09
std	0.09	0.11	0.14	0.27

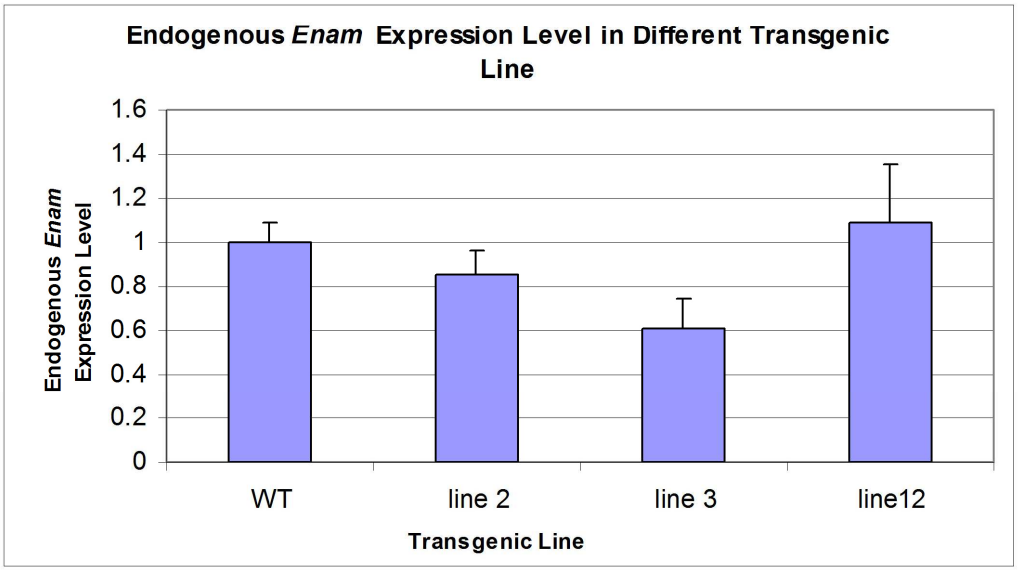

Fig 3.6 Endogenous *Enam* expression levels in different transgenic lines.
Real-time PCR was used to check mRNA expression level among transgenic lines. Day 5 first molars were extracted from offspring of Enamelin transgenic mice breeding with C57BL/6 wild-type mice. From each transgenic line, littermates were divided into two groups: transgene positive (tg) group and transgene negative (wt) group. One upper and one lower first molar from each animal were used to isolate mRNA. cDNA was obtained by reverse transcription from mRNA. *Enam* primer detects both endogenous enamelin and transgenic enamelin. "*Enam* tg" primer detects only enamelin from transgene. Each transgenic line has 3-5 transgenic mice and 3-5 wild-type mice. All wild-type animals from each line were averaged as the final "wt" group. Lines 2, 3, 12 are check in this experiment. Primer used is "*Enam* Endo" primer ("primer 3" in table 3.2), which recognizes only endogenous enamelin, not enamelin transgene mRNA.

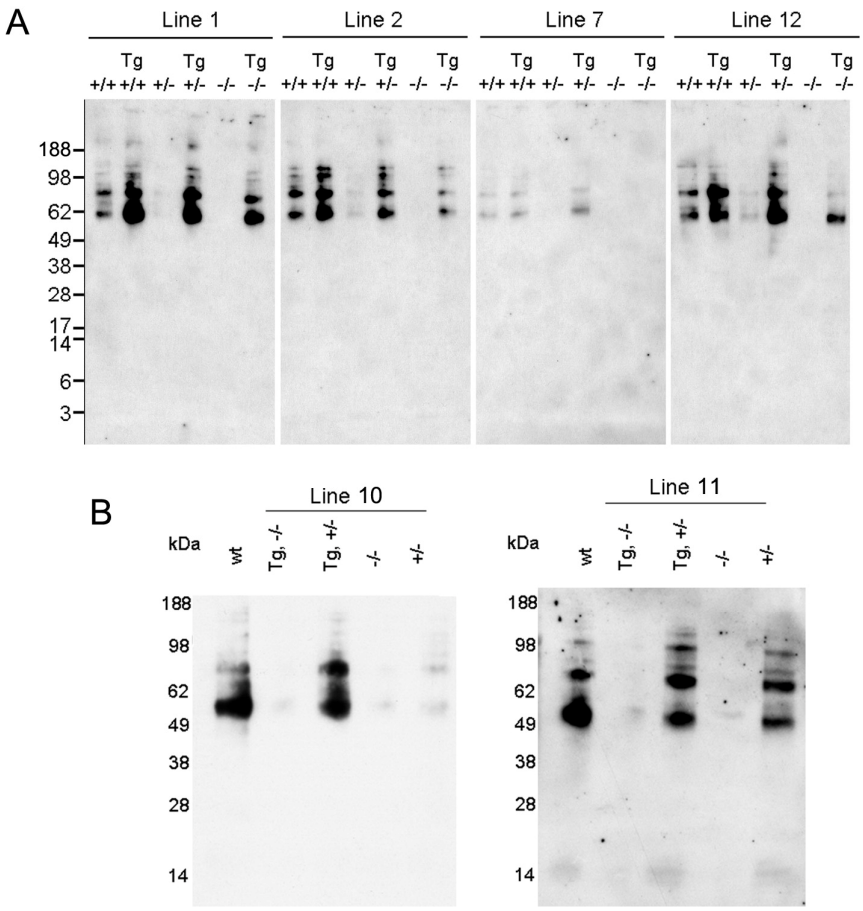

Fig 3.7 *Enam* transgene expression at the protein level. Western blots immunostained using an antibody raised against a mouse enamelin peptide starting at residue 223 and was used to examine protein expression level on F2 offspring of transgenic lines as noted. A, transgenic mouse line 1, 2, 7, 12 have all the six transgenic background from the two breeding strategy (as described in Chapter 2), including wild-type (lane +/+), transgene expressed in wild-type background (lane tg +/+), heterozygous (lane +/-), transgene expressed in heterozygous background (lane tg +/-), enamelin knockout (lane -/-), transgene expressed in knockout background (lane tg -/-). B, for line 10 and 11, four genotypes from breeding of enamelin transgenic mouse with knockout mice were compared with non-littermate wild-type animal sample. Equal fractions of enamel proteins extracted from day 5 one first upper and one first lower molar from *Enam* wild-type (lanes wt, or +/+), *Enam* knockout mice expressing an transgene (lanes tg,-/-), *Enam* heterozygotes expressing an *Enam* transgene (lane tg, +/-), *Enam* homozygous knockout mice (lanes -/-) and *Enam* heterozygotes (lanes +/-).

Table 3.1 Real-time PCR primer sequences

Primers	Sequences	Product size (bp)
Enam F	5'AACACATTGGTTGGGTTAGC3'	114
Enam R	5'GTCCTGTGGACTGGTTCCTT3'	
Enam tg F	5'ACTCAAAGAACCATCAAGGGC3'	96
Enam tg R	5'CATTTGGTACCAGGCCACAT3'	
Enam Endo F	5'TTTGGGTACTGAACATGACACC3'	99
Enam Endo R	5'CAAACTGCTGAAGCCAGAGA3'	
Gapdh F	5'TGACGTGCCGCCTGGAGAAA3'	98
Gapdh R	5'AGTGTAGCCCAAGATGCCCTTCAG3'	

Basically the PCR condition is to maintain the DNA at 95 ℃ for 3 minutes followed by 50 cycles of denaturation at 95 ℃ for 15 seconds, annealing at 60 ℃ for 25 seconds, extension at 72 ℃ for 35 seconds and then maintain the reaction at 95 ℃ for 1 minutes, then at 55 ℃ for 1 minutes followed by 68 cycles of graduate temperature increase reaction starting at 68 ℃ with 0.5 ℃ increasing each time for 10 seconds each cycle to complete final reaction.

Table 3.2 Real-time PCR done on different *Enam* transgenic lines of different gene background by three primer sets

primer set	Genotype	Line 1	Line 2	Line 3	line 4	Line 7	Line 10	Line 11	Line 12
primer 1 (*Enam* F/R)	+/+		√	√	√		√	√	√
	+/-	√				√	√		√
	-/-	√				√	√		√
	tg,+/+		√	√	√		√	√	√
	tg,+/-	√				√	√		√
	tg,-/-	√				√	√		√
primer 2 (*Enam* tg F/R)	+/+		√	√	√		√	√	√
	tg,+/+		√	√	√		√	√	√
primer 3 (*Enam* Endo F/R)	+/+		√	√					√
	tg,+/+		√	√					√

Primer 1: This primer set amplifies the total *Enam* expression level, including the endogenous *Enam* and *Enam* transgene.

Primer 2: This primer set amplifies only the *Enam* transgene.

Primer 3: This primer set to amplifies only the endogenous *Enam*. It PCR the sequence between the 5' UTR and exon-- of endogenous *Enam* gene.

+/+: Wide type mice.
+/-: Heterozygous *Enam* knock out mice.
-/-: Homozygous *Enam* Knock out mice.
tg,+/+: *Enam* transgenic mice on wild-type background.
tg,+/-: *Enam* transgenic mice on heterozygous *Enam* knock out mice.
tg,-/-: *Enam* transgenic mice on homozygous *Enam* knock out mice.

Table 3.3 Result of Western-Blot representing enamelin protein level of mice with different genotype from various transgenic lines background

Antibody	Genotype	Line 1	Line 2	Line 3	Line 4	Line 7	Line 10	Line 11	Line 12
Mouse *Enam* 223	+/+	√	√			√			√
	+/-	√	√			√	√	√	√
	-/-	√	√			√	√	√	√
	tg,+/+	√	√			√			√
	tg,+/-	√	√			√	√	√	√
	tg,-/-	√	√			√	√	√	√

Table 3.4 Converted relative *Enam* transgene gene expression levels in different lines by real-time PCR.

	wt	line 2	line 3	line 4	line 10	line 11	line 12
average	0	1.32	17.47	0.29	0.15	0.24	1.00
Converted (avg X 31%)	0	0.40	5.42	0.09	0.05	0.07	0.31

Table 3.5 Comparison of real-time PCR results from two primers.

	wt	line 2	line 3	line 4	line 10	line 11	line 12
Primer 1 (*Enam* F/R)	0	47%	485%	1%	11%	22%	31%
Primer 2 (*Enam* tg F/R)	0	40%	542%	6%	5%	7%	31%

Table 3.6 Percentage of *Enam* transgene expression in different transgenic lines and different gene backgrounds

	Line 1	Line 2	Line 3	Line 4	Line 7	Line 10	Line 11	Line 12
Percentage of transgene expression on wild-type background	n/a	47%	485%	1%	n/a	11%	22%	31%
Percentage of transgene expression on heterozygous background	127%	n/a	n/a	n/a	20%	4%	n/a	56%
Percentage of transgene expression on null background	154	n/a	n/a	n/a	13%	9%	n/a	91%
Averaged transgene expression level	140%	47%	485%	1%	14%	8%	22%	59.3%

Chapter IV

PHENOTYPIC RESCUE OF ENAMELIN KNOCKOUT MICE BY AN ENAMELIN TRANSGENE

Abstract

In *Enam* null mice the mineralization front associated with the secretory surface of the ameloblast membrane fails to initiate and elongate enamel mineral ribbons, so no true enamel forms. The mineralization front is a complex of enamel proteins that cannot be reconstituted *in vitro*. This study is to establish an *in vivo* system for assaying enamelin structure-function relationships by developing an enamelin transgene that can recover normal enamel formation in *Enam* null mice. A mouse expression vector was constructed using 4.6 kb of 5' amelogenin gene up to the translation initiation codon, the enamelin 3.8 kb cDNA, and 1.2 kb of amelogenin 3' noncoding sequence. Transgenic mice established using this construct was bred with *Enam* null mice for two generations. Offspring of this breeding strategy have the following four genotypes: enamelin transgene expressed in the *Enam* null background ($Enam^{tg,-/-}$), enamelin transgene expressed in the *Enam* heterozygous background ($Enam^{tg,+/-}$), enamelin null mice ($Enam^{-}$

$^{/-}$) and enamelin heterozygous mice (*Enam*$^{+/-}$). The enamel was characterized by scanning electron microscopy (SEM) and oral photographs to see whether the enamelin transgene rescued the enamel phenotype of *Enam* null mice. Offspring of founder 12, which were median expressers of the *Enam* transgene (transgene is similar as endogenous enamelin level), fully recovered the enamel phenotype in the *Enam*$^{-/-}$ background. SEM evaluation of *Enam*$^{tg,-/-}$ mice demonstrated that the enamel layer was the same thickness as wild-type mice and had well-defined, decussating enamel rods. Von Kossa staining of histological sections showed enamel mineralization from the DEJ to the enamel surface. Offspring of founders 10, which were low expressers of the *Enam* transgene (around 8% of the endogenous enamelin level), did not recover the phenotype in the null background, but recovered the phenotype in the heterozygous background. Similar was the result from founder 1, which is a high expresser (transgene is around 140% of endogenous enamelin level): when transgene is expressed in null background, the enamel defect was not recovered; when transgene is expressed in heterozygous background, the phenotype is fully recovered. This study confirms the importance of enamelin in the enamel formation and that its role is dosage-dependent. This study also shows that appropriate expression of *Enam* transgene was can rescue the defective phenotype of enamelin knockout mice. This system is useful to study enamelin structure-function relationships *in vivo*.

Introduction

Trying to rescue the defective phenotype of a mutant gene using another gene, mutated version of the same gene, fragment of the same gene, etc., is a useful approach to study the structure and function of a gene in many fields, including tooth development area.

This approach was used to study gene regulation in early stage tooth development. Tooth development is arrested at the bud stage in *Msx1* deficient mice (Houzelstein et al., 1997; Satokata and Maas, 1994). *Bmp4* is a downstream gene of *Msx1* in early mouse tooth development. In one study, it was found that ectopic expression of a *Bmp4* transgene driven by the mouse *Msx1* promoter in the dental mesenchyme restored the expression of *Lef-1* and *Dlx2* but neither *Fgf3* nor syndecan-1 in the *Msx1* mutant molar tooth germ. The mutant phenotype of molar but not incisor could be partially rescued to progress to the cap stage (Zhao et al., 2000). By using the rescue approach, the authors in this study learned that *Bmp4* can bypass *Msx1* function to partially rescue molar tooth development *in vivo*, and to support alveolar process formation (Zhao et al., 2000). Another example of tooth development gene regulation study using a rescuing approach is that using the keratin 14 promoter to target expression of an activated form of TNF family receptor Edar in transgenic mice. Expression of this transgene is able to rescue the tooth phenotype in Tabby (Eda) and Sleek (Edar) mutant mice (Tucker et al., 2004), which has ectodermal dysplasia phenotype including missing teeth and smaller teeth with reduced cusps (Pispa et al., 1999). Rescuing approach can also be used to study the function of a gene in different developmental stages. This approach is used in one study on dentin development. Dentin matrix protein 1 (Dmp1) is expressed in both pulp and odontoblast cells and deletion of the *Dmp1* gene leads to defects in odontogenesis and mineralization (Ye et al., 2004). Re-expression of Dmp1 in early and late odontoblasts under control of the Col1a1 promoter rescued the defects in mineralization as well as the defects in the dentinal tubules and third molar development. In contrast, re-expression of Dmp1 in mature odontoblasts, using the Dspp promoter, produced only a partial rescue of the

mineralization defects (Lu et al., 2007). In this study, the results suggest that Dmp1 is a key regulator of odontoblast differentiation and it is required in both early and late odontoblasts for normal odontogenesis to proceed (Lu et al., 2007). Rescuing approach is also used in the studies of enamel matrix proteins. Amelogenin is the most abundant protein in developing enamel (Fincham et al., 1999b). Amelogenin and its cleavage products make up over 90% of the enamel matrix (Fincham et al., 1999b; Termine et al., 1980). There are several studies that use the rescuing approach to study the function of amelogenin by using fragments or modulated version of this gene to try to rescue the defective phenotype of the amelogenin knockout mice. Amelogenin null mice show a phenotype similar to human *amelogenesis imperfecta*, with a thin surface layer of mineral lacking a typical rod pattern (Gibson et al., 2001). Transgenic expression of bovine leucine-rich amelogenin protein (LRAP) in the enamel-secreting ameloblasts in amelogenin knockout mice, did not rescue the enamel phenotype (Chen et al., 2003). When they use transgenic mice that express LRAP (a 59 amino acid leucine-rich amelogenin peptide) under control of the *AmelX* regulatory regions to breed with amelogenin knockout mice, they found the organization of the enamel rod pattern was altered by the presence of the LRAP transgene (Gibson et al., 2009). In another study, amelogenin null (KO) mice were bred with two transgenic mouse lines, one expresses the most abundant amelogenin (TgM180), which has normal enamel; another expresses a mutated amelogenin (TgP70T), which leads to amelogenesis imperfecta in humans (Li et al., 2008a). The resultant TgM180KO offspring showed evidence of rescue in enamel thickness, mineral density, and volume in molar teeth. Rescue was not observed in the molars from the TgP70TKO mice (Li et al., 2008a). In the study of ameloblastin, another

major enamel matrix protein, transgenic mouse established using full-length ameloblastin gene expressed driven by amelogenin promoter were bred with *Ambn* mutant mice. Appropriate expression level of transgene fully recovered the defective phenotype of *Ambn* mutant mice (Chun et al., 2010 in press).

The objective of this study was to establish an *in vivo* system for assaying enamelin structure-function relationships by developing an effective transgenic model that can recover normal enamel formation in *Enam* null mice. The mouse amelogenin (*AmelX*) 5' transcriptional regulatory region has been successfully used to drive transgenic expression specifically in ameloblasts (Snead et al., 1996; Snead et al., 1998b; Wen et al., 2008b). We established transgenic mouse lines that express *Enam* gene driven by amelogenin promoter, and used different transgenic mouse lines to breed with enamelin null mice to see whether the transgene can recover the defective phenotype of null mice, which show no true enamel layer and chalky-white teeth phenotype (Hu et al., 2008).

Materials and Methods

Von Kossa staining of secretory stage molars. Day 4 mandibles of F2 offspring from line 12 were fixed with 4% paraformaldehyde/0.1% glutaraldehyde, dehydrated in ethanol, embedded in paraffin and sectioned at 6mm. Von Kossa staining for mineral was performed by applying 1% silver nitrate to the sections and exposing them to ultraviolet light for 20 min. Unreacted silver was removed with 5% sodium thiosulfate. Sections were counterstained using toluidine blue.

Scanning electron microscopy (SEM) of mandibular incisors using fracture method. The soft tissue was removed from left and right half mandibles at 7 weeks. We used a rotating diamond disc (BRASSELER Dental Instruments, Savannah, GA, Cat. No. 934.11.180) to cut a notch on mandibular incisor from the dentin side (lingual side) at the level of the labial alveolar crest and fractured the incisor at the notch. SEM imaging of the broken surface highlights the decussating rods. A second, parallel cut was made through the incisors 5-6 mm apical to the first cut. This cut surface was glued to an SEM stub so that the electron beam would be aimed directly perpendicular to the fracture surface. The surface was sputter coated with gold and analyzed by SEM to determine enamel thickness and structure.

Scanning electron microscopy (SEM) of mandibular incisors using polish and etch method. The soft tissue was removed from left and right half mandibles at 7 weeks. We used a rotating diamond disc to cut through mandibular incisor at the level of the labial alveolar crest. The broken edge of the incisor was polished with two different Extra Thin Contouring and Polishing Disc (3M ESPE Dental Products, St. Paul, MN. REF 2381F, REF 2381SF) for about 1 minute each, using the orange colored disk (REF 2381F) first and the yellow colored disk (REF 2381SF) second. After polished the cutting surface, the sample was washed with 0.75 % Bleach for 10 seconds and then lightly etched with 0.1% nitric acid (RICCA CHEMICAL co. Arlington, TX. Cat. No. 5320-16) for exactly 15 seconds three times. Samples were washed with water in between etching. A second, parallel cut was made through the incisors 5-6 mm apical to the first cut. This cut surface was glued to an SEM stub so that the electron beam would be aimed directly

perpendicular to the first cut to accurately measure the thickness of the enamel layer. The surface was sputter coated with gold and analyzed by SEM to determine enamel thickness and structure.

Oral photographs. Oral photographs of teeth were taken using Nikon DIGITAL CAMERA DXM1200 combined with microscope. For each sample, intraoral picture of upper and lower incisors in the head with skin (0.8x), labial view of lower incisor (2x), mesial view of lower mandible (1.3x) and mesial view of lower molars (3x) were taken.

Results

We have characterized four lines of *Enam* transgenic mice bred with *Enam* null mice.

Phenotype of F2 offspring from transgenic line 7. Based on the Western blotting and real-time PCR results, line 7 is a low expresser. Line 7 has a minimum transgene expression level that is hardly detectable at the protein level and is around 14% of wild-type *Enam* based on real-time PCR result. Transgene expressing in null background showed no enamel recovery. The phenotype of this genotype, *i.e.* $Enam^{tg,\ -/-}$, has severer defects than heterozygous mouse (Fig 4.1 E-H, compared with Q-T). However when transgene of this line expressed in heterozygous background, i.e. $Enam^{(tg,\ +/-)}$, the teeth look much better than *Enam* heterozygous mouse (Fig 4.1 I-L compared with Q-T) based on the oral photographs. On intraoral photograph, the incisors look yellowish in color, similar to wild-type animals (Fig 4.1 I). From the mesial view of the lower mandible, the enamel layer can be seen in the $Enam^{(tg,\ +/-)}$ mice from this line (Fig 4.1 K), similar as the

wild-type mice (Fig 4.1 C). On the Scanning Electron Microscopy (SEM) pictures, when the transgene from this line is expressed in null background, i.e., *Enam*$^{(tg, -/-)}$, no true enamel layer was found (Fig 4.2 and Fig 4.4 column 2). The molars of this genotype look rough on the surface and small in size (Fig 4.3 column 2, row 3 and 4). High magnification SEM (10,000x and 20,000x) pictures show no decussation pattern was found in the enamel microstructure in this phenotype (Fig 4.3 column 2, row 1 and 2). But when the transgene is expressed in heterozygous background, i.e., *Enam*$^{(tg, +/-)}$, the enamel thickness is completely normal, and the decussation pattern of enamel rod-interrod structure is evident (Fig 4.2, 4.3, 4.4 column 3). Molars of mice from this genotype look similar to the wild-type animals (Fig 4.3 column 3 row 3 and 4).

Phenotype of F2 offspring from transgenic line 10. Based on the Western blotting and real-time PCR results, line 10 is also a low expresser. Line 10 has a minimum transgene expression level that is hardly detectable at the protein level and is around 8% of wild-type *Enam* based on real-time PCR result. The phenotype of 7 weeks old mice from line 10 is similar to those of line 7. When the transgene is expressed in *Enam* null background, no enamel thickness recovery is found (Fig 4.6 and 4.8, column 2). On high magnification SEM pictures, the enamel layer has some rod-interrod-like decussation structures coming back (Fig 4.7 column2, row 1 and 2). But when the transgene is expressed in *Enam* heterozygous background, the enamel thickness and decussation pattern is fully recovered (Fig 4.6, 4.7, 4.8 column3). The lower incisor for this genotype looks smooth on surface and yellowish in color (Fig 4.5 I), similar as those of wild-type

(Fig 4.5 A), much better than those of heterozygous mouse, which have chalky-white lower incisors (Fig 4.5 Q).

Phenotype of F2 offspring from transgenic line 12. Line 12 has a transgene expression level similar as endogenous gene expression level. Transgene from line 12 successfully recovered the defects of the *Enam* null mice as shown by the oral photographs of adult F2 offspring. When expressing an *Enam* transgene, both the null mice and heterozygous mice have their teeth appear normal (Fig 4.9, E-H and I-L individually). The teeth look smooth on the surface and yellowish in color for both genotypes (Fig 4.9 E and I individually). Scanning Electron Microscope (SEM) sections showed the *Enam* transgene in both null and heterozygous background recovered the enamel thickness. Enamel of these mice has well-defined, decussating enamel rods (Fig. 4.10, 4.11, 4.12 column 2 and 3). In secretory stage, enamel formation is recovered by the transgene from line 12 in the *Enam* null background, *i.e.* genotype $Enam^{(tg,\ -/-)}$, as shown by von Kossa staining on sections from day 4 F2 offspring (Fig 4.13A and B column1). The enamel layer has mineralization staining, while in the *Enam* null mice, no mineralization was found in enamel layer (Fig 4.13A and B column 4).

Phenotype of F2 offspring from transgenic line 1. Based on the Western blotting and real-time PCR results, line 1 showed about 140% as much as those of wild-type *Enam* expression. In line 1, the transgene did not recover the phenotype in null background but recovered the phenotype well in the heterozygous background. $Enam^{(tg,\ +/-)}$ mouse in this line showed full enamel thickness and well defined decussation pattern under SEM (Fig

4.15-4.17 column 3) and smooth surface and yellowish in color on oral photographs (Fig 4.14 I-L), similar to those of wild-type mouse.

Discussion

Based on our current results, phenotype of *Enam*$^{(tg, +/-)}$ mice from all four transgenic lines have their teeth look normal, fully recovered the phenotype of *Enam*$^{(+/-)}$ mouse. Each genotype from each line has more than 3 animals characterized and demonstrated similar results. In line 12, which has a transgene expression level similar to wild-type *Enam* gene, F2 offspring in genotype of *Enam*$^{(tg, -/-)}$ showed full recovery of enamel phenotype. Secretory stage enamel formation is also recovered. Line 7 and line 10 have a transgene with a low expression level. For these two transgenic mouse lines, transgene recovered the phenotype in the heterozygous background but not in the null background. Line 1 has an expression level higher than normal, however, the *Enam*$^{(tg, -/-)}$ has a similar expression level as *Enam*$^{(tg, +/-)}$ yet with a different phenotype. Based on the current study, except the *Enam*$^{(tg, -/-)}$ mice from line 1, enamelin expression higher than 70% is adequate for facilitating enamel formation. When *Enam* expression level is lower than 50% (like around 10% in line 7 and 10) of the normal, the enamel defect cannot be recovered.

The recovery of the enamel phenotype in *Enam* null mice by transgenic expression of functional *Enam* confirms the previous observation that *Enam* is essential for proper dental enamel formation. Another finding of this study is that variation in transgene expression by ameloblasts among different transgenic lines dictated the degree of phenotypic rescue of *Enam* null mice. It further confirmed that there is a dose-dependent

effect of enamelin and that proper expression level of this gene is critical for proper enamel formation.

Figures and Legends

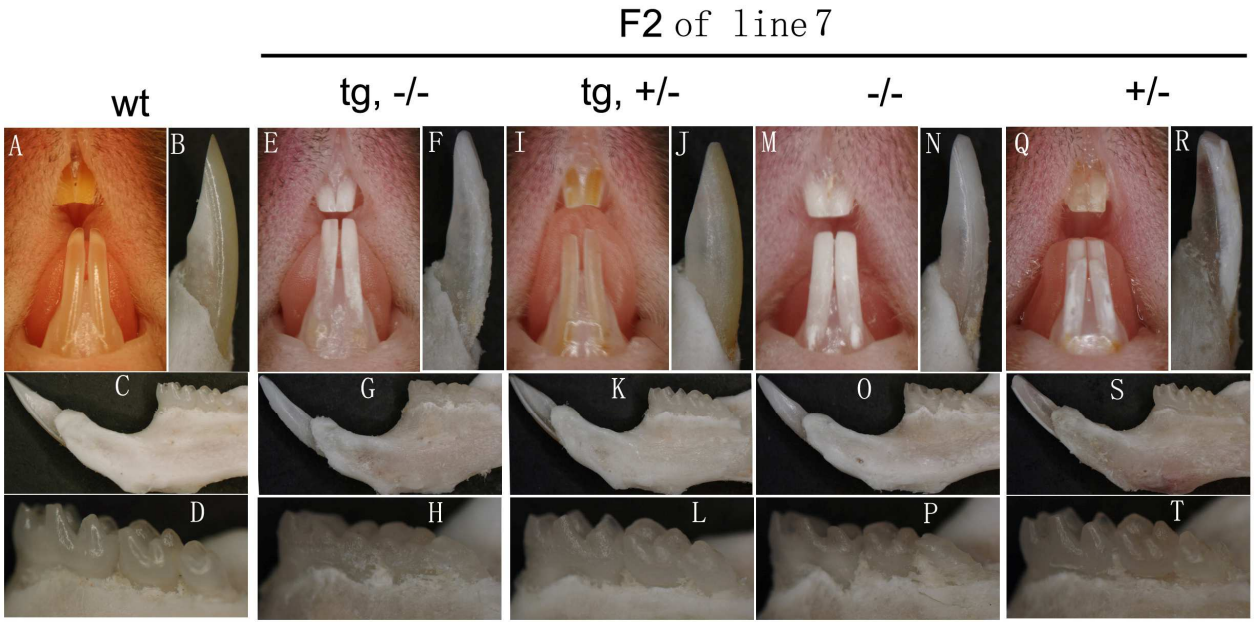

Fig 4.1 Oral photograph of F2 offspring from transgenic mouse line 7. Intraoral photographs of 7 weeks old mice of wild-type mouse (A-D), F2 offspring from transgenic line 12 (E-T) are shown. Oral photograph of genotype *Enam*$^{(tg, -/-)}$ (E-H), *Enam*$^{(tg, +/-)}$ (I-L), *Enam*$^{(-/-)}$ (M-P) and *Enam*$^{(+/-)}$ (Q-T) are noted. These photographs includes direct intraoral photograph (A, E, I, M, Q), distal view of lower incisor (B, F, J, N, R), mesial view of lower incisor and mandible (C, G, K, O, S) and mesial view of molars (D, H, L, P, T).

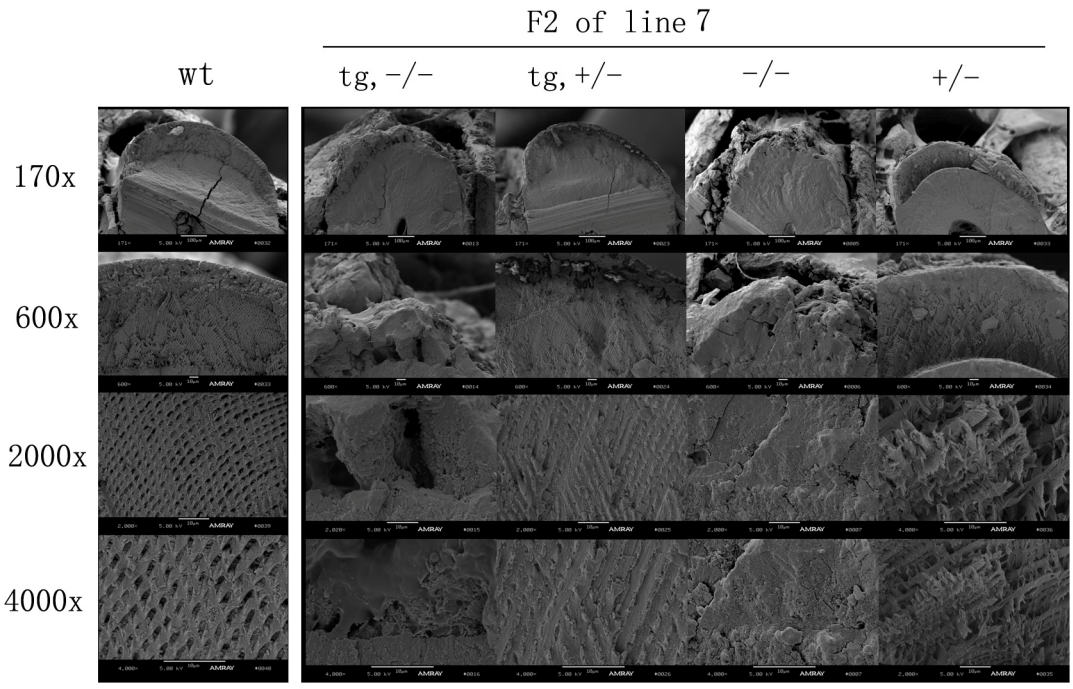

Fig 4.2 SEM analysis of F2 offspring of line 7: low magnification. Mandibular incisors from 7-week-old F2 offspring were cut at the level of labial alveolar crest for SEM evaluation. SEM results of F2 offspring from transgenic mouse line 7 (column 2-5) and wild-type control were shown (column 1) with whole incisor (row 1), enamel layer (row 2) and middle enamel (2000x in row 3 and 4,000x in row 4) are shown. Genotypes of groups are: wild-type (wt) (column 1), *Enam*$^{(tg, -/-)}$ (column 2), *Enam*$^{(tg, +/-)}$ (column 3), *Enam*$^{(-/-)}$ (column 4) and *Enam*$^{(+/-)}$ (column 5).

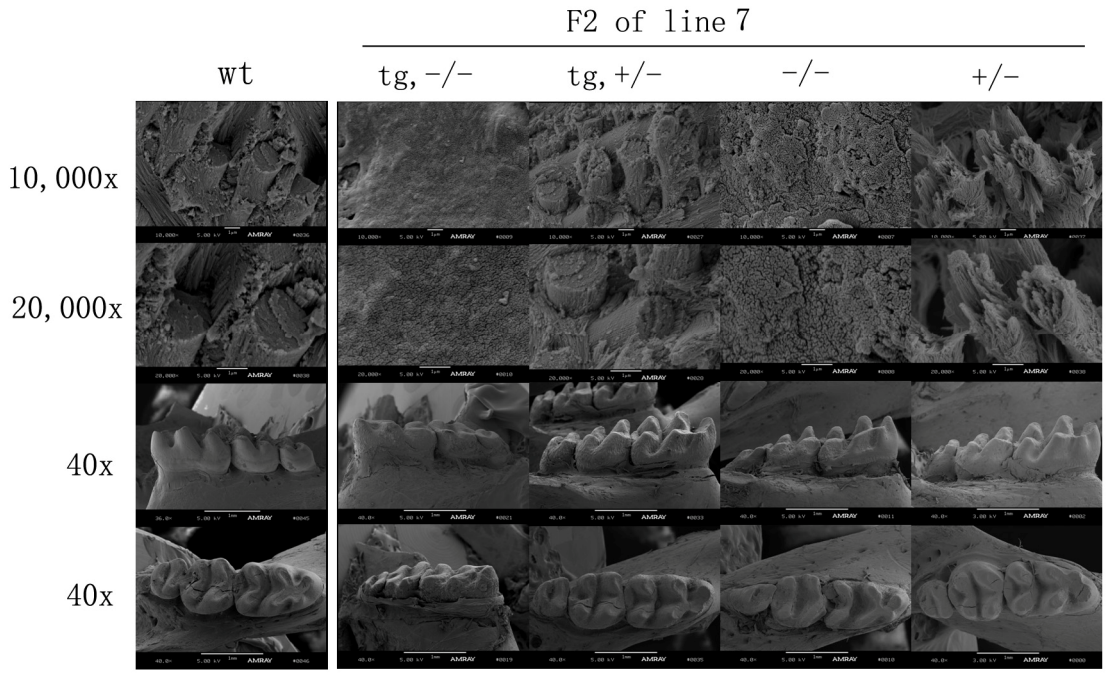

Fig 4.3 SEM analysis of F2 offspring of line 7: high magnification and molars. Mandibular incisors from 7-week-old F2 offspring were cut at the level of labial alveolar crest for SEM evaluation. SEM results of F2 offspring from transgenic mouse line 7 (column 2-5) and wild-type control (column 1) are shown. High magnification of enamel microstructure (10,000x in row 1, 20,000x in row 2) and the surface SEM of molars (mesial view in row 3, occlusal view in row 4) are shown. Genotypes of groups are: wild-type (wt) (column 1), *Enam*$^{(tg, -/-)}$ (column 2), *Enam*$^{(tg, +/-)}$ (column 3), *Enam*$^{(-/-)}$ (column 4) and *Enam*$^{(+/-)}$ (column 5).

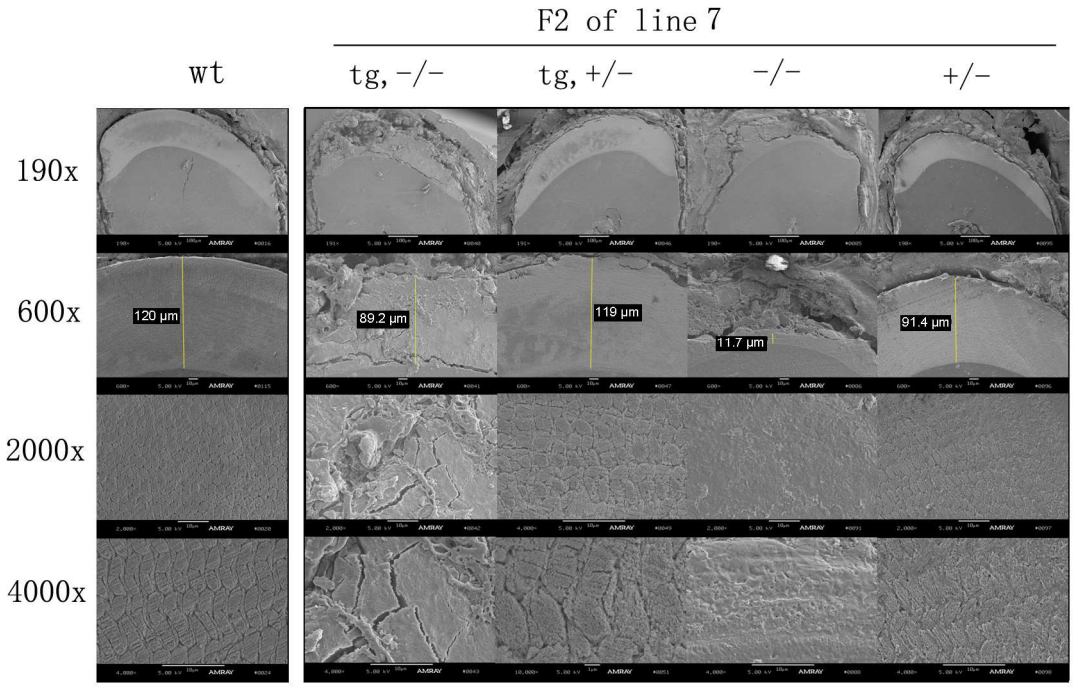

Fig 4.4 SEM analysis of F2 offspring of line 7 using polish and etch method. Mandibular incisors from 7-week-old F2 offspring were cut at the level of labial alveolar crest and processed for polish and etch for SEM evaluation to examine enamel thickness. SEM results of F2 offspring from transgenic mouse line 7 (column 2-5) and wild-type control were shown (column 1) with cross section of incisor (row 1), enamel layer (row 2) and middle enamel (2000x in row 3 and 4,000x in row 4) are shown. Genotypes of groups are: wild-type (wt) (column 1), *Enam*$^{(tg, -/-)}$ (column 2), *Enam*$^{(tg, +/-)}$ (column 3), *Enam*$^{(-/-)}$ (column 4) and *Enam*$^{(+/-)}$ (column 5).

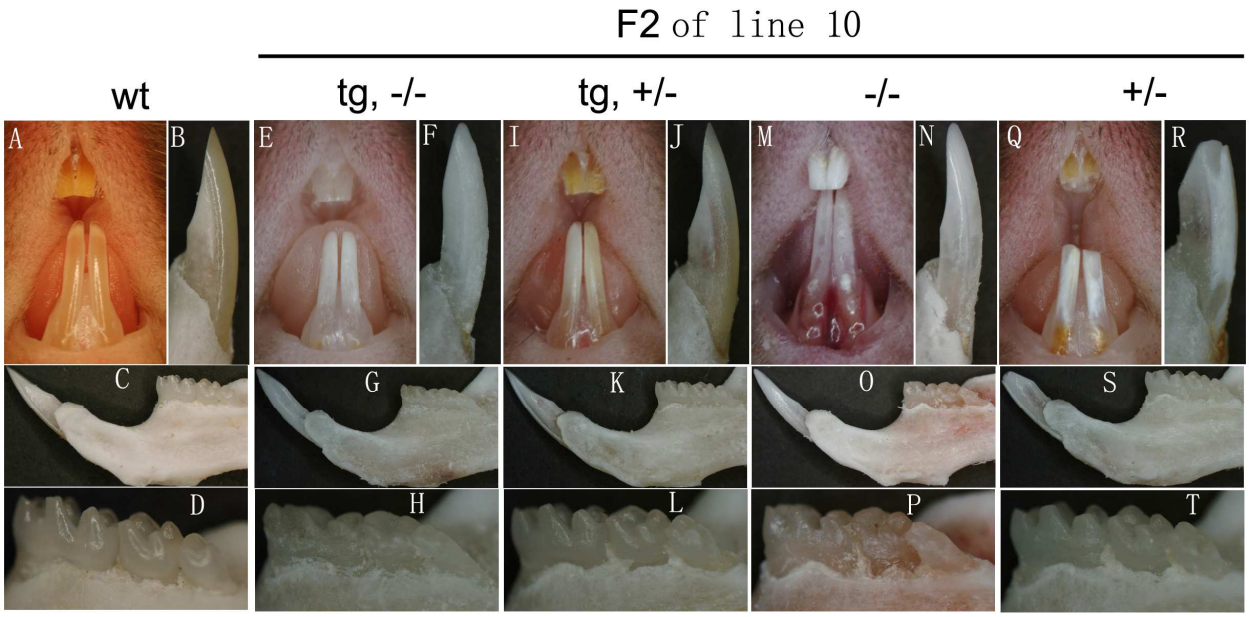

Fig 4.5 Oral photograph of F2 offspring from transgenic mouse line 10. Intraoral photographs of 7 weeks old mice of wild-type mouse (A-D), F2 offspring from transgenic line 10 (E-T) are shown. Oral photograph of genotype *Enam*$^{(tg, -/-)}$ (E-H), *Enam*$^{(tg, +/-)}$ (I-L), *Enam*$^{(-/-)}$ (M-P) and *Enam*$^{(+/-)}$ (Q-T) are noted. These photographs include direct intraoral photograph (A, E, I, M, Q), distal view of lower incisor (B, F, J, N, R), mesial view of lower incisor and mandible (C, G, K, O, S) and mesial view of molars (D, H, L, P, T).

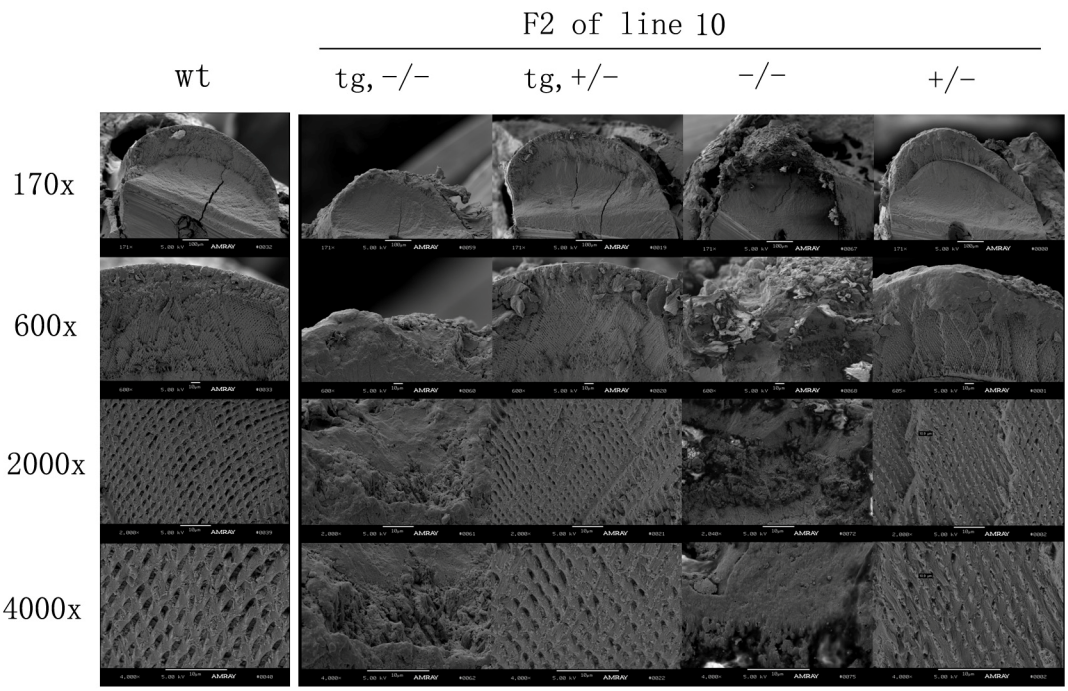

Fig 4.6 SEM analysis of F2 offspring of line 10: low magnification. Mandibular incisors from 7-week-old F2 offspring were cut at the level of labial alveolar crest for SEM evaluation. SEM results of F2 offspring from transgenic mouse line 10 (column 2-5) and wild-type control were shown (column 1) with cross section of incisor (row 1), enamel layer (row 2) and middle enamel (2000x in row 3 and 4,000x in row 4) are shown. Genotypes of groups are: wild-type (wt) (column 1), *Enam*$^{(tg, -/-)}$ (column 2), *Enam*$^{(tg, +/-)}$ (column 3), *Enam*$^{(-/-)}$ (column 4) and *Enam*$^{(+/-)}$ (column 5).

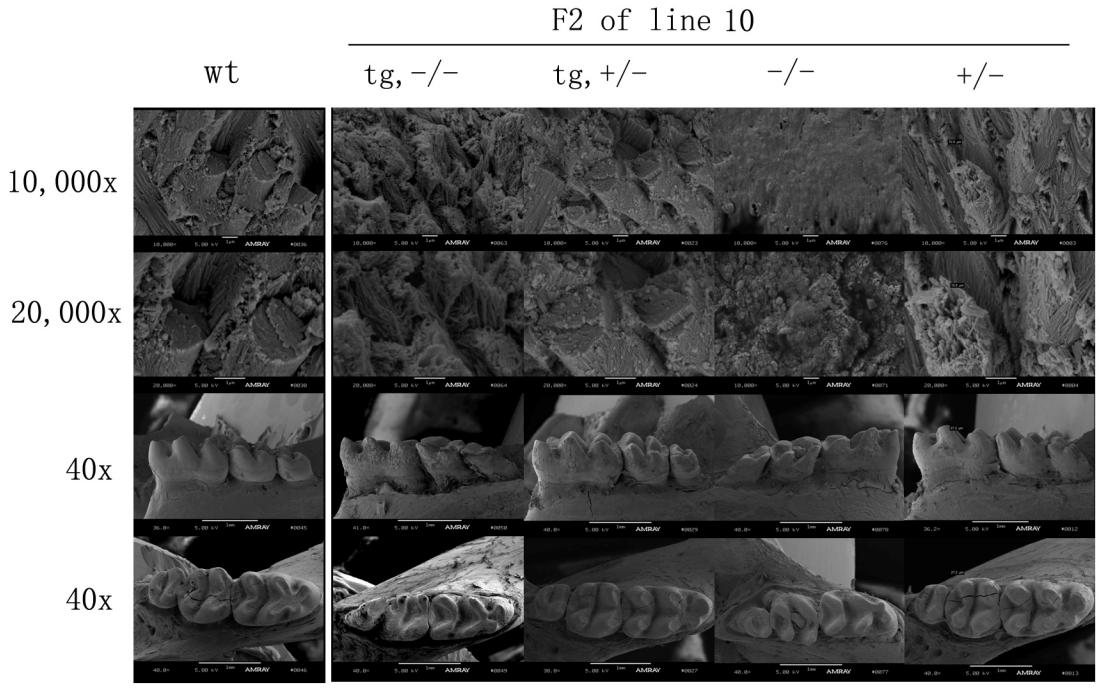

Fig 4.7 SEM analysis of F2 offspring of line 10: high magnification and molars. Mandibular incisors from 7-week-old F2 offspring were cut at the level of labial alveolar crest for SEM evaluation. SEM results of F2 offspring from transgenic mouse line 10 (column 2-5) and wild-type control (column 1) are shown. High magnification of enamel microstructure (10,000x in row 1, 20,000x in row 2) and the surface SEM of molars (mesial view in row 3, occlusal view in row 4) are shown. Genotypes of groups are: wild-type (wt) (column 1), *Enam*$^{(tg, -/-)}$ (column 2), *Enam*$^{(tg, +/-)}$ (column 3), *Enam*$^{(-/-)}$ (column 4) and *Enam*$^{(+/-)}$ (column 5).

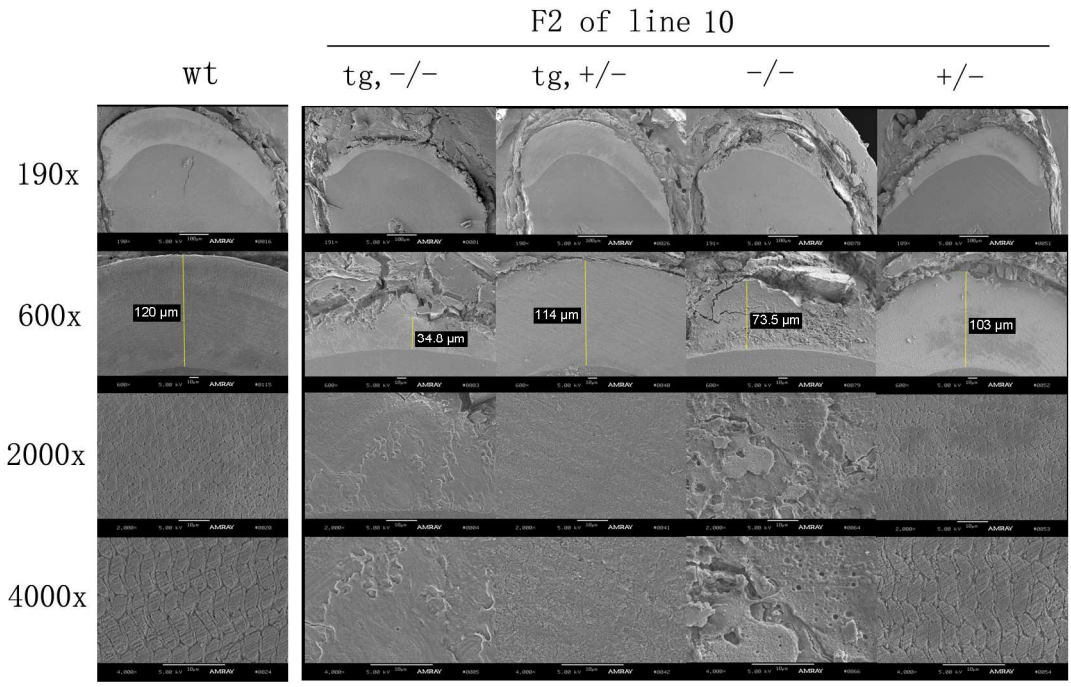

Fig 4.8 SEM analysis of F2 offspring of line 10 using polish and etch method. Mandibular incisors from 7-week-old F2 offspring were cut at the level of labial alveolar crest and processed for polish and etch for SEM evaluation to examine enamel thickness. SEM results of F2 offspring from transgenic mouse line 10 (column 2-5) and wild-type control were shown (column 1) with whole incisor (row 1), enamel layer (row 2) and middle enamel (2000x in row 3 and 4,000x in row 4) are shown. Genotypes of groups are: wild-type (wt) (column 1), *Enam*$^{(tg, -/-)}$ (column 2), *Enam*$^{(tg, +/-)}$ (column 3), *Enam*$^{(-/-)}$ (column 4) and *Enam*$^{(+/-)}$ (column 5).

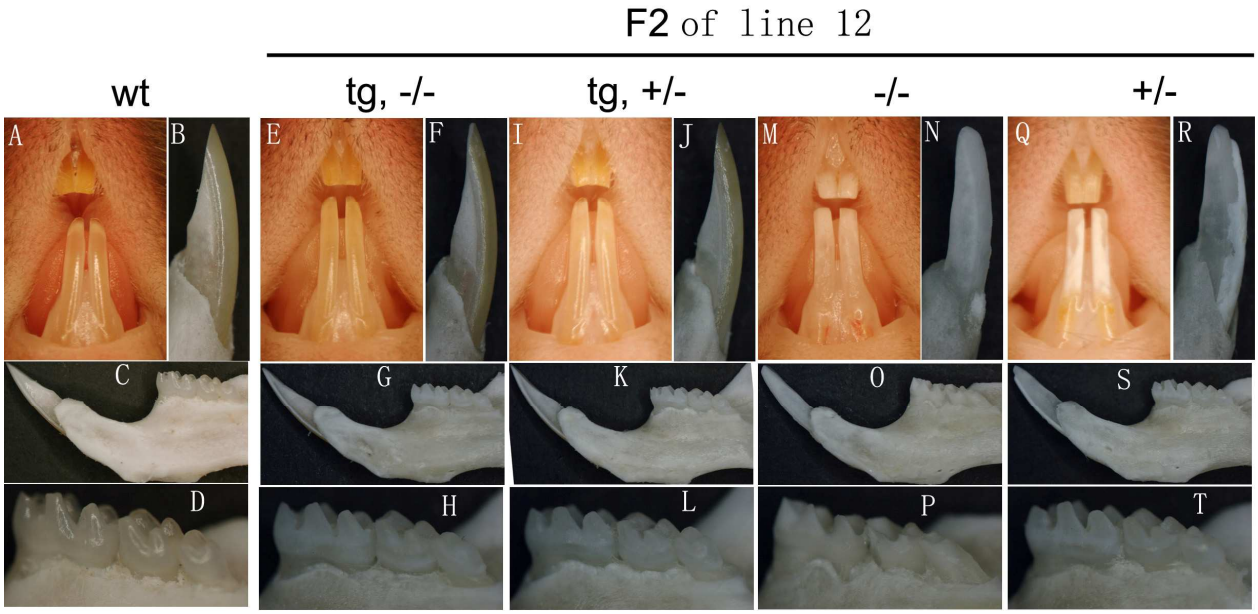

Fig 4.9 Oral photograph of F2 offspring from transgenic mouse line 12. Intraoral photographs of 7 weeks old mice of wild-type mouse (A-D), F2 offspring from transgenic line 12 (E-T) are shown. Oral photograph of genotype *Enam*$^{(tg, -/-)}$ (E-H), *Enam*$^{(tg, +/-)}$ (I-L), *Enam*$^{(-/-)}$ (M-P) and *Enam*$^{(+/-)}$ (Q-T) are noted. These photographs include direct intraoral photograph (A, E, I, M, Q), distal view of lower incisor (B, F, J, N, R), mesial view of lower incisor and mandible (C, G, K, O, S) and mesial view of molars (D, H, L, P, T).

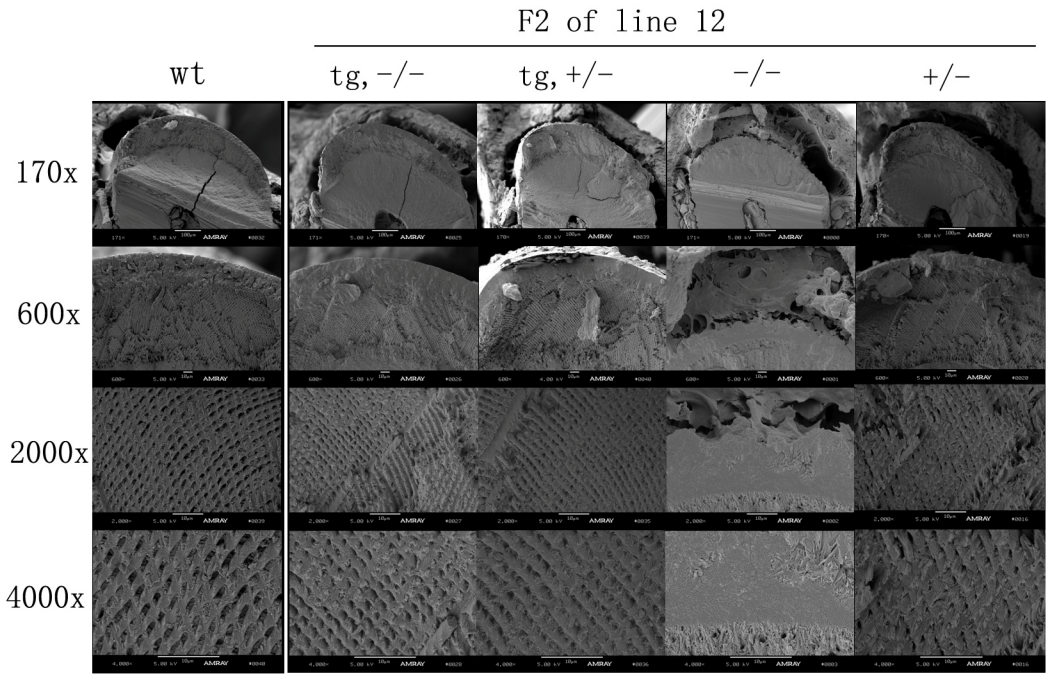

Fig 4.10 SEM analysis of F2 offspring of line 12: low magnification. Mandibular incisors from 7-week-old F2 offspring were cut at the level of labial alveolar crest for SEM evaluation. SEM results of F2 offspring from transgenic mouse line 12 (column 2-5) and wild-type control were shown (column 1) with whole incisor (row 1), enamel layer (row 2) and middle enamel (2000x in row 3 and 4,000x in row 4) are shown. Genotypes of groups are: wild-type (wt) (column 1), *Enam*$^{(tg, -/-)}$ (column 2), *Enam*$^{(tg, +/-)}$ (column 3), *Enam*$^{(-/-)}$ (column 4) and *Enam*$^{(+/-)}$ (column 5).

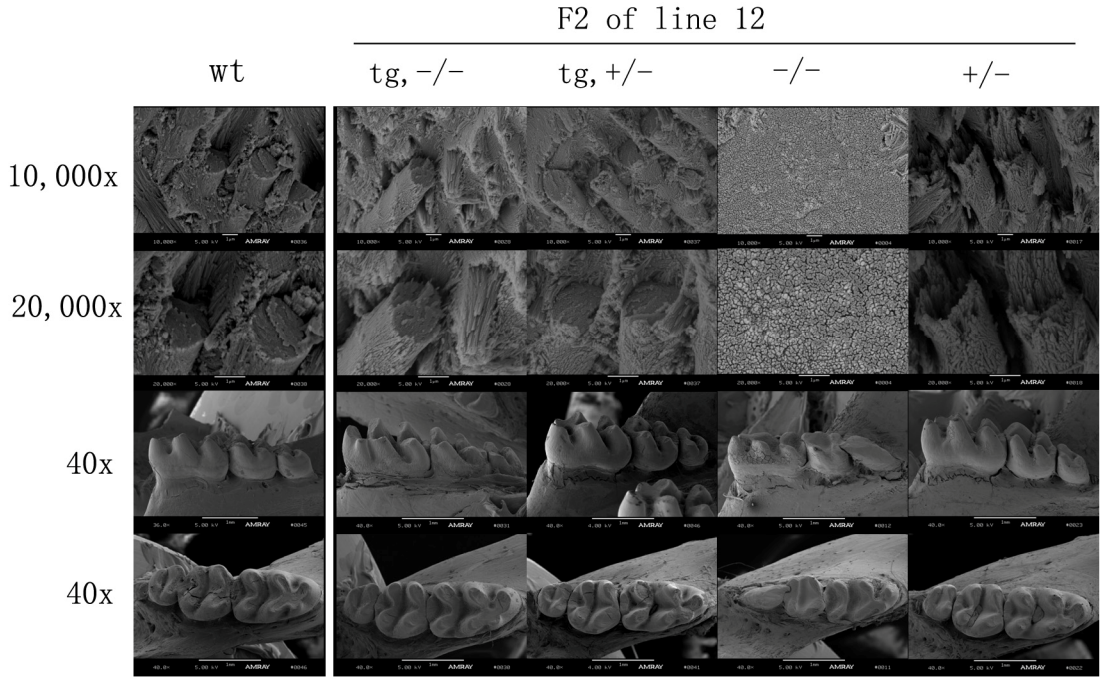

Fig 4.11 SEM analysis of F2 offspring of line 12: high magnification and molars. Mandibular incisors from 7-week-old F2 offspring were cut at the level of labial alveolar crest for SEM evaluation. SEM results of F2 offspring from transgenic mouse line 12 (column 2-5) and wild-type control (column 1) are shown. High magnification of enamel microstructure (10,000x in row 1, 20,000x in row 2) and the surface SEM of molars (mesial view in row 3, occlusal view in row 4) are shown. Genotypes of groups are: wild-type (wt) (column 1), *Enam*$^{(tg, -/-)}$ (column 2), *Enam*$^{(tg, +/-)}$ (column 3), *Enam*$^{(-/-)}$ (column 4) and *Enam*$^{(+/-)}$ (column 5).

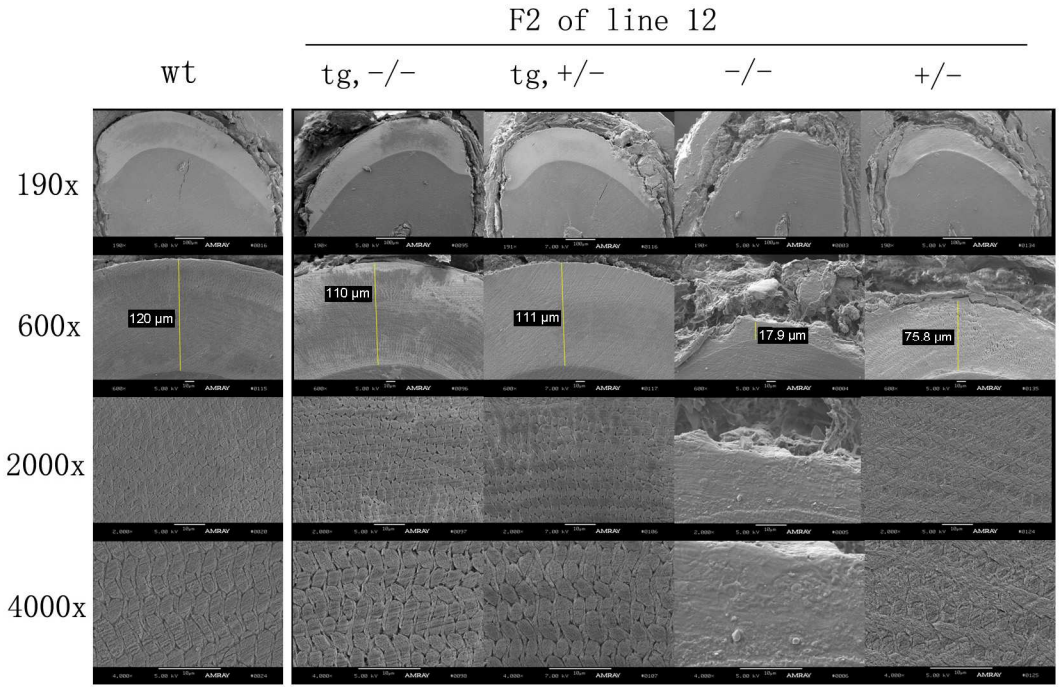

Fig 4.12 SEM analysis of F2 offspring of line 12 using polish and etch method. Mandibular incisors from 7-week-old F2 offspring were cut at the level of labial alveolar crest and processed for polish and etch for SEM evaluation to examine enamel thickness. SEM results of F2 offspring from transgenic mouse line 12 (column 2-5) and wild-type control were shown (column 1) with whole incisor (row 1), enamel layer (row 2) and middle enamel (2000x in row 3 and 4,000x in row 4) are shown. Genotypes of groups are: wild-type (wt) (column 1), *Enam*$^{(tg, -/-)}$ (column 2), *Enam*$^{(tg, +/-)}$ (column 3), *Enam*$^{(-/-)}$ (column 4) and *Enam*$^{(+/-)}$ (column 5).

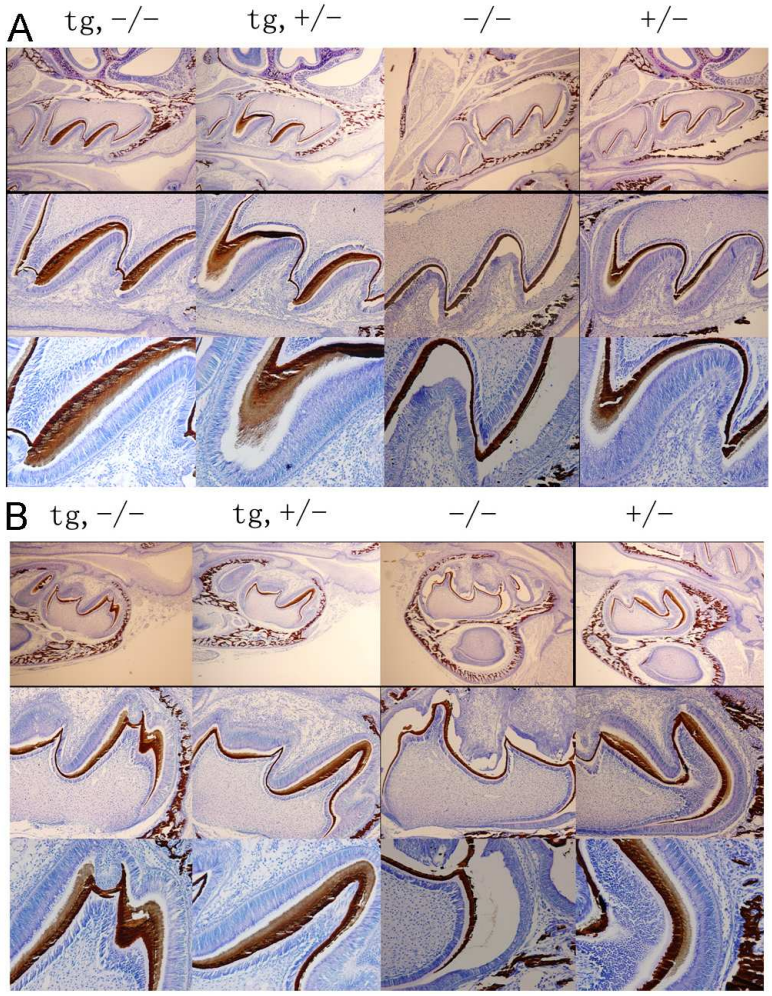

Fig 4.13 Secretory stage enamel formation of F2 offspring from transgenic mouse line 12. Von Kossa staining of day 4 molar sections from F2 offspring of line 12, upper molar (A) and lower molar (B). Upper row, 4x microscope; middle row, 10x microscope; lower row, 20x microscope. Genotype of these mice are: *Enam*$^{(tg,,-/-)}$(First column), *Enam*$^{(tg,,+/-)}$ (Second column); *Enam*$^{(-/-)}$ (third column) and *Enam*$^{(+/-)}$ (fourth column).

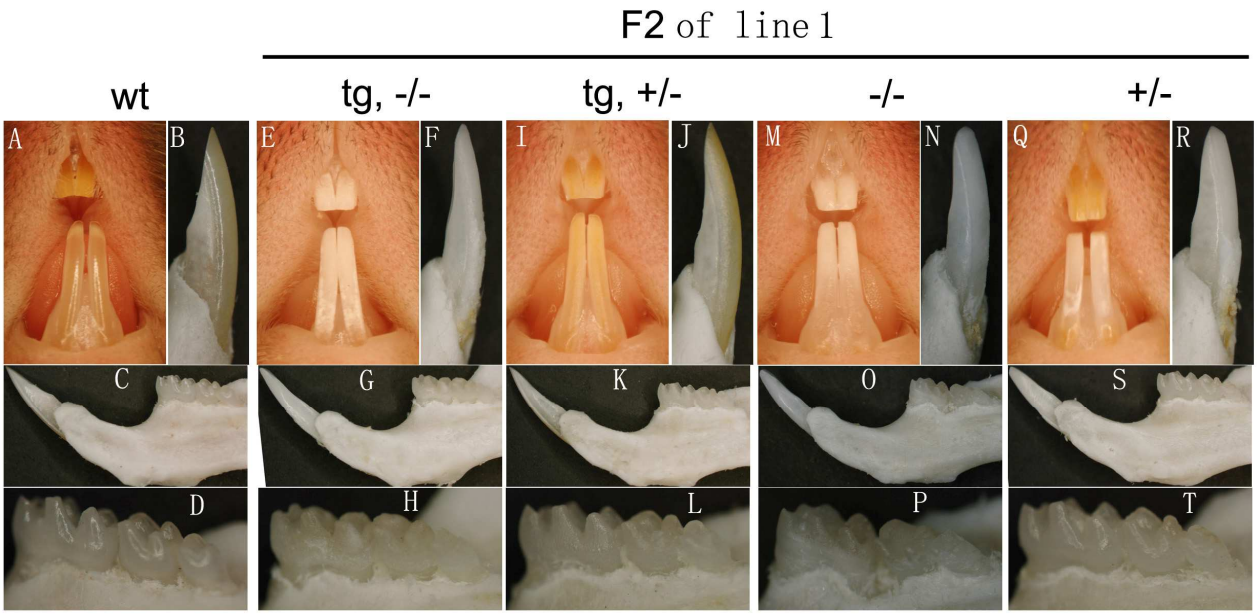

Fig 4.14 Oral photograph of F2 offspring from transgenic mouse line 1. Intraoral photographs of 7 weeks old mice of wild-type mouse (A-D), F2 offspring from transgenic line 1(E-T) are shown. Oral photograph of genotype *Enam*$^{(tg, -/-)}$ (E-H), *Enam*$^{(tg, +/-)}$ (I-L), *Enam*$^{(-/-)}$ (M-P) and *Enam*$^{(+/-)}$ (Q-T) are noted. These photographs include direct intraoral photograph (A, E, I, M, Q), distal view of lower incisor (B, F, J, N, R), mesial view of lower incisor and mandible (C, G, K, O, S) and mesial view of molars (D, H, L, P, T).

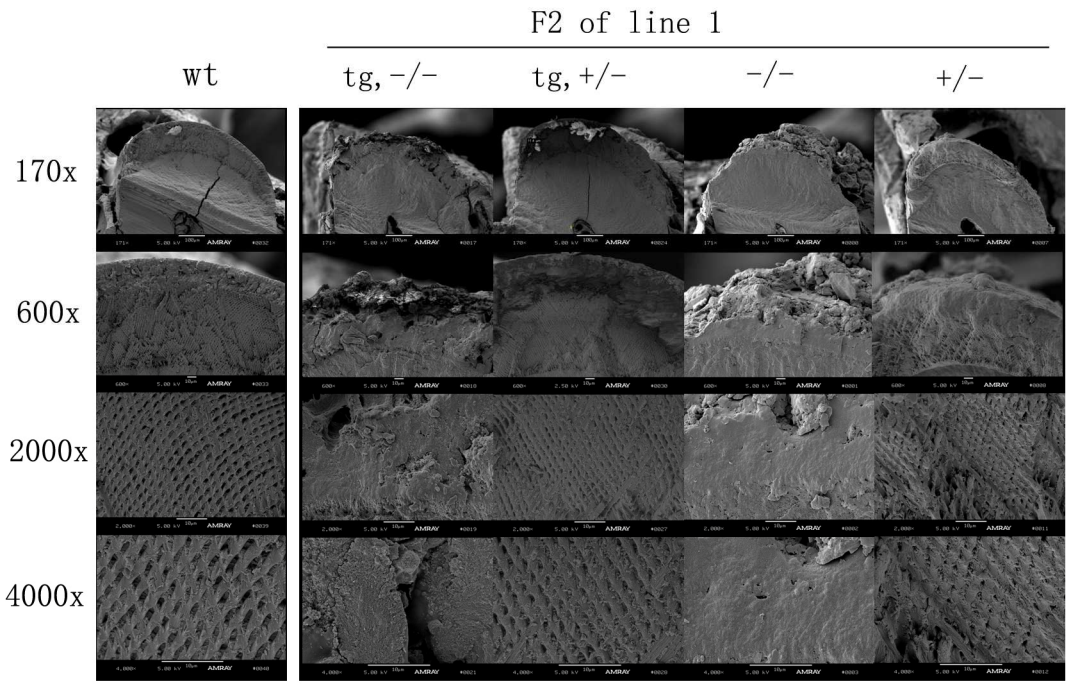

Fig 4.15 SEM analysis of F2 offspring of line 1: low magnification. Mandibular incisors from 7-week-old F2 offspring were cut at the level of labial alveolar crest for SEM evaluation. SEM results of F2 offspring from transgenic mouse line 1 (column 2-5) and wild-type control were shown (column 1) with whole incisor (row 1), enamel layer (row 2) and middle enamel (2000x in row 3 and 4,000x in row 4) are shown. Genotypes of groups are: wild-type (wt) (column 1), *Enam*$^{(tg, -/-)}$ (column 2), *Enam*$^{(tg, +/-)}$ (column 3), *Enam*$^{(-/-)}$ (column 4) and *Enam*$^{(+/-)}$ (column 5).

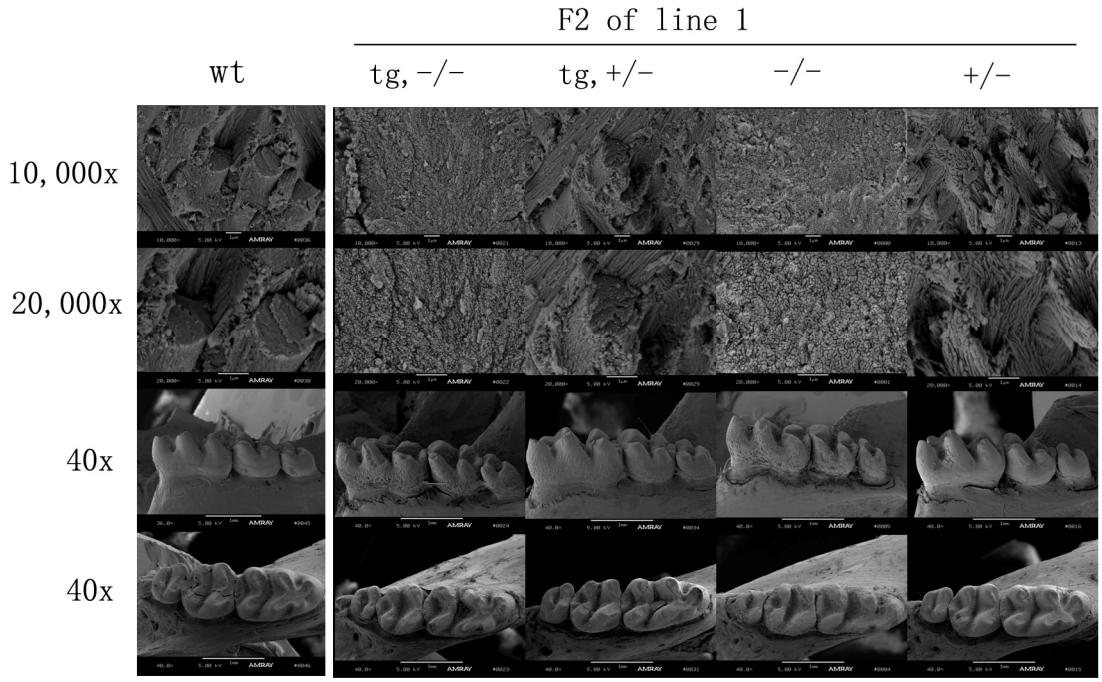

Fig 4.16 SEM analysis of F2 offspring of line 1: high magnification and molars. Mandibular incisors from 7-week-old F2 offspring were cut at the level of labial alveolar crest for SEM evaluation. SEM results of F2 offspring from transgenic mouse line 1 (column 2-5) and wild-type control (column 1) are shown. High magnification of enamel microstructure (10,000x in row 1, 20,000x in row 2) and the surface SEM of molars (mesial view in row 3, occlusal view in row 4) are shown. Genotypes of groups are: wild-type (wt) (column 1), *Enam*$^{(tg, -/-)}$ (column 2), *Enam*$^{(tg, +/-)}$ (column 3), *Enam*$^{(-/-)}$ (column 4) and *Enam*$^{(+/-)}$ (column 5).

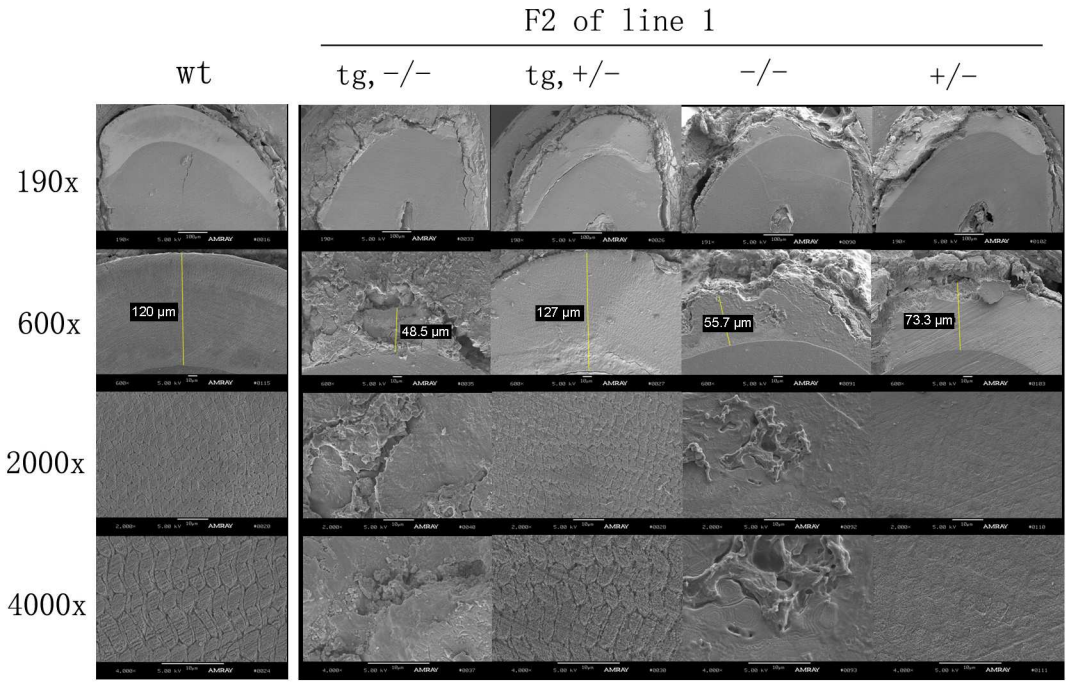

Fig 4.17 SEM analysis of F2 offspring of line 1 using polish and etch method. Mandibular incisors from 7-week-old F2 offspring were cut at the level of labial alveolar crest and processed for polish and etch for SEM evaluation to examine enamel thickness. SEM results of F2 offspring from transgenic mouse line 1 (column 2-5) and wild-type control were shown (column 1) with whole incisor (row 1), enamel layer (row 2) and middle enamel (2000x in row 3 and 4,000x in row 4) are shown. Genotypes of groups are: wild-type (wt) (column 1), *Enam*$^{(tg, -/-)}$ (column 2), *Enam*$^{(tg, +/-)}$ (column 3), *Enam*$^{(-/-)}$ (column 4) and *Enam*$^{(+/-)}$ (column 5).

References

Chen E, Yuan ZA, Wright JT, Hong SP, Li Y, Collier PM, et al. (2003). The small bovine amelogenin LRAP fails to rescue the amelogenin null phenotype. *Calcif Tissue Int* 73(5)*:*487-95.

Fincham AG, Moradian-Oldak J, Simmer JP (1999). The structural biology of the developing dental enamel matrix. *J Struct Biol* 126(3)*:*270-99.

Gibson CW, Yuan ZA, Hall B, Longenecker G, Chen E, Thyagarajan T, et al. (2001). Amelogenin-deficient mice display an amelogenesis imperfecta phenotype. *J Biol Chem* 276(34)*:*31871-5.

Gibson CW, Li Y, Daly B, Suggs C, Yuan ZA, Fong H, et al. (2009). The leucine-rich amelogenin peptide alters the amelogenin null enamel phenotype. *Cells Tissues Organs* 189(1-4)*:*169-74.

Houzelstein D, Cohen A, Buckingham ME, Robert B (1997). Insertional mutation of the mouse Msx1 homeobox gene by an nlacZ reporter gene. *Mech Dev* 65(1-2)*:*123-33.

Hu JC, Hu Y, Smith CE, McKee MD, Wright JT, Yamakoshi Y, et al. (2008). Enamel defects and ameloblast-specific expression in *Enam* knockout/lacz knock-in mice. *J Biol Chem* 283(16)*:*10858-71.

Li Y, Suggs C, Wright JT, Yuan ZA, Aragon M, Fong H, et al. (2008). Partial rescue of the amelogenin null dental enamel phenotype. *J Biol Chem* 283(22)*:*15056-62.

Lu Y, Ye L, Yu S, Zhang S, Xie Y, McKee MD, et al. (2007). Rescue of odontogenesis in Dmp1-deficient mice by targeted re-expression of DMP1 reveals roles for DMP1 in early odontogenesis and dentin apposition in vivo. *Dev Biol* 303(1)*:*191-201.

Pispa J, Jung HS, Jernvall J, Kettunen P, Mustonen T, Tabata MJ, et al. (1999). Cusp patterning defect in Tabby mouse teeth and its partial rescue by FGF. *Dev Biol* 216(2)*:*521-34.

Satokata I, Maas R (1994). Msx1 deficient mice exhibit cleft palate and abnormalities of craniofacial and tooth development. *Nat Genet* 6(4)*:*348-56.

Snead ML, Paine ML, Chen LS, Luo BY, Zhou DH, Lei YP, et al. (1996). The murine amelogenin promoter: developmentally regulated expression in transgenic animals. *Connect Tissue Res* 35(1-4)*:*41-7.

Snead ML, Paine ML, Luo W, Zhu DH, Yoshida B, Lei YP, et al. (1998). Transgene animal model for protein expression and accumulation into forming enamel. *Connect Tissue Res* 38(1-4)*:*279-86; discussion 295-303.

Termine JD, Belcourt AB, Miyamoto MS, Conn KM (1980). Properties of dissociatively extracted fetal tooth matrix proteins. II. Separation and purification of fetal bovine dentin phosphoprotein. *J Biol Chem* 255(20)*:*9769-72.

Tucker AS, Headon DJ, Courtney JM, Overbeek P, Sharpe PT (2004). The activation level of the TNF family receptor, Edar, determines cusp number and tooth number during tooth development. *Dev Biol* 268(1)*:*185-94.

Wen X, Zou Y, Luo W, Goldberg M, Moats R, Conti PS, et al. (2008). Biglycan over-expression on tooth enamel formation in transgenic mice. *Anat Rec (Hoboken)* 291(10)*:*1246-53.

Ye L, MacDougall M, Zhang S, Xie Y, Zhang J, Li Z, et al. (2004). Deletion of dentin matrix protein-1 leads to a partial failure of maturation of predentin into dentin, hypomineralization, and expanded cavities of pulp and root canal during postnatal tooth development. *J Biol Chem* 279(18)*:*19141-8.

Zhao X, Zhang Z, Song Y, Zhang X, Zhang Y, Hu Y, et al. (2000). Transgenically ectopic expression of Bmp4 to the Msx1 mutant dental mesenchyme restores downstream gene expression but represses Shh and Bmp2 in the enamel knot of wild-type tooth germ. *Mech Dev* 99(1-2)*:*29-38.

Chapter V

OVER-EXPRESSION OF ENAMELIN CAUSES ENAMEL DEFECTS AND IS DOSAGE DEPENDENT

Abstract

In *Enam* null mice the mineralization front associated with the secretory surface of the ameloblast membrane fails to initiate and elongate enamel mineral ribbons. True enamel was not formed in *Enam* null mice. While the phenotype of enamelin loss-of-function *in vivo* is clearly described in the enamelin null mouse study, no report has shown what happens when the enamelin is over-expressed *in vivo* yet. We established enamelin transgenic mouse lines using the amelogenin promoter. In these transgenic mouse lines, the enamel expression level varies. We show here when over-expression of enamelin is in median level (around one and half times as much as endogenous enamelin), enamel surface start to lose its smoothness, the enamel surface has some round protrusive structures. When the over-expression of enamelin is in a high level (around five times as much as endogenous enamelin), the enamel layer is almost lost: the teeth look chalky and white on oral photographs. Scanning electron microscopy showed the enamel portion underneath the protrusive structure on the surface (roughness on enamel surface) start to

lose its rod-interrod decussation pattern. The higher the level of enamelin over-expression, the more decussation pattern of the enamel is lost. On micro-CT analysis, mineral content of enamel layer decreased in the enamelin transgenic mouse compared to wild-type mice. We then concluded that enamelin expression level is critical for proper enamel formation. Over-expression of enamelin *in vivo* caused defective enamel phenotype, the severity of defects is correlated with the level of enamelin over-expression.

Introduction

Mature enamel crystallites are about 70 nm wide and 30 nm thick, and organized into bundles called enamel rods (prisms), with about 10,000 parallel crystals in a rod (Daculsi and Kerebel, 1978; Nanci, 2003). Each rod is made by one ameloblast cell, the cell type which is responsible of secreting enamel matrix and orchestrating enamel formation (Nanci, 2003). Enamel crystals grow primarily in length in secretory stage. As the crystals extend, the enamel layer expands. Because enamel crystals grow longer at this mineralization front, the ameloblasts retreat away from the growing tooth.

Studies of enamelin null (*Enam*$^{-/-}$) mice showed that the teeth of homozygous mouse look chalky and white and no enamel layer is present, while in heterozygous mice, the upper incisors look close to normal, and lower incisors look chalky and white. Histological sections of one week old developing enamel showed there is no mineralization in the enamel layer at the secretory surface of the ameloblast (Hu et al., 2008).

While the phenotype of a tooth when lacking enamelin is clearly described in the enamelin null mice study, no report has shown what happens when the enamelin is

overexpressed *in vivo*. Over-expressing a gene in a tissue specific manner is an effective approach to investigate the role a protein in the context of a developing animal. We targeted enamelin over-expression to ameloblasts by generating transgenic animals in which enamelin expression was under the control of the ameloblast-specific amelogenin promoter. Amelogenin is the most abundant protein in developing enamel (Fincham et al., 1999b). The mouse amelogenin (*AmelX*) 5' transcriptional regulatory region has been successfully used to drive transgenic expression specifically in ameloblasts (Snead et al., 1996; Snead et al., 1998b; Wen et al., 2008b). In this study, we characterized the dental enamel phenotype of these transgenic mice and found over-expression of enamelin causes defects on enamel formation and this effect is dose dependent.

Materials and Methods

Oral photographs. Similar as previously described in Chapter 4, oral photographs of teeth were taken using Nikon DIGITAL CAMERA DXM1200 combined with microscope. As showed in Fig5.2 A, for each sample, intraoral picture of upper and lower incisors in the head with skin(0.8x), labial view of lower incisor (2x), mesial view of lower mandible (1.3x) and mesial view of lower molars (3x) were taken as noted magnification. Labial view of lower incisor with increased magnification (2x, 3x, 4x, 6x, 8x individually) were also taken (Fig 5.2B).

Assessing *Enam* transgene expression level by real-time PCR. The material and method for real-time PCR experiment was described in detail in Chapter 3. To further explain the data in this chapter, Table 5.1 and 5.2 was generated. For "*Enam*" primer, all

the wild-type animal relative expression levels were averaged (column 3 in Table 5.1). All the fold change numbers were divided by this average number to make the wild-type animal enamelin expression levels in each transgenic line close to 1, so it is easier to compare the transgenic animal enamelin expression levels with wild-type animal groups. In other words, for each comparison, fold change were assessed relative to the expression level of the wild-type animal which was set as 1.

Assessing *Enam* transgene expression level by Western blotting. The material and method of Western-blotting was described in detail in chapter 3. From each transgenic mouse line, littermates of the offspring from enamelin transgenic mouse breed with C57BL/6 wild-type mouse were divided into two groups after genotyping: wild-type group and transgene positive group. Sample from all genotypes were loaded on SDS-PAGE, wild-type animals (wt1-wt4) first followed by transgenic animals (tg1-tg5) (Fig5.1 D, E, F).

Micro-computed tomography. Mouse hemimandibles were imaged using a cone-beam micro-computed tomography (μCT) system (eXplore Locus SP, Amersham Biosciences Pre-Clinical Imaging, London, Ontario, Canada) in the Orthopaedic Research Laboratory at the University of Michigan Department of Orthopaedic Surgery, as described previously (Park et al., 2007). In brief, hemimandibles were exposed to polychromatic x-rays on a rotating stage. Measurements were taken at an operating voltage of 80 kV and 80 mA of current, with an exposure time of 1600ms. The effective voxel size of the reconstructed image was 18 ×18 × 18 μm^3.

Results

Gene expression levels in enamelin transgenic mice. The transgene expression levels vary in different transgenic lines. Here we show three transgenic mouse lines which have different enamelin expression level. Line 12 have the lowest enamelin expression level among these three, with around 130% of enamelin expression in the transgenic mouse compared with wild-type littermates; line 2 have the middle expression level, with around 150% of enamelin expressed in transgenic mouse; line 3 have the highest expression, have as much as five times enamelin expressed in transgenic mouse as in wild-type littermates (Fig 5.1 A and Table 5.1 last column). When using the real-time PCR primer set which detects only enamelin transgene, the result correlates well to the result of enamelin primer in Fig 5.1 A. That is, the enamelin expression level from low to high in line 12, 2 and 3 (Fig 5.1 B) was determined to be accurate. On protein level, it is consistent that the transgenic mice have higher enamelin expression than wild-type littermates in line 12 and 2 (Fig 5.1 C, D). This confirms that our strategy to establish enamelin over-expression transgenic mouse line is working and we have a range of enamelin over-expression *in vivo*.

Phenotype of enamelin transgenic mouse. Seven weeks old enamelin transgenic mouse and wild-type controls were oral-photographed. On the intraoral photograph for this three transgenic mouse lines, line 12 and 2 show some roughness (not smooth and shiny) on the surface of incisor (e and i in Fig 5.2A individually), while line 3 has incisor appear chalky and white (m in Fig 5.2A), similar to the phenotype of enamelin null mice (Hu et

al., 2008). The wild-type mouse incisors have yellowish and smooth surface (a in Fig 5.2A). The roughness of the enamel surface on the incisors of transgenic mouse line 12 and 2 can also be seen on the distal view of lower incisors (f and j in Fig 5.2A individually). For line 3, most enamel is lost, leaving the dentin exposed but sometimes, a little chalky rough materials left on top of dentin (n in Fig 5.2A). The surface roughness is associated with round, protrusive bumps which are hard and cannot be removed by hand instruments. From the mesial view of mandible, the enamel layer can be seen in line 12 (g in Fig 5.2A) and line 2 (k in Fig 5.2A) incisors, similar to the enamel layer in wild-type controls (c in Fig 5.2A). Transgenic mice of line 2 have more protrusive bumps than line 12, it can be seen even on the mesial view of mandible (k in Fig 5.2A). But for line 3, no enamel layer is seen on the mesial view of lower incisor (o in Fig 3.2A). Molars of line 12 look similar to that of the wild-type mouse (h in Fig 5.2A); molar of line 2 seems to have some roughness on the surface (l in Fig 5.2A), not as smooth and shiny as wild-type molars (d in Fig 5.2A); molars of line 3 are smaller and do not seem to have enamel layer or have a very thin enamel layer (p in Fig 5.2A). Under higher magnification of the lower incisor surface, we can clearly see the round, protrusive structure on the enamel surface of transgenic mouse line 12 (f-j in Fig 5.2B) and line 2 (k-o in Fig 5.2B), with line 2 having a severer presentation. The protrusive structure in line 2 is slightly larger than in line 12 and the texture seem to change a bit, because some bumps look whiter and chalkier than the others. While in line 3, covering most of the exposed dentin surface is sporadic chalky white material, which is similar but not identical to the protrusive bumps observed in line 2 and 12 (p-t in Fig 5.2B).

On the surface SEM (scanning electron microscopy) analysis, we can clearly see the round protrusive structures of enamel on enamel surface of lower incisors in line 12 (e-h in Fig 5.3) and line 2 (i-l in Fig 5.3), compare with a smooth enamel surface for wild-type control animals (a-d in Fig 5.3).

Enamel microstructure in enamelin transgenic mice. On the SEM photos of fractured surface, we can examine the micro-structures of enamel in the enamelin transgenic mice. Transgenic mice from line 12 and 2 still have an enamel layer as shown in SEM (Fig 5.4B and C individually), while line 3 loses its enamel layer (Fig5.4 D). The rod-interrod decussation of enamel in wild-type mouse is shown (Fig 5.4 A, E, F, G). Most parts of enamel layer from enamelin transgenic mouse founder line 12 have similar decussating pattern as wild-type (a, b, c in Fig 5.5 A), however, where there are protrusive bumps on the surface of enamel, the underneath enamel start to lose its decussating pattern (g, h, i in Fig 5.5 A). There are areas that the enamel has not completely lost its decussation pattern, the crystallite seems to have difficulty in forming bundle-like structures, but only in a longitudinal dimension. It seems only rod-like structures is there, but not much interrod-like structures present (d, e, f in Fig 5.5 A). Transgenic mice from line 2 still have an enamel layer, but most part of the enamel has lost its decussating pattern (d, e, f in Fig 5.5 B). Small portion of enamel has a decussating pattern (a, b, c in Fig 5.5 B), similar to the wild-type mouse. Enamel structure of the protrusive bumps has the long crystallite-like structures (g, h, i in Fig 5.5 B). Transgenic mouse from line 3 almost lost its enamel layer. The decussating pattern of enamel is gone. Some areas of the enamel layer where some protrusive bumps are located contain crystallite-like structure (a, b, c in Fig 5.5 C), some

other areas just have a thin layer of amorphous material on the dentin surface (d, e, f in Fig 5.5 C), similar to what we have seen on enamelin null mice (Hu et al., 2008).

Micro-computed tomographic analysis of enamel in enamelin transgenic mice. Seven weeks old transgenic mice and wild-type control mice were also used for micro-CT analysis to evaluate mineral content of the dental enamel. Sagittal sections through the incisor (Fig.5.6 B, F, J) showed strong contrast between enamel and dentin in both the wild-type enamelin transgenic mice. The three-dimensional micro-computed tomography reconstructions of the hemimandibles using a low arbitrary density demarcation displayed the entire mandible (Fig.5.6 A, E, I). Similar reconstructions were made using an arbitrary density demarcation that eliminated all of the dentin and bone of the wild-type hemimandibles but displayed the entire enamel layer of the molars and the maturation stage enamel of the incisors (Fig. 5.6 D, H, L). On pictures of the two-dimensional sagittal section of incisors (Fig 5.6 B, F, J), and pictures of the three-dimensional outline of the hemimandibles (Fig 5.6 A, E, I), the protrusive structure on the incisor surface from line 2 can be seen (Fig 5.6 I, J), while line 12 (Fig 5.6 E, F) transgenic mouse has a similar profile as wild-type mice (Fig 5.6 A, B). On the three-dimensional image which shows only the enamel layer of molars and maturation stage enamel of the incisors, the mineral density of the maturation incisors from line 2 mice (Fig 5.6 K and L) is obviously decreased than that of the line 12 (Fig 5.6 G and H) and wild-type mice (Fig 5.6 C and D). The mineral density of the maturation incisor of line 12 (Fig 5.6 G and H) does not have an obvious difference when compared to that of the wild-type animals.

Discussion

This is the first study that shows over-expression of enamelin resulting in the formation of round and hard protrusive structures on the enamel surface. Transgenic mouse line 2 has more of these protrusive structures on the incisor surface than transgenic mouse line 12. Since line 2 has a slightly higher enamelin expression than line 12, we suspect that this defect of enamel may be dose-dependent. When enamelin expression level is too high, like in transgenic line 3 (more than five times as much as wild-type enamelin), the enamel formation is completely disrupted. The enamel layer is almost all lost in this transgenic line. The fact that wherever there are protrusive structures on the surface of enamel, the underlying enamel also lost its rod-interrod decussation pattern is quite interesting. The crystallites in these areas seem to have a longitudinal dimension extending from the dentino-enamel junction to the outer-enamel portion. It seems that the enamel crystals have the tendency to grow too long, instead of assuming the rod-interrod pattern. In transgenic mouse line 12, enamel in areas between the “good” and “bad” enamel, has crystallite attempted to form bundles of rods, but the interrod-like structure was lacking (Fig 5.5 A, d, e, f). We have learned from a previous study that ameloblastin over-expression caused interrod enamel to dominate the enamel structure, with the crystallites of interrod enamel growing longer in ameloblastin transgenic mice than in the wild-type (Paine et al., 2003). This is just opposite to the result of our study. Our data indicates that in enamelin null mice and enamelin heterozygous mice, where enamelin expression is decreased or obliterated, the ameloblastin expression level is also decreased. We also know that in the secretory stage pig tooth, immunostaining showed ameloblastin fragments was localized to a honeycomb pattern and enamelin was expressed in a reverse

honeycomb pattern (Uchida et al., 1991b). Enamelin is expressed in the enamel rod area and ameloblastin is expressed in the interrod area. Taking these pieces of evidence together, I hypothesized that during secretory stage enamel formation, enamelin and ameloblastin play a role in the rod and interrod structure formation separately. The expression level of these two proteins was maintained by ameloblasts in a specific manner. When enamelin expression level is low, the cells try to make less ameloblastin as well and try to maintain the proportional expression of these two proteins to sustain a rod-interrod decussating pattern. When the proportional expression level of these two proteins was disrupted as in the enamelin transgenic mice and ameloblastin transgenic mice, the ameloblasts begin to fail to make enamel in a rod-interrod decussating pattern. In enamelin over-expression transgenic mouse, the median level of over-expression cause protrusive structures on the enamel surface, probably because the enamel rod structure to grow faster and longer than the interrods of enamel. When the enamelin over-expression is too high as in transgenic mouse line 3, the ameloblasts fail to make proper enamel. More detailed experimental design is needed to test this hypothesis. But this study is the first to provide information about the defective enamel phenotype of enamelin over-expression *in vivo* supporting this hypothesis of enamel formation: the enamelin plays a role in enamel rod formation while ameloblastin plays a role in the interrod formation in the secretory stage amelogenisis; ameloblasts maintain the expression level of enamelin and ameloblastin in a specific manner to maintain the rod-interrod decussating pattern of enamel formation.

Figures and Legends

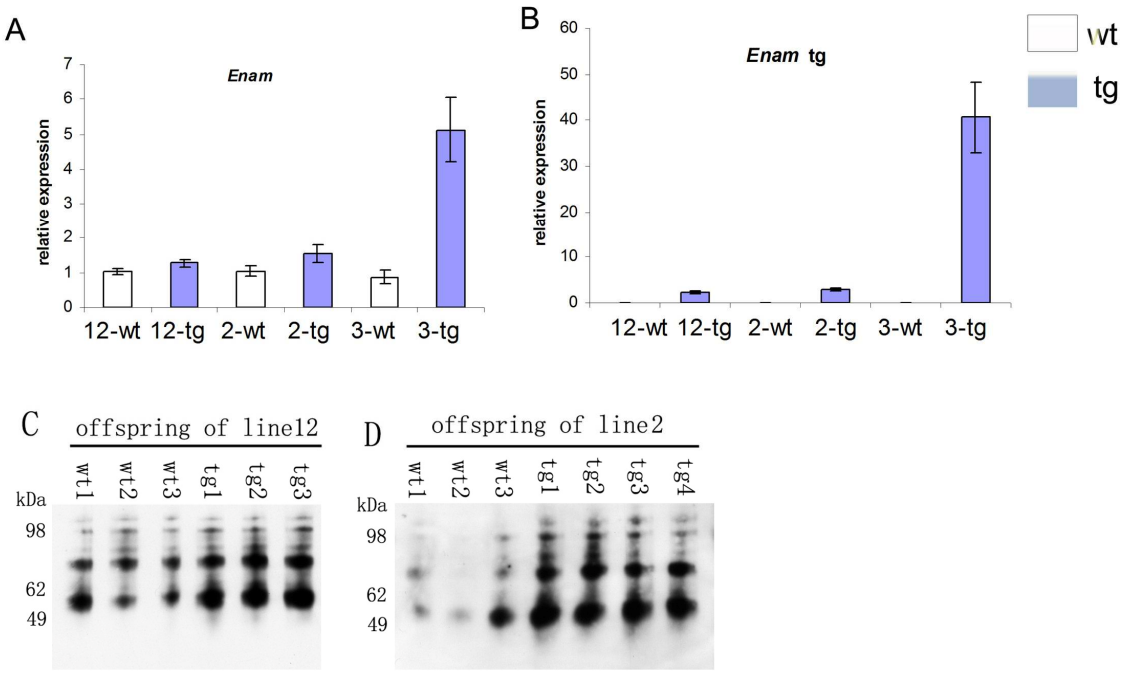

Fig 5.1 Enamelin expression level in transgenic mouse. Enamelin expression level is tested in three transgenic mouse line on both mRNA (A and B) expression and protein level (C, D, E). Day 5 first molars were extracted from offspring of enamelin transgenic mice breeding with C57BL6 wild-type mice. From each transgenic line, littermates were divided into two groups: transgene positive (tg) group and transgene negative (wt) group. One upper and one lower first molar from each animal were used to isolate mRNA. The other upper and lower first molars were used to isolate protein. *Enam* primer detects both endogenous enamelin and transgenic enamelin. "*Enam* tg" primer detects only enamelin from transgene. For real-time PCR analysis, animal numbers in each group are as follow: n(12-wt)=3, n(12-tg)=3, n(2-wt)=5, n(2-tg)=4, n(3-wt)=3, n(3-tg)=5. **A:** Enamelin (detects both endogenous enamelin and enamelin from transgene) expression level in wild-type mouse and transgenic littermates from three transgenic lines. **B:** Enamelin transgene (only from transgene, not endogenous enamelin) expression level in transgenic mice and wild-type mice groups from six transgenic lines. **C, D:** Western-blots immunostained using an antibody raised against mouse enamelin peptide starting at residue 223. Equal fractions of enamel proteins extracted from day 5 upper and lower first molars from *Enam* wild-type mice (lanes *wt1* to *wt3*) group and *Enam* transgenic mice group (lanes *tg1* to *tg5*) from littermates were loaded on SDS-PAGE gel. Enamelin expression levels from transgenic mice line 12 (C), line 2 (D) is shown.

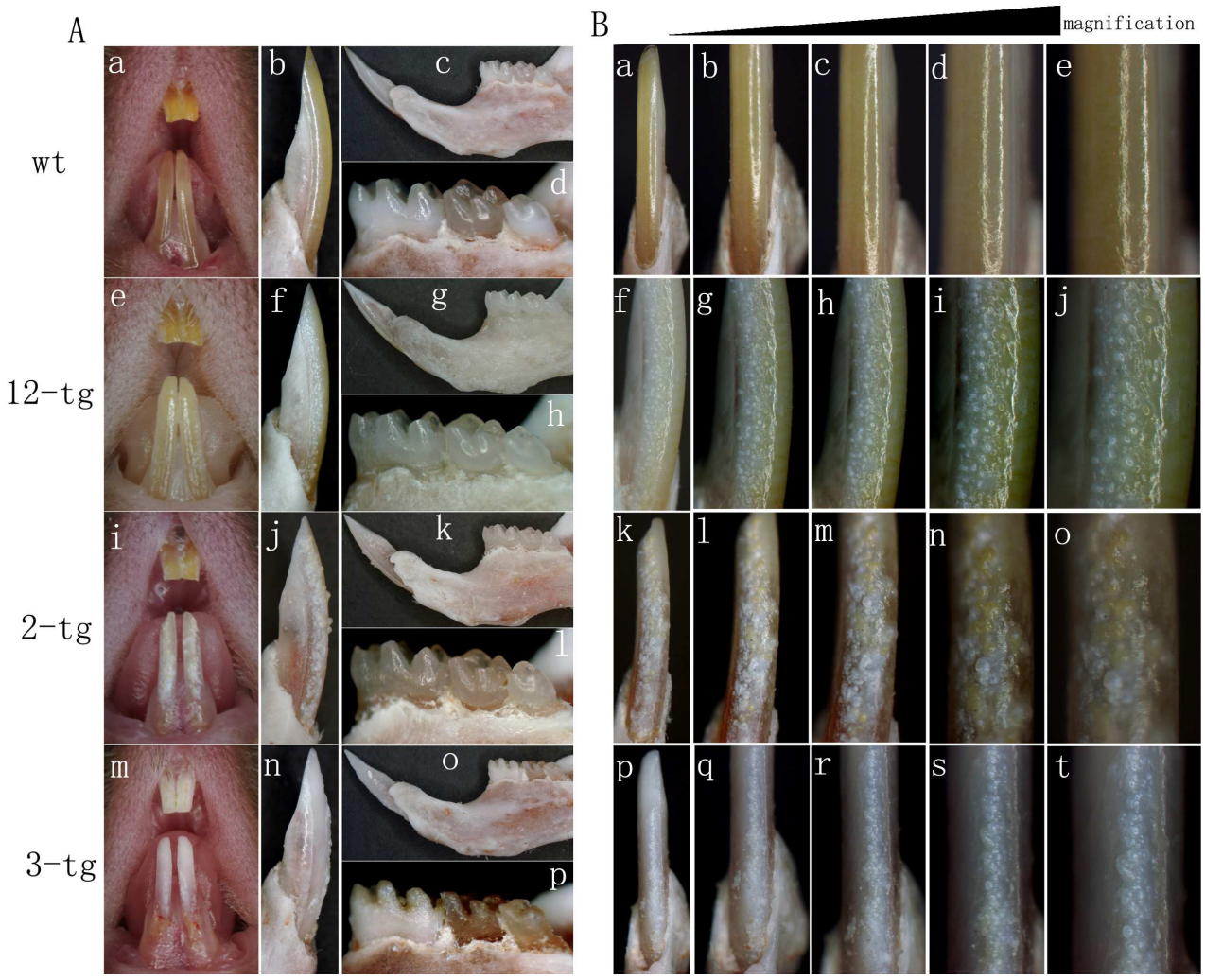

Fig 5.2 Oral photograph of enamelin transgenic mouse. A: Intraoral photographs of 7 weeks old mice of wild-type mouse (a-d), offspring from transgenic line 12 (e-h), line 2 (i-l) and line 3(m-p) are shown. These photographs includes direct intraoral photograph (a, e, i, m), distal view of lower incisor (b, f, j, n), mesial view of lower incisor and mandible (c, g, k, o) and mesial view of molars (d, h, l, p). **B:** Labial view of lower incisor from mice showed in A, i.e., wild-type mouse (a-e), offspring from transgenic line 12 (f-j), line 2 (k-o) and line 3(p-t). In each row, the magnification is increased from left to right, 2x (a, f, k, p), 3x (b, g, l, q), 4x (c, h, m, r), 6x (d, i, n, s) and 8x (e, j, o, t).

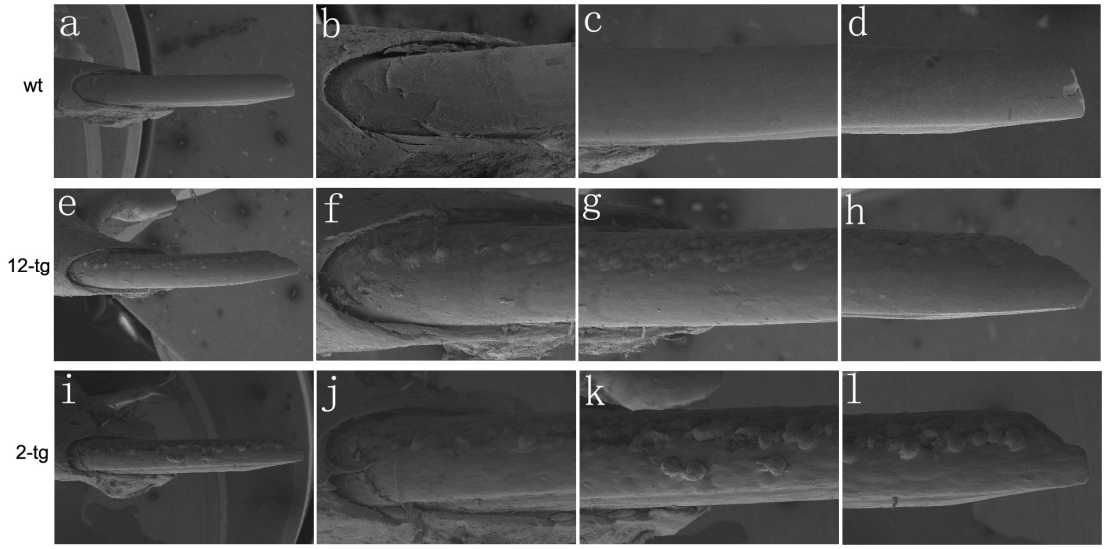

Fig 5.3 SEM analysis of incisor surface. Surface SEM is examined to show the roughness (protrusive structure) of enamel from transgenic mouse line 12(e-h) and line 2 (i-l) compare to the smooth enamel in wild-type mouse (a-d). Enamel surface of the lower incisor (a, e, i), at apical third of lower incisor (b, f, j), middle third of lower incisor (c, g, k) and incisal third of lower incisor (d, h, l) are shown.

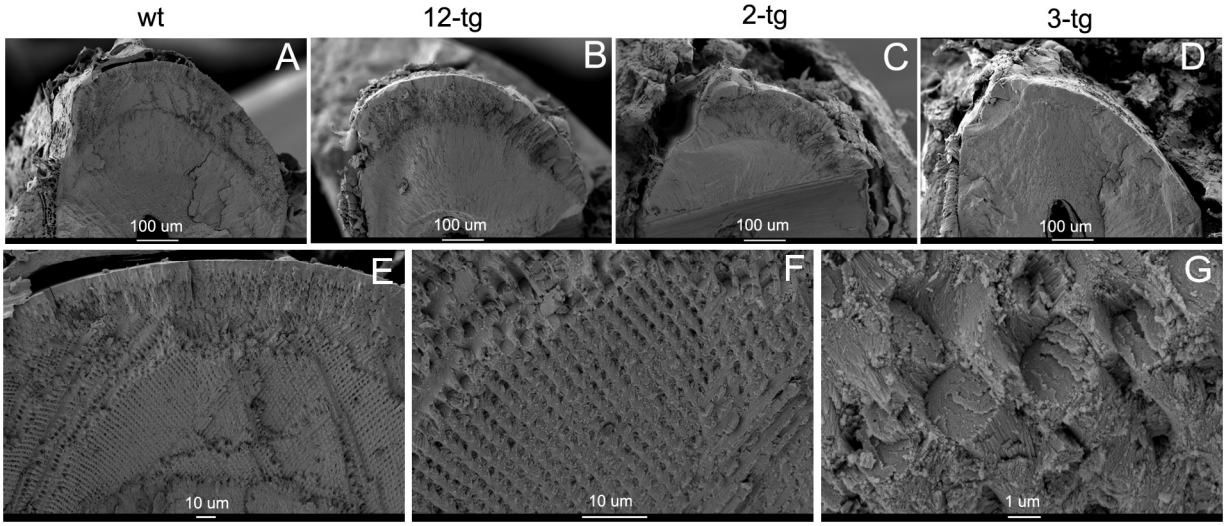

Fig 5.4 SEM analysis of the wild-type and enamelin transgenic mice. Seven weeks old mice were used for SEM (Scanning Electron Microscopy) analysis. Whole enamel from wild-type mouse (A), offspring from enamelin transgenic mouse line 12(B), line 2 (C) and line 3 (D) is shown. Enamel decussation pattern for wild-type mouse is also shown at the magnification of 600x (E), 2000x (F) and 10,000x (G).

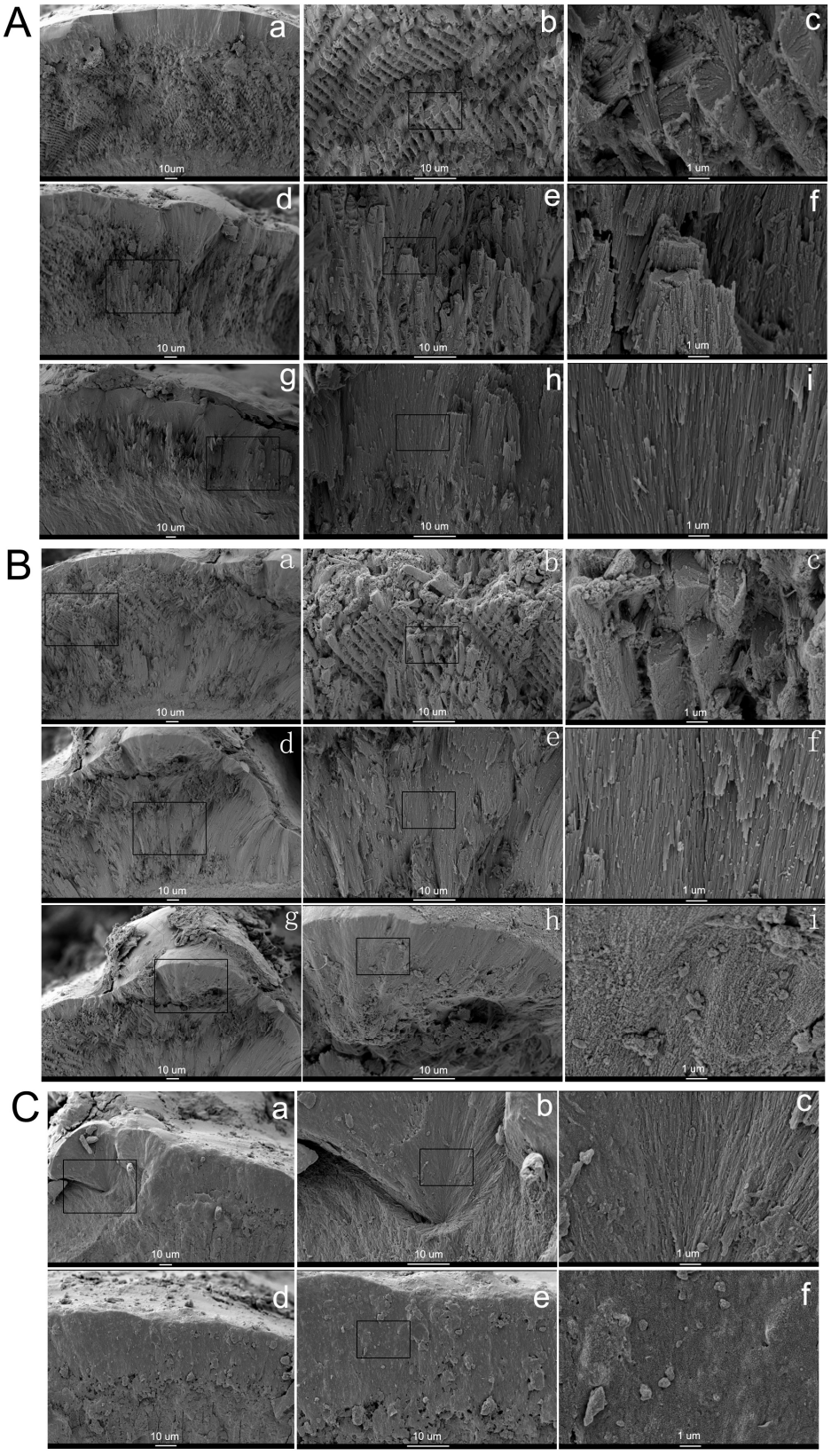
A
a
10um
b
10 um
c
1 um
d
10 um
e
10 um
f
1 um
g
10 um
h
10 um
i
1 um
B
a
10 um
b
10 um
c
1 um
d
10 um
e
10 um
f
1 um
g
10 um
h
10 um
i
1 um
C
a
10 um
b
10 um
c
1 um
d
10 um
e
10 um
f
1 um

Fig 5.5 SEM analysis of enamelin transgenic mouse line 12, 2 and 3. Detailed structure of enamel is shown for offspring from enamelin transgenic mouse line 12 (A), line 2 (B) and line 3(C) by SEM. **A:** Most parts of enamel layer from enamelin transgenic mouse founder line 12 have similar decussation pattern as wild-type (600x in a, 2000x in b and 10,000x in c), while where there are protrusive bumps on the surface of enamel, the underneath middle enamel start to lose its decussation pattern (600x in g, 2000x in h and 10,000x in i). There are areas that the enamel has not completely lost its decussation pattern (600x in d, 2000x in e and 10,000x in f). **B:** Transgenic mouse from line 2 still have an enamel layer, but most part of the enamel lost its decussation pattern (600x in d, 2000x in e and 10,000x in f). Small portion of enamel has a decussation pattern (600x in a, 2000x in b and 10,000x in c) similar as wild-type mouse. Enamel structure of the protrusive area is also shown (600x in g, 2000x in h and 10,000x in i). **C:** Transgenic mouse from line 3 almost lost its enamel layer. The decussation pattern of enamel is gone. Some area of enamel layer where protrusive bumps are located has some crystallite-like structure (600x in a, 2000x in b and 10,000x in c), some other areas just have a thin layer of material on the dentin surface (600x in d, 2000x in e and 10,000x in f).

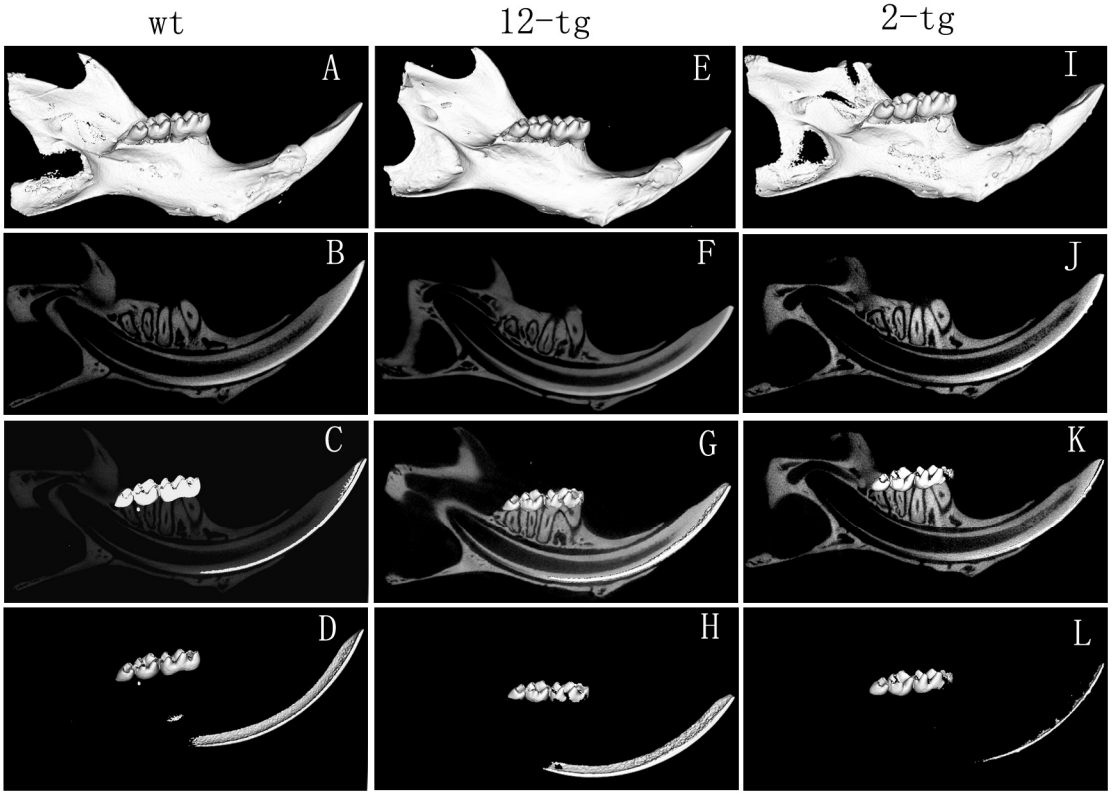

Fig.5.6 uCT analysis of enamelin transgenic mice. Mandibles from 7-week old mouse were used for micro-CT analysis of wild-type group (A-D), transgenic mouse line 12 (E-H) and line 2 (I-L). For every group of mice, 3-dimensional mandible (A, E, I), 2-dimensional incisors (B, F, J), 2-dimensional incisors plus 3-dimensional enamel (C, G, K) and 3-dimensional enamel only (D, H, L) are shown.

Table 5.1 Raw data from real-time PCR experiment plotted for Fig 5.1 A

samples	*Enam* fold change	wt expression average	*Enam* expression/avg wt	average	Standard deviation	Ratio of tg/wt
12-wt 1	**1.9652421**	(12-wt1 + 12-wt2 + 12-wt3 + 2-wt1 + 2-wt2 + 2-wt3 + 2-wt4 + 2-wt5 + 3-wt1+3-wt2+3-wt3)/11= 1.757389	1.118273814			
12-wt 2	**1.862622**		1.059880311			
12-wt 3	**1.6741447**		0.952631831	1.043595	0.084013	
12-tg 1	**2.2988266**		1.308092062			
12-tg 2	**2.4089127**		1.370733913			
12-tg 3	**2.0338578**		1.15731793	1.278715	0.109699	1.225297
2-wt 1	**1.6792271**		0.955523848			
2-wt 2	**1.8291224**		1.040818168			
2-wt 3	**1.7073953**		0.971552286			
2-wt 4	**2.2538085**		1.282475593			
2-wt 5	**1.7364913**		0.988108666	1.047696	0.135105	
2-tg 1	**3.3050502**		1.880659433			
2-tg 2	**2.6437149**		1.504342465			
2-tg 3	**2.7218759**		1.548818105			
2-tg 4	**2.149491**		1.223116225	1.539234	0.269451	1.469161
3-wt 1	**1.9401212**		1.103979369			
3-wt 2	**1.3773149**		0.783727962			
3-wt 3	**1.3057891**		0.743027924	0.876912	0.197696	
3-tg 1	**7.274665**		4.139473389			
3-tg 2	**9.1700262**		5.217983156			
3-tg 3	**8.9793776**		5.109499149			
3-tg 4	**8.0136903**		4.559997986			
3-tg 5	**11.605036**		6.603566996	5.126104	0.933479	5.845633

Table 5.2 Raw data from real-time PCR experiment plotted for Fig 5.1 B

samples	*Enam* TG fold change	average	Standard deviation
12-wt 1	**3.21E-06**		
12-wt 2	**8.02E-07**		
12-wt 3	**6.04E-07**	1.54E-06	1.45E-06
12-tg 1	**1.838011565**		
12-tg 2	**2.764589055**		
12-tg 3	**2.288000472**	2.296867031	0.463352
2-wt 1	**1.59E-06**		
2-wt 2	**4.15E-06**		
2-wt 3	**1.48E-06**		
2-wt 4	**7.65E-06**		
2-wt 5	**4.78E-06**	3.93E-06	2.55E-06
2-tg 1	**3.361381845**		
2-tg 2	**2.799421227**		
2-tg 3	**3.353104467**		
2-tg 4	**2.76306158**	3.06924228	0.332903
3-wt 1	**3.48E-06**		
3-wt 2	**4.88E-06**		
3-wt 3	**0.000319356**	1.09E-04	0.000182
3-tg 1	**38.00715029**		
3-tg 2	**34.16794541**		
3-tg 3	**39.7676823**		
3-tg 4	**37.62824166**		
3-tg 5	**53.99287086**	40.7127781	7.696163

References

Daculsi G, Kerebel B (1978). High-resolution electron microscope study of human enamel crystallites: size, shape, and growth. *J Ultrastruct Res* 65(2)*:*163-72.

Fincham AG, Moradian-Oldak J, Simmer JP (1999). The structural biology of the developing dental enamel matrix. *J Struct Biol* 126(3)*:*270-99.

Fukumoto S, Kiba T, Hall B, Iehara N, Nakamura T, Longenecker G, et al. (2004). Ameloblastin is a cell adhesion molecule required for maintaining the differentiation state of ameloblasts. *J Cell Biol* 167(5)*:*973-83.

Gibson CW, Yuan ZA, Hall B, Longenecker G, Chen E, Thyagarajan T, et al. (2001). Amelogenin-deficient mice display an amelogenesis imperfecta phenotype. *J Biol Chem* 276(34)*:*31871-5.

Hu CC, Simmer JP, Bartlett JD, Qian Q, Zhang C, Ryu OH, et al. (1998). Murine enamelin: cDNA and derived protein sequences. *Connect Tissue Res* 39(1-3)*:*47-61; discussion 63-7.

Hu JC, Zhang CH, Yang Y, Karrman-Mardh C, Forsman-Semb K, Simmer JP (2001). Cloning and characterization of the mouse and human enamelin genes. *J Dent Res* 80(3)*:*898-902.

Hu JC, Hu Y, Smith CE, McKee MD, Wright JT, Yamakoshi Y, et al. (2008). Enamel defects and ameloblast-specific expression in *Enam* knockout/lacz knock-in mice. *J Biol Chem* 283(16)*:*10858-71.

Kallenbach E (1971). Electron microscopy of the differentiating rat incisor ameloblast. *J Ultrastruct Res* 35(5)*:*508-31.

Karrman C, Backman B, Dixon M, Holmgren G, Forsman K (1997). Mapping of the locus for autosomal dominant amelogenesis imperfecta (AIH2) to a 4-Mb YAC contig on chromosome 4q11-q21. *Genomics* 39(2)*:*164-70.

Margolis HC, Beniash E, Fowler CE (2006). Role of macromolecular assembly of enamel matrix proteins in enamel formation. *J Dent Res* 85(9)*:*775-93.

Nagano T, Oida S, Ando H, Gomi K, Arai T, Fukae M (2003). Relative levels of mRNA encoding enamel proteins in enamel organ epithelia and odontoblasts. *J Dent Res* 82(12)*:*982-6.

Nanci N (2003). Ten Cate's Oral Histology: Development, Structure, and Function. 6th edition).

Paine ML, Wang HJ, Luo W, Krebsbach PH, Snead ML (2003). A transgenic animal model resembling amelogenesis imperfecta related to ameloblastin over-expression. *J Biol Chem* 278(21)*:*19447-52.

Park CH, Abramson ZR, Taba M, Jr., Jin Q, Chang J, Kreider JM, et al. (2007). Three-dimensional micro-computed tomographic imaging of alveolar bone in experimental bone loss or repair. *J Periodontol* 78(2)*:*273-81.

Rajpar MH, Harley K, Laing C, Davies RM, Dixon MJ (2001). Mutation of the gene encoding the enamel-specific protein, enamelin, causes autosomal-dominant amelogenesis imperfecta. *Hum Mol Genet* 10(16)*:*1673-7.

Reith EJ (1970). The stages of amelogenesis as observed in molar teeth of young rats. *J Ultrastruct Res* 30(1)*:*111-51.

Ronnholm E (1962). The amelogenesis of human teeth as revealed by electron microscopy. II. The development of the enamel crystallites. *J Ultrastruct Res* 6(249-303.

Snead ML, Paine ML, Chen LS, Luo BY, Zhou DH, Lei YP, et al. (1996). The murine amelogenin promoter: developmentally regulated expression in transgenic animals. *Connect Tissue Res* 35(1-4)*:*41-7.

Snead ML, Paine ML, Luo W, Zhu DH, Yoshida B, Lei YP, et al. (1998). Transgene animal model for protein expression and accumulation into forming enamel. *Connect Tissue Res* 38(1-4)*:*279-86; discussion 295-303.

Stephanopoulos G, Garefalaki ME, Lyroudia K (2005). Genes and related proteins involved in amelogenesis imperfecta. *J Dent Res* 84(12)*:*1117-26.

Termine JD, Belcourt AB, Miyamoto MS, Conn KM (1980). Properties of dissociatively extracted fetal tooth matrix proteins. II. Separation and purification of fetal bovine dentin phosphoprotein. *J Biol Chem* 255(20)*:*9769-72.

Uchida T, Tanabe T, Fukae M, Shimizu M, Yamada M, Miake K, et al. (1991). Immunochemical and immunohistochemical studies, using antisera against porcine 25 kDa amelogenin, 89 kDa enamelin and the 13-17 kDa nonamelogenins, on immature enamel of the pig and rat. *Histochemistry* 96(2)*:*129-38.

Wen X, Zou Y, Luo W, Goldberg M, Moats R, Conti PS, et al. (2008). Biglycan over-expression on tooth enamel formation in transgenic mice. *Anat Rec (Hoboken)* 291(10)*:*1246-53.

Witkop CJ, Jr. (1988). Amelogenesis imperfecta, dentinogenesis imperfecta and dentin dysplasia revisited: problems in classification. *J Oral Pathol* 17(9-10)*:*547-53.

Yoshizaki K, Yamamoto S, Yamada A, Yuasa K, Iwamoto T, Fukumoto E, et al. (2008). Neurotrophic factor neurotrophin-4 regulates ameloblastin expression via full-length TrkB. *J Biol Chem* 283(6):3385-91.

Chapter VI

SUMMARY AND FUTURE DIRECTIONS

Summary of Thesis Findings

There are four portions of work that have been done in this dissertation: 1) The enamelin transgenic construct was fabricated and enamelin transgenic mice were established; 2) the enamelin transgenic mouse were bred with wild-type mouse as well as enamelin knockout mice, the transgene expression levels from different transgenic mouse lines were examined; 3) Phenotype of mouse with enamelin transgene expressed in knockout background and heterozygous background were described to determined whether enamelin transgene can rescue the defective phenotype of knockout mice; 4) Phenotype of enamelin transgenic mouse were described and found to be defective when the transgene is expressed at high level.

Enamelin is one of the major enamel matrix proteins that play an important role in tooth enamel formation. Enamelin knockout mice showed white and chalky teeth and the enamel layer is lost (Hu et al., 2008). Amelogenin is the most abundant enamel matrix

protein (Fincham et al., 1999b). Amelogenin promoter has been used to drive enamel protein expression successfully in previous studies (Snead et al., 1996; Snead et al., 1998b; Wen et al., 2008b). Transgenic mice over-expressing enamelin that was driven by amelogenin promoter has never been made before. In chapter 2, I described the design and procedure of fabricating an enamelin transgene with an amelogenin promoter and the establishment of enamelin transgenic mouse made using this transgene. This transgene construct have rare restriction enzyme recognition sites so that can be and already being used to make other enamel protein transgene constructs.

In Chapter 3, I described the examination of enamelin transgene expression level in different transgenic mouse lines and when transgene is expressed in different gene background. I used the real-time PCR and Western-blot methods to check transgene expression at both the mRNA and the protein level. We found that enamelin expression level varies, from very little to as high as around 5 times the amount of endogenous gene expression.

In Chapter 4, I showed how enamelin transgene can rescue the defective phenotype of enamelin knockout mice. In one transgenic mouse line which has a moderate expression level, the transgene successfully rescued the defective phenotype of enamelin knockout mice. The enamel thickness and microstructure of enamel are same as the enamel of wild-type mouse with this transgene expressed in knockout background mice. Other transgenic mouse lines all have a normal enamel thickness and normal decussation pattern when the transgene is expressed in heterozygous background, the teeth look yellowish and smooth,

which is similar to the wild-type mouse. These mice have better enamel than the heterozygous mice which do not have any enamelin transgene expression.

In Chapter 5, I described the effects of enamelin over-expression on dental enamel formation. I found in moderate to high expression level enamelin transgenic mouse lines, the enamel starts to have defective phenotypes: with moderate expression level, the enamel surface is not smooth and has protrusive structure on the surface of enamel; with high transgene expression, the enamel layer is almost lost, similar as the phenotype of enamelin knockout mice. This is the first time in the literature that the effect of over-expression of enamelin in developing enamel is described. The effect of transgene over-expression is dosage dependent.

Future Directions

Enamelin is a gene that is specific to dental enamel formation. Defects in *ENAM* cause autosomal dominant *amelogenesis imperfecta*. In *Enam* null mice, the mineralization front fails and no enamel forms. We focus on the mineralization front, which is the center of enamel formation. We now know that enamelin transgene with full-length enamelin cDNA and proper expression level can rescue the defective phenotype of enamelin knockout mice. We established an *in vivo* system to study the structural and functional relationship of enamelin gene in dental enamel formation. We can further make modification of enamelin gene to the area of interests to study the functional domains of this gene and their corresponding roles with other proteins and other genes. By discovering the molecular mechanisms of enamel formation we will gain important

insights into the mechanism of biomineralization in general, and pathological conditions that cause enamel defects. We know the list of extracellular matrix proteins that are critical for dental enamel formation. By understanding how they work together and by properly reconstituting the enamel matrix *in vitro*, we may ultimately synthesize enamel that can be used for clinical applications.

References

Fincham AG, Moradian-Oldak J, Simmer JP (1999). The structural biology of the developing dental enamel matrix. *J Struct Biol* 126(3)*:*270-99.

Hu JC, Hu Y, Smith CE, McKee MD, Wright JT, Yamakoshi Y, et al. (2008). Enamel defects and ameloblast-specific expression in *Enam* knockout/lacz knock-in mice. *J Biol Chem* 283(16)*:*10858-71.

Snead ML, Paine ML, Chen LS, Luo BY, Zhou DH, Lei YP, et al. (1996). The murine amelogenin promoter: developmentally regulated expression in transgenic animals. *Connect Tissue Res* 35(1-4)*:*41-7.

Snead ML, Paine ML, Luo W, Zhu DH, Yoshida B, Lei YP, et al. (1998). Transgene animal model for protein expression and accumulation into forming enamel. *Connect Tissue Res* 38(1-4)*:*279-86; discussion 295-303.

Wen X, Zou Y, Luo W, Goldberg M, Moats R, Conti PS, et al. (2008). Biglycan over-expression on tooth enamel formation in transgenic mice. *Anat Rec (Hoboken)* 291(10)*:*1246-53.

Appendix A

PORCINE DENTIN SIALOPHOSPHOPROTEIN: LENGTH POLYMORPHISMS, GLYCOSYLATION, PHOSPHORYLATION, AND STABILITY

Abstract

Dentin sialophosphoprotein (DSPP) is critical for proper mineralization of tooth dentin, and mutations in *DSPP* cause inherited dentin defects. Dentin phosphoprotein (DPP) is the C-terminal cleavage product of DSPP that binds collagen and induces intrafibrillar mineralization. We isolated DPP from individual pigs and determined that its N-terminal and C-terminal domains are glycosylated, and that DPP averages 155 phosphates per molecule. Porcine DPP is unstable at low pH and high temperatures, and complexing with collagen improves its stability. Surprisingly, we observed DPP size variations on SDS-PAGE for DPP isolated from individual pigs. These variations are not due to differences in proteolytic processing or degrees of phosphorylation or glycosylation, but rather to allelic variations in *Dspp*. Characterization of the DPP coding region identified 4 allelic variants. Among the 4 alleles, 27 sequence variations were identified, including 16 length polymorphisms ranging from 3 to 63 nucleotides. None of the length variations shifted the reading frame, and all localized to the highly redundant

region of the DPP code. The four alleles encode DPP domains having 551, 575, 589 or 594 amino acids and completely explain the DPP size variations. DPP length variations are polymorphic and not associated with dentin defects.

Introduction

About 85% of the organic material in tooth dentin is type I collagen. The non-collagenous proteins in dentin are predominantly cleavage products of dentin sialophosphoprotein (DSPP). DSPP is processed by proteases into numerous parts. In pig, the three major cleavage products are dentin sialoprotein (DSP) (Yamakoshi et al., 2005a), dentin glycoprotein (DGP) (Yamakoshi et al., 2005b), and dentin phosphoprotein (DPP). The linear order of the structural domains in porcine DSPP is DSP-DGP-DPP. In the rat, the designation DSP is used to include all of the non-DPP region of DSPP (DSP-DPP). The initial proteolytic cleavage of DSPP is in a conserved context and releases DPP so that DPP proteins isolated from various mammals share the same N-terminal sequence: AspAspProAsn (DDPN) (Butler et al., 1983; Huq et al., 2000). The early work on rat DSP and DPP was performed without knowing that DSP and DPP are initially part of the same protein and must be secreted in equal amounts. Based upon the results of these early studies, it became generally accepted that DPP is ten times more abundant than DSP in dentin extracts (Butler et al., 1981; Butler, 1998; ibarPatel, 2001). As DPP and DSP are expressed in a 1:1 ratio (MacDougall et al., 1997), to get to a 10:1 ratio DSP must be rapidly degraded, and/or there must be alternative forms of DSP that were not previously recognized that, when counted, bring the ratio back to 1:1. In fact, high

molecular weight forms of DSP have been discovered in rat dentin (Qin et al., 2003). Porcine DSP is a highly glycosylated proteoglycan that forms covalent dimers (Yamakoshi et al., 2005a). These glycosylations protect some parts of the protein from detection by DSP polyclonal antibodies, so it seems likely that DSP cleavage products may be more abundant than was originally thought.

Defects in human *DSPP* cause various types of inherited dentin defects, including dentin dysplasia type II, and dentinogenesis imperfecta types II and III (Hart and Hart, 2007; Kim and Simmer, 2007). *Dspp* knockout mice exhibit dentin defects reminiscent of those observed in human dentinogenesis imperfecta (Sreenath et al., 2003). The *DSPP* mutations reported so far are primarily along intron-exon borders near the 5' end of the gene (Holappa et al., 2006; Kim et al., 2004; Kim et al., 2005a; Malmgren et al., 2004; Song et al., 2006; Xiao et al., 2001; Zhang et al., 2007). This region encodes DSP, the N-terminal DSPP cleavage (Ritchie et al., 1994). The DPP coding region in the last exon of *DSPP* (exon 5) has a highly redundant region that is prone to artifacts during reverse transcription and polymerase chain reactions (Yamakoshi et al., 2003). Technical difficulties have so far thwarted mutational analyses of the DPP code in kindreds with inherited dentin defects. The only sequence variation reported to be disease-causing in the DPP region was a compound insertion (6 codons) and a deletion (12 codons) in the repetitive region (Dong et al., 2005). These insertions and deletions, however, are apparently normal sequence variations (polymorphisms) that do not cause the dental disease in that kindred. Alignment of four human *DSPP* sequences in GenBank identified 10 length variations in the DPP redundant region, ranging in length from 3 to 153 nucleotides, and all maintaining the reading frame (Kim and Simmer, 2007). An

independent analysis of the kindred with the compound insertion/deletion found similar (but not identical) deletions and insertions in the DPP redundant region in normal controls, and identified a missense mutation (p.P17S) in the DSP code that functional studies showed caused retention the DSPP protein in the endoplasmic reticulum (Hart and Hart, 2007). Separately, a p.P17S missense alteration was found in the affected members of another family with inherited dentin defects and was thought to be causing the disease (Zhang et al., 2007). These findings suggest that there may be extensive sequence length variations in the human DPP redundant region and that these length variations are compatible with normal function.

DPP protein has never been extensively characterized, and it is still not known if DPP is glycosylated (Qin et al., 2004). In this study we isolate porcine DPP, determine its abundance relative to DSP, characterize its post-translational modifications, and determine the molecular basis for variability in the size of DPP protein in dentin extracts.

Material and Methods

All experimental procedures involving the use of animals were reviewed and approved by the Institutional Animal Care and Use Program at the University of Michigan.

Preparation of Dentin Powder. Tooth germs of permanent second molars were surgically and extracted with a hammer and chisel from the maxillae and mandibles of six-month-old pigs, within minutes of each animal's termination at the Michigan State University Meat Laboratory (East Lansing, MI). Typically two maxillary and two mandibular second molars were obtained from each animal. The developmental stage of

the molars was advanced in crown formation, but prior to the onset of root formation. The soft tissue was removed with forceps and secretory and maturation stage enamel was scraped off with a curette. The remaining hard tissue was reduced to powder using a jaw crusher (Retsch, Newtown, PA).

Extraction of proteins from dentin powder. Dentin powder (1.7-4.4 gm each) obtained from 22 pigs individually, or combined from ~8 pigs (40 gm) for large-scale preparations, was suspended with 50 mM Tris-HCl/4M guanidine buffer (pH 7.4) containing Protease Inhibitor Cocktail Set III (1 mM AEBSF, 0.8 µM aprotinin, 50 µM bestatin, 15 µM E-64, 20 µM leupeptin and 10 µM pepstatin) (Calbiochem, San Diego, CA) and 1 mM 1,10-phenanthroline (Sigma, St. Louis, MO, USA). Each sample was intensively agitated with an orbital shaker for 24 h at 4 °C. Insoluble material was pelleted by centrifugation (15,900 x g) and the guanidine extraction repeated for two more days. The insoluble guanidine extracts were dialyzed against 16 L of 0.5 M acetic acid (HAc) containing 5 mM benzamidine (Sigma, St. Louis, MO, USA), 1 mM PMSF (Sigma, St. Louis, MO, USA) and 1 mM 1,10-phenanthroline. Each day the calcium concentration in the reservoir was measured using the Calcium Reagent Set (Pointe Scientific, Canton, MI, USA) and the HAc/protease inhibitor solution was replaced. After five days, the calcium ion concentration of the HAc reservoir fell below 0.2 mM, indicating that the tooth mineral has fully dissolved. The dialysis bag contents were centrifuged and the pellet was extracted with 0.5 M acetic acid/ 2 M NaCl (AN), which dissolved dentin phosphoprotein (DPP) and DSP proteoglycan products. The AN supernatant was fractioned to purify DPP and high molecular weight DSP-containing proteoglycan.

Purification of P\porcine DPP. AN extracts (~10-28 mg each) were dissolved in 0.05% trifluoroacetic acid (TFA) and fractionated by reversed phase-high performance liquid chromatography (RP-HPLC) using a Discovery C-18 column (1.0 cm x 25 cm, Sigma-Aldrich / Supelco, Bellefonte, PA) run at a flow rate of 1.0 mL/min and monitored at 220 nm (Buffer A: 0.05% TFA; Buffer B: 80% acetonitrile/buffer A).

Sodium Dodecyl Sulfate-Polyacrylamide Gel Electrophoresis (SDS-PAGE). SDS-PAGE was performed using Novex 4-20% Tris-Glycine or NuPage 3-8% Tris-Acetate Gels (Invitrogen, Carlsbad, CA, USA). Samples were dissolved in Laemmli sample buffer (Bio-Rad) and electrophoresis was carried out using a current of 20 mA for 65 min or 150V for 1 h, respectively. The gels were stained with Simply Blue Safe Stain (Invitrogen) or Stains-all (Sigma, St. Louis, MO, USA). The apparent molecular weights of protein bands were estimated by comparison with SeeBlue® Plus2 Pre-Stained Standard (Invitrogen).

Release of N- and O-linked Glycan Chains by Glycopeptidase A and O-glycanase Digestion. Acid phosphatase treated DPP (0.2 mg each) in 0.1M citrate-phosphate buffer (pH 5.0) or in 0.25 M sodium phosphate buffer (pH 5.0) was incubated with 1 mU of glycopeptidase A (Seikagaku America, East Falmouth, MA, USA) or a mixture of 2.5 mU of O-glycosidase and 5 mU of sialidase Au (QA-Bio, LLC, Palm Desert, CA) containing the Protease Inhibitor Cocktail Set II (0.08 mM of AEBSF, 6.8 µM of Bestatin, 0.8 µM of E-64, 0.35 mM of EDTA and 8 µM of Pepstatin A; Calbiochem, San Diego,

CA, USA) for 48 h or 2 h at 37 °C, respectively. At the end of the incubation period, aliquots were analyzed by SDS-PAGE. The six purified pronase digested DPP peptides were digested with glycopeptidase A, precipitated with three volumes of ice-cold ethanol and pelleted by centrifuged for 10 min at 10,000 x g. Glycans in the supernatant were evaporated and stored at -80°C.

Quantitative Determination of Phosphoserine in DPP. DPP from individual 22 pigs (0.5-0.7 mg each) was partially hydrolyzed with 0.2 ml of 6 N HCl for 3 h at 110 °C. After the reaction, the sample was evaporated and dissolved in 1 ml of deionized (DI) water, and 0.25 ml was fractionated on a TSK-gel SAX column (4.6 mm x 15 cm, TOSOH, Tokyo, JPN). The column was equilibrated with 40 mM potassium phosphate buffer (pH 4.0), and eluted with the same buffer at a flow rate of 1.5 ml/min at the room T. Phosphoserine was detected by monitoring absorbance at 210 nm and authentic phosphoserine, phosphothreonine and phosphotyrosine (Sigma, St. Louis, MO, USA) were used as references. The moles of phosphates released was divided by the starting weight times 100 g/mole (100-kDa molecular weight) to calculate phosphate per molecule.

Quantitative Determination of DPP Phosphorylation by Acid Phosphatase Digestion. DPP (150 µg each) in 150 ml of 10 mM sodium acetate/ 50 mM EDTA buffer (pH 5.8), from individual pigs was incubated with 0.2 unit of acid phosphatase (White potato) (Sigma, St. Louis, MO, USA) containing the Protease Inhibitor Cocktail Set II (0.08 mM of AEBSF, 6.8 µM of Bestatin, 0.8 µM of E-64, 0.35 mM of EDTA and 8 µM of

Pepstatin A; Calbiochem, San Diego, CA, USA) for 48 h at 37 °C. Free phosphorus in aliquots (20 ml) of acid phosphatase digests was measured by colorimetric assay using the Inorganic Phosphorus Reagent Set (Pointe Scientific, Canton, MI, USA). The number of phosphates per molecule was calculated assuming a molecular weight of 100-kDa.

Extraction of DPP from gels. Three DPP protein bands from large-scale dentin preparations were excised from a polyacrylamide gel after Stains-all staining. Each gel slice was transferred to a D-Tube Dialyzer (midi size) (Novagen/EMD Chemicals, Inc., Gibbstown, NJ) and electroeluted with 25 mM Tris/ 250 mM Tricine/ 0.025% SDS buffer (pH 8.5) at 150 volts for 3 h. The eluate (DPP) was precipitated with 20% trichloroacetic acid. The pellet was incubated in acetone overnight at -20 ℃ and centrifuged at 4 ℃ for 30 min at 14,000 x g. The supernatant was decanted, the pellet dried under a hood, and characterized by Edman sequencing.

Purification of DPP Glycopeptide by Pronase Digestion. DPP (25 mg) was digested with acid phosphatase, dialyzed against water for 2 days, and lyophilized. Acid phosphatase treated DPP (18 mg) was dissolved with 1 ml of 50 mM Tris-HCl buffer (pH 8.0). This solution was incubated with 0.1 mg of pronase (Calbiochem) for 15 h at 37 °C. The digest was fractionated by size exclusion chromatography using a Sephadex G-15 column (1.6 cm x 100 cm, GE Healthcare Life Sciences) equilibrated with 50 mM Tris-HCl buffer (pH 8.0). DPP peptides were eluted with the same buffer at a flow rate of 0.2 ml/min at 4 °C with absorbance monitored at 220 nm, and analyzed for glycosylations using a phenol-sulfuric acid assay at 490 nm. The fraction of peptides containing DPP

glycopeptide were eluted in the first peak and this fraction was separated by hydrophilic interaction liquid chromatography (HILIC) using a PolyHYDROXYETHYL A column (4.6 mm ID x 20 cm, The Nest Group, Inc., Southborough, MA, USA) equilibrated with 15 mM triethylamine-phosphate (TEAP) in 95% acetonitrile (pH 3.0). Peptides were eluted with a linear acetonitrile gradient containing 15 mM TEAP in 5% acetonitrile (pH 3.0) at a flow rate of 0.5 ml/min at room T, while monitoring the absorbance at 220 nm. Six peaks were collected and evaporated. Aliquots were used for both amino acid sequence and glycosylation analyses.

Preparation and Isolation of 2-AA-labeled Glycans. Glycans released by glycopeptidase A were labeled with 2-aminobenzoic acid (2-AA) Labeling Kit (QA-Bio, Palm Desert, CA) and labeled glycans were purified by LudgerClean S cartridge (QA-Bio). The 2-AA-glycans were fractionated by normal phase (NP) HPLC using a SUPELCOSIL LC-NH2 column (4.6 mm x 25 cm, Sigma-Aldrich/ Supelco, Bellefonte, PA). The column was equilibrated with 2% acetic acid and 1% tetrahydrofuran in acetonitrile. Glycans were eluted with a linear gradient using 5% acetic acid/ 1% tetrahydrofuran/ 3% triethylamine in water at a flow rate of 0.7 ml/min at room T. For the detection of 2-AA-glycans, an excitation wavelength of 230 nm and an emission wavelength of 420 nm were used.

Effect of pH and Temperature for Stability of DPP Structure. DPP (1 mg) was dissolved with 0.2 ml of DI water. An 20 µl aliquot was mixed with 180 µl of 50 mM sodium acetate or 50 mM Tris-HCl or 50 mM carbonate buffers to achieve a final pH of 4,

5, 6, 7, 8, 9, 10 or 11 (50 mM sodium acetate for pH 4 and 5, 50 mM Tris-HCl for pH 6-8, or 50 mM carbonate buffer for pH 9-11), respectively. Each sample was divided into five tubes (40 µl each). One tube was immediately stored at -80 °C, another one tube was incubated for 5 min at 95 °C, and other three tubes were incubated for 20 h at 4°, 20°, or 37 °C, respectively. Aliquots (20 µl) of samples were separated by SDS-PAGE and visualized with Stains-all.

Effect of Collagen on the Stability of DPP. DPP (0.2 mg) was dissolved with 0.2 ml of 0.5 M acetic acid. An aliquot of sample (50 µl) was then mixed with 0.2 ml of 0.5 M acetic acid containing 0.2 mg of acid-soluble human placenta type I collagen (Abcam, Cambridge, MA). Another aliquot (50 µl) were mixed with 0.2 ml of 0.5 M acetic acid only. Two samples with and without the collagen were divided into five tubes (50 µl each). Each sample was incubated and analyzed by SDS-PAGE.

Amino Acid Analysis. The purified peptide samples (0.02-0.03 mg) were hydrolyzed with 6 N HCl at 115 °C for 16 h. The amino acid analyses were performed using a Beckman Model 7300 automatic amino acid analyzer.

***Automated Edman Degradation*.** Automated Edman degradation used the Applied Biosystems Procise 494 cLC protein sequencer at the W.M. Keck Facility at Yale University.

Characterization of DPP Genomic Sequences. Genomic DNA was isolated from the ear auricles of the 22 pigs investigated using the DNeasy Tissue Kit (QIAGEN, Valencia, CA). The DNA from eight pigs (B, J, H, M, N, P, R, V) was used as template to clone and characterize the DPP coding region. A segment from *Dspp* exon 5 containing the entire DPP coding region was amplified by polymerase chain reaction (PCR) using the primer pair 5'-TGGACCCAGCAAAAC ACATA and 5'-AATCGTAGCCAAGCTGG AGA). The reactions ran for 35 cycles, with denaturing at 94 ˚C for 30 s, annealing at 56 ˚C for 30 s, and extension at 72 ˚C for 3 min using the Expand High Fidelity plus PCR system (Roche, Indianapolis, IN). The amplification products for each pig were separated on 1% agarose gels containing ethidium bromide. The DNA bands were visualized with long wavelength UV light, excised with a razor blade, purified using a QIAquick gel extraction kit (QIAGEN), ligated into pCR2.1-topo vector (Invitrogen, Carlsbad, CA) and used to transform Top10 competent cells (Invitrogen). Individual colonies were grown in LB broth and DNA isolated using the SV Minipreps DNA Purification System (Promega, Madison, WI). Sequencing was carried out at the University of Michigan DNA Sequencing Core using four separate primers, the two used for the original amplification and two internal primers (5' AGTGATGGCAATGGTGACAA and 5'-GATTG CTGTCACTGCCTTCA3'). Due to the cloning and characterization of some PCR artifacts, a second set of PCR/cloning reactions was conducted and only clones isolated from multiple independent PCR reactions were accepted as being the true DPP alleles.

Results

Relative abundance of DSP and DPP in porcine dentin. Previously we developed a strategy for sequentially extracting proteins from porcine dentin and used DSP and DGP antibodies to identify where DSPP-derived cleavage products fractionated during the procedure (Yamakoshi et al., 2005a; Yamakoshi et al., 2005b; Yamakoshi et al., 2006). This extraction scheme is shown in Fig. A.1A. Dentin powder is first homogenized in guanidine. Dialysis of the guanidine extract causes some precipitation, separating it into guanidine soluble "GS" and guanidine pellet "GP" extracts. The original guanidine pellet is demineralized with acetic acid yielding an acid or "A" extract. The acid pellet is extracted with acetic acid/NaCl, generating the "AN" extract. The GS and GP extracts contain primarily enamel protein cleavage products and proteases (Yamakoshi et al., 2005b; Yamakoshi et al., 2006). The A extract contains soluble collagen, 32-kDa enamelin (from enamel), osteocalcin, and relatively small cleavage products from the non-DPP portion of DSP (the N-terminal fragments of DSP, DGP and extended DGP). Very little protein in the AN extract stains with CBB, but this extract is rich in Stains-all positive DSPP-derived dentin proteins (Fig. A.1B). Lower molecular weight protein is removed from the AN extract by size exclusion chromatography and the high molecular weight DSPP-derived proteins are separated into DPP and DSP components by RP-HPLC. Five RP fractions are evident in the chromatogram (Fig. A.1C). R1 contains DPP fragments, R2 contains intact DPP and DPP fragments, R3 contains the central proteoglycan core of DSP, R4 contains DSP, and R5 contains DSP-DGP, or the entire non-DPP region of DSPP (Fig.A.1D) (Yamakoshi et al., 2006).

To quantify the relative abundance of DPP and high molecular weight DSP, we isolated and weighed the AN extract from the second molars of 22 individual pigs and

isolated the five RP-HPLC fractions containing DSPP-derived proteins. We normalized for variations in protein quantity among the pig extracts by dividing the quantity of protein in each RP fraction by the total amount of protein in the AN extract and calculated the total amount of DPP (R1+R2) relative to the total amount of high molecular weight DSP in fractions (R3+R4+R5). On a weight basis, porcine dentin in the second molars of six month old pigs contains between 1.2 and 2.0 times more DPP than high molecular weight DSP (Fig. A.1E). There are, however, low molecular weight DSP cleavage products outside of the AN extract (Lanes A, Fig. A.1B). These cannot be efficiently isolated and their quantity was not determined for individual pigs, but including the small DSP cleavage products in the A extract would have brought the ratio of DSP to DPP (on a weight basis) very close to 1:1, which is consistent with the fact that DPP and DSP are synthesized from the same mRNA transcript in 1:1 molar ratios (MacDougall et al., 1997; Yamakoshi et al., 2003).

DPP post-translational modifications. An estimate of the gross levels of post-translational modifications in porcine dentin phosphoprotein was made by examining DPP before and after dephosphorylation and deglycosylation (Fig. A.2). Porcine DPP in our large-scale preparations (that combine dentin powder from 8 pigs) typically appears as two prominent bands, often accompanied by a one or two distinct but weaker DPP bands. We originally assumed that the multiple DPP bands, all migrating near 100-kDa on SDS-PAGE, to be due to variations in the amount of DPP post-translational modifications. Dephosphorylation of DPP with acid phosphatase, however, causes these DPP bands to shift to a lower apparent molecular weight on SDS-PAGE (Fig. A.2A), but

does not alter the pattern of multiple bands. N-deglycosylation (Fig. A.2B) and O-deglycosylation (Fig. A.2C) of the dephosphorylated DPP does not appreciably alter the mobility of DPP on SDS-PAGE and also does not alter the pattern of multiple bands. Each DPP band was excised from the gel and characterized by N-terminal sequencing. All three DPP bands gave the same N-terminus: DDPNxxE. These results demonstrate that the various DPP bands extracted from porcine dentin do not differ from each other because of variations in the levels of phosphorylation, glycosylation, or through the use of multiple cleavage sites to release DPP from the parent DSPP protein. We then characterized the number of phosphates on DPP and identified DPP glycosylations sites.

We isolated DPP from 22 individual pigs and determined the numbers of phosphate per molecule using two independent methods. One method measures the amount of phosphoserine released after acid hydrolysis, the other measures inorganic phosphate released by acid phosphatase. Using the apparent molecular weight of DPP (100-kDa) on SDS-PAGE to convert from grams to moles, the number of phosphates per molecule of DPP came to an average of 212 per molecule. This number of phosphates would contribute 17-kDa to the mass of the protein.

To identify specific glycosylation sites, DPP was digested with pronase, a cocktail of proteolytic enzymes that digests glycoproteins down to short glycopeptides, which are protected from further degradation by their bulky carbohydrate chains. The pronase digestion products were fractionated by size exclusion chromatography and assayed for the presence of glycosylations (Fig. A.3A). The glycosylation-positive peak was separated into six fractions (labeled Pr-DPP-1 through Pr-DPP-6) by HILIC (Fig. A.3B). The protein in each fraction was deglycosylated and characterized by N-terminal

sequencing (Table A.2). The glycosylations were fluorescently labeled and analyzed by NP-HPLC (Fig. A.3C-3H). No labeled glycosylations were observed for Pr-DPP-1, Pr-DPP-5, and Pr-DPP-6. Two N-linked glycosylation sites were identified in the other fractions: at Asn^{525} (Pr-DPP-2 and Pr-DPP-3) and Asn^{937} (numbered for the smallest DSPP allele; Pr-DPP-4). Based upon its retention time on the NP-HPLC column, the glycosylation at Asn^{525} can have either no sialic acid (Pr-DPP3) or two sialic acids (Pr-DPP2). The glycosylation at Asn^{937} has two sialic acids (Pr-DPP4). These results demonstrate that porcine DPP is glycosylated at two positions, and that variations in glycosylation cannot account for the multiple bands of DPP observed on SDS-PAGE.

Allelic polymorphisms as the source of DPP length variations. DPP protein was separately isolated from 22 pigs and analyzed by SDS-PAGE (Fig. A.4A). Each pig showed either one or two DPP bands of equal intensity, migrating near 100-kDa. DPP bands from six pigs representing the full range of DPP size variations were characterized by Edman sequencing and all displayed the same N-terminal sequence: DDPNxxE. Dephosphorylation caused the DPP bands to shift to a lower position on the gel, but did not alter the pattern of bands (Fig. A.4B). We amplified the DPP coding region (which is not interrupted by any introns) using genomic DNA isolated from the same 22 pigs used to obtain the DPP protein and found length variations in the DPP code that closely correlated with the length variations observed at the protein level (Fig. A.4C).

The DPP PCR products from eight of the pigs were cloned and characterized. Some length variations in the DPP amplification products were identified as PCR artifacts (data not shown), as they could not be reproduced by repeating the experiment.

PCR products that represented singular events were consistently ignored in favor of only reproducible outcomes. We characterized four groups of DPP cDNAs that were generated from multiple independent PCR cloning experiments, and these clones can account for all of the DPP size variability observed at the protein level. The DPP clones correspond to four allelic variations of the DPP code in the *Dspp* genes of this group of pigs. The four clones varied in length due to the presence of multiple in-frame deletions or insertions. All of the length variations localized to the highly redundant region of the DPP code (Fig. A.5A). The DPP coding region has 27 sequence variations among the four alleles (Fig. A.5B). Of these, 11 are point mutations (changing 5 amino acids) and 16 are length variations ranging from 3 to 63 bp that maintain the open reading frame (Table 1, suppl).

The DPP coding regions in the four alleles are 1656 (EU419998), 1728 (EU419999), 1770 (EU420000), and 1785 bp (EU419997) in length (Fig. A.5C). Because the lengths of the DPP coding region closely correlate with the apparent sizes of the protein bands on SDS-PAGE (Figs. A.3A, A.3B), it was possible to deduce the distribution of the four DPP alleles in the 22 pigs investigated. In these pigs there are 44 DPP alleles in total: 20 (1656 bp), 18 (1728 bp), 3 (1770 bp) and 3 (1785 bp). Thus, the two smallest DPP alleles (1656 bp and 1728 bp) predominate among the pigs in this group. These commercial pigs have no apparent dental phenotype and the observed DPP sequence variations are not associated with any loss of function.

DPP stability. The effects of pH and temperature on the stability of DPP were examined (Fig. A.6). Dentin phosphoprotein is stable for at least 20 h at 4 ˚C and at 20 ˚C within the entire range of p 4 to pH 11). At 37 ˚C, DPP is sensitive to hydrogen ion

concentration and a significant reduction in the amount of DPP is observed after 20 h at pH 5 and below. The degradation of DPP at low pH 5 occurs more rapidly if the protein is heated at 95 ˚C for 5 min. The instability of DPP observed at low pH and high T is reduced in the presence of type I collagen (Fig. A.7A-7C).

Discussion

Relative abundance of DSP and DPP. Using the porcine animal model, which provides abundant dentin proteins, and having previously surveyed dentin extracts for the presence of DSPP-derived proteins, we were able to quantify levels of DSPP-derived proteins from developing pig molars and determine that there are approximately equal weights of DSPP cleavage products from the DSP-DGP and DPP regions in our dentin extracts. There are differences, however in the way these proteins are degraded. After the release of DPP, DSP-DGP is processed into numerous relatively small cleavage products (~17 to 35-kDa) that can be found in the A extract. Larger DSP-DGP pieces that contain the two long chondroitin sulfate attachments are in the AN extract. DPP degradation products do not form discrete bands, but rather show a continuum of all sizes that make a Stains-all positive smear on SDS-PAGE (Fig. A.1D, R1 and R2). This pattern might reflect an inherent chemical instability rather than processing by proteases (Ibaraki et al., 1991).

DPP post-translational modifications. DPP is the most acidic protein known and has an isoelectric point of 1.1 (Jonsson and Fredriksson, 1978). The low electric point is due to its large number of acidic amino acids and phosphorylated serines. Porcine DPP migrates at about 100-kDa on SDS-PAGE. When DPP is isolated from individual pigs, either one

or two DPP bands are observed. We have demonstrated that the presence of multiple bands is due to allelic variation. Porcine DPP is relatively homogeneous with respect to its post-translational modifications. This contrasts with rat DPP where multiple forms have been proposed that vary according to their degree of phosphorylation (Butler et al., 1983).

We determined that the average number of phosphates per DPP molecule is 212 when using DPPs apparent molecular weight (100-kDa) on SDS-PAGE to calculate moles of DPP in a weighed sample. The results of the cloning and post-translational modification studies, however, suggest that 73-kDa might be a better estimate for the molecular weight of porcine DPP. The predominant forms of DPP in our population of pigs contain 551 or 575 amino acids. Without post-translational modifications, the common DPP forms have calculated molecular weights of 54.6-kDa and 57.1-kDa. If DPP were 73-kDa, the average number of phosphates per molecule would be 155 (73-kDa/mol x 212 P/100-kDa/mol = 155 P). This number of phosphates (155/molecule) has a mass of 12.4-kDa (155 P x 80 Da/P = 12.4-kDa). The breakdown for the 73-kDa native protein is: 56-kDa protein + 12.4-kDa P + 4.6 kDa N-glycos = 73 kDa. As there are 310 serines per molecule, half of the serines in DPP are phosphorylated.

The DPP deduced amino acid sequences of the four DPP alleles are aligned in Fig. 8. There are eight potential N-linked glycosylation sites (NxS, where x≠P) in the N-terminal region of DPP and five in the C-terminal region. Pronase digests of DPP generated short glycopeptides derived from one site in each of these regions. It seems unlikely that additional sites are glycosylated as the mobility of DPP on SDS-PAGE does not change appreciably following deglycosylation.

DPP length polymorphisms. The size of DPP varies among species. Rat, bovine, and porcine DPPs have an apparent molecular mass just under 100-kDa (Butler et al., 1983; Termine et al., 1980), while human DPP migrates at about 140-kDa on SDS-PAGE (Chang et al., 1996). It is becoming increasingly apparent that the size of DPP also varies within species. These observations suggest that DPP function is not affected by length variations in its repeat region. The functional significance (or insignificance) of DPP length variations is important when considering whether a particular sequence variation is disease-causing or simply a polymorphism. It is also important when considering DPP function.

Our studies of 22 commercial pigs demonstrate that DPP allelic variations at the DNA level translate into size variations at the protein level. The four *Dspp* alleles showed 16 DPP length variations ranging from 1 to 21 amino acids and 5 single amino acid substitutions. There is no apparent loss of function due to this variability. Previously we reported the cloning of two porcine DSPP (pDSPP) cDNA clones encoding a total of 600 and 593 amino acids, respectively: $pDSPP_{600}/DPP_{128}$ (Acc# AY161863) and $pDSPP_{593}/pDPP_{121}$ (Acc# AY161862). The DPP part of these clones was short and apparently had most of the DPP region deleted during the cloning procedure, possibly during the reverse transcription reaction (Yamakoshi et al., 2003). Only the DPP region was affected by artifacts, and the early DSPP clones demonstrated that porcine DPP begins at Asp^{473} of DSPP. Therefore, the four DPP allelic variants identified in the 22 pigs can be designated $pDSPP_{1023}/DPP_{551}$, $pDSPP_{1047}/DPP_{575}$, $pDSPP_{1061}/ DPP_{589}$, and $pDSPP_{1066}/DPP_{594}$. The $pDSPP_{1023}/ DPP_{551}$ and $pDSPP_{1047}/DPP_{575}$ alleles predominate

(38/44 alleles) in our group of pigs and express the two major DPP bands observed in protein preparations from the same animals. By comparison, rat DSPP protein has 970 amino acids, 523 of which are in the DPP portion of the protein ($rDSPP_{970}/DPP_{523}$, Acc# AJ403971) (George et al., 1996), while human DSPP is larger and may also show allelic length variations ($hDSPP_{1301}/DPP_{839}$, Acc# NM_014208; $hDSPP_{1253}/DPP_{791}$ Acc# AAF42472) (Gu et al., 2000).

DPP instability. The DPP domain is inherently unstable and degrades when heated *in vitro* (Ibaraki et al., 1991). Increasing concentrations of SDS helped protect against thermal degradation. We confirm these findings and add that DPP is unstable at low pH, and that type I collagen helps protect DPP from thermal degradation, presumably by forming Col I-DPP complexes.

DPP is an intrinsically disordered protein. Proteins that do not appear to adopt a well-defined conformation under native conditions are increasingly being categorized as intrinsically disordered proteins (IDP) (Hansen et al., 2006). The tendency for proteins to be intrinsically disordered can be predicted from their amino acid sequences. DPP is 29% aspartic acid and 54% serine, with half of the serines being phosphorylated. The PONDR computational software for predicting naturally disordered structures gives DPP its highest possible score (1.0) over a continuous region extending for more than 350 amino acids (Yamakoshi, in press). NMR analysis showed that bovine DPP is a molecule of uniformly high mobility, which is consistent with it being an intrinsically disordered protein (Cross et al., 2005).

In summary our results demonstrate that the amounts of protein in porcine dentin extracts that are derived from the DSP-DGP and DPP regions of DSPP are about equal. Porcine DPP is extensively phosphorylated, averaging 155 phosphates per molecule, and is glycosylated in its N-terminal and C-terminal domains. Although porcine DPP shows an apparent molecular weight of 100-kDa on SDS-PAGE, we estimate its actual size to be 73-kDa, based upon the deduced weights of its amino acid chain and post-translational modifications. Allelic length variations in the DPP coding region translate into size variations at the protein level. Such length variations are exceedingly rare in proteins. They occur, however, within the highly redundant DPP region and represent normal variations that do not interfere with protein function.

Figures and Legends

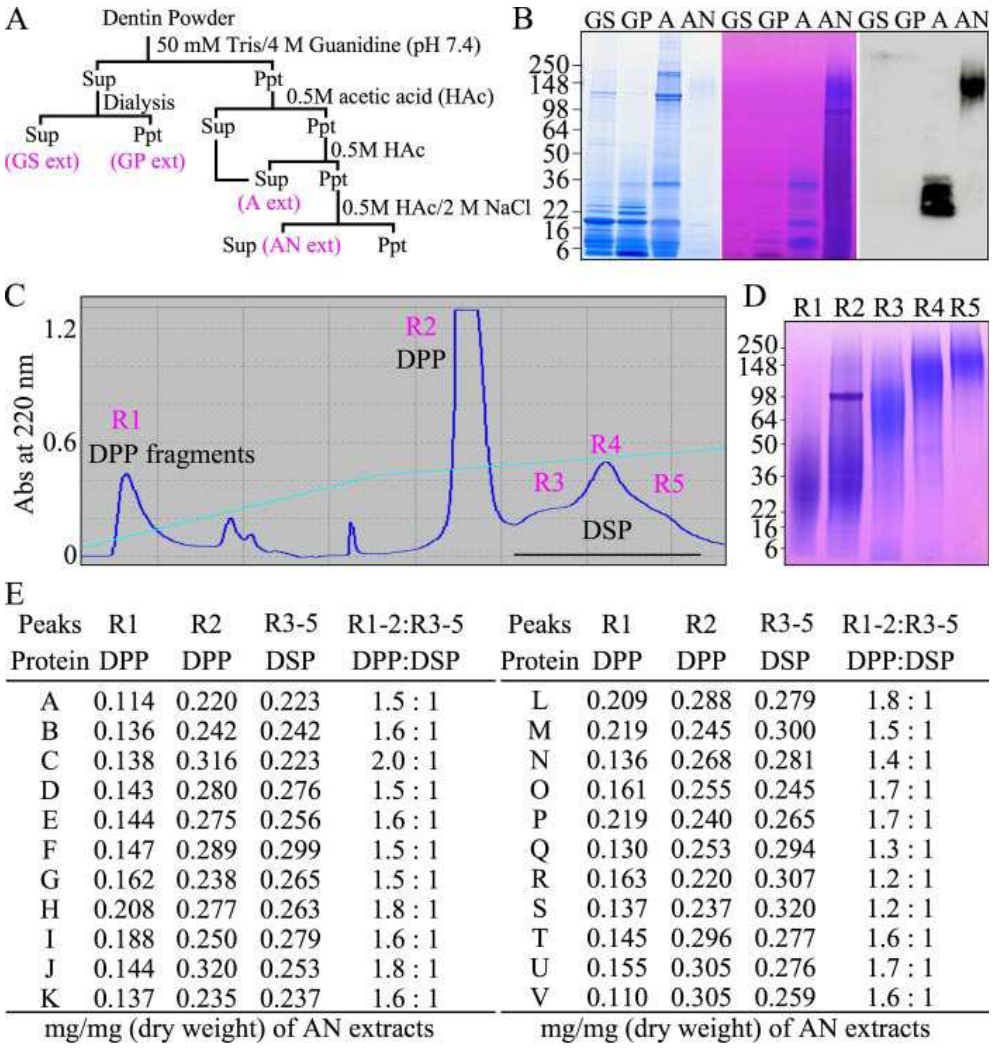

E

Peaks	R1	R2	R3-5	R1-2:R3-5	Peaks	R1	R2	R3-5	R1-2:R3-5
Protein	DPP	DPP	DSP	DPP:DSP	Protein	DPP	DPP	DSP	DPP:DSP
A	0.114	0.220	0.223	1.5 : 1	L	0.209	0.288	0.279	1.8 : 1
B	0.136	0.242	0.242	1.6 : 1	M	0.219	0.245	0.300	1.5 : 1
C	0.138	0.316	0.223	2.0 : 1	N	0.136	0.268	0.281	1.4 : 1
D	0.143	0.280	0.276	1.5 : 1	O	0.161	0.255	0.245	1.7 : 1
E	0.144	0.275	0.256	1.6 : 1	P	0.219	0.240	0.265	1.7 : 1
F	0.147	0.289	0.299	1.5 : 1	Q	0.130	0.253	0.294	1.3 : 1
G	0.162	0.238	0.265	1.5 : 1	R	0.163	0.220	0.307	1.2 : 1
H	0.208	0.277	0.263	1.8 : 1	S	0.137	0.237	0.320	1.2 : 1
I	0.188	0.250	0.279	1.6 : 1	T	0.145	0.296	0.277	1.6 : 1
J	0.144	0.320	0.253	1.8 : 1	U	0.155	0.305	0.276	1.7 : 1
K	0.137	0.235	0.237	1.6 : 1	V	0.110	0.305	0.259	1.6 : 1
mg/mg (dry weight) of AN extracts					mg/mg (dry weight) of AN extracts				

Fig A.1: Relative abundance of DSP and DPP in developing porcine molars. *A*. Strategy for isolating dentin proteins from dentin powder that generates four extracts: the guanidine supernatant (GS extract), guanidine pellet (GP extract), acid extract (A extract), and acid/NaCl (AN extract). *B*. SDS-PAGE (4-20% gradient gel) stained with CBB (left), Stains-all (center) and a Western blot immunostained with an anti-DSP Ab (right). High molecular weight DSPP-derived proteins in the AN extract do not stain with CBB, but stain deeply with Stains-all. High molecular weight DSPP-derived proteins are in the AN extract are purified by size exclusion chromatography (not shown) followed by RP-HPLC. *C*. The RP-HPLC chromatogram exhibits five peaks, labeled R1 through R5. *D*. SDS-PAGE (4-20% gradient gel) stained with Stains all shows DPP fragments (R1), intact DPP with DPP fragments (R2), DSP proteoglycan core (R3), DSP proteoglycan (R4), and DSP-DGP proteoglycan (R5). The weight of the AN extract and fractions R1 through R5 was measured for dentin obtained from each of 22 pigs (labeled A through V). *E*. Table showing the dry weights of fractions R1, R2, and R3 through R5 divided by the total dry weight of the AN extract, and the dry weight of DPP (R1+R2) relative to DSP (R3-R5) in the AN extracts.

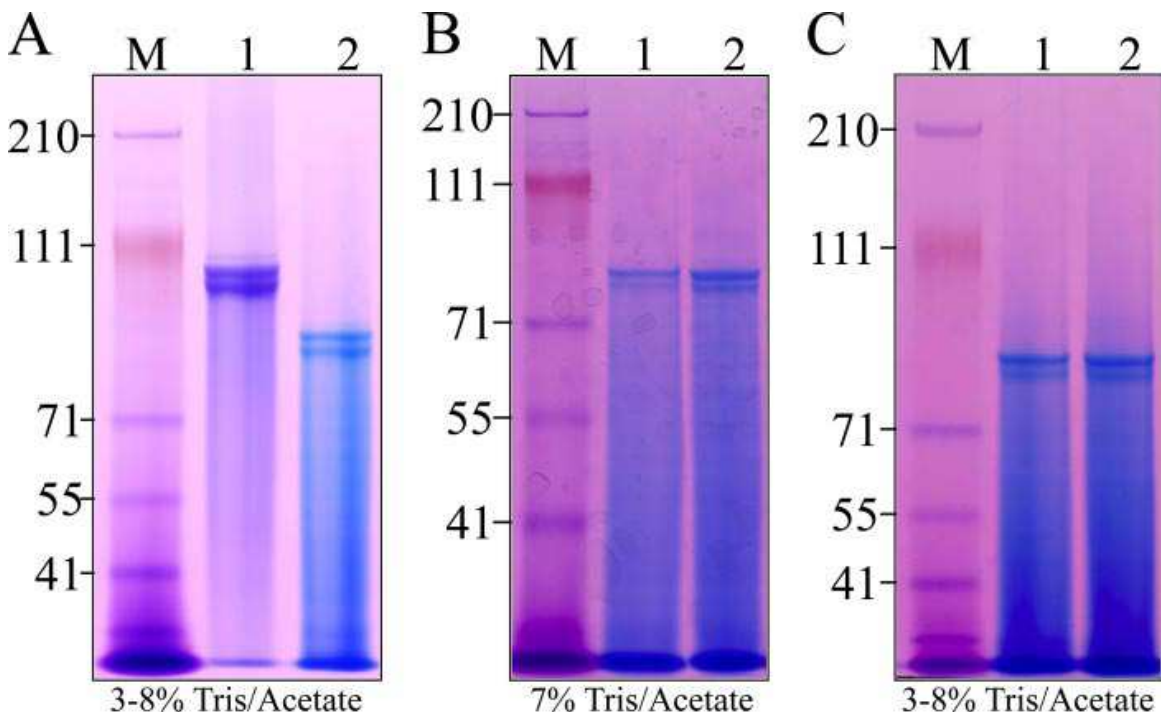

Fig A.2. Multiple DPP bands are not due to variable levels of phosphorylation or glycosylation. *A.* DPP in large scale preparations (from 8 pigs) typically shows 2 prominent bands and 1 or 2 additional feint bands (lane 1). Dephosphorylation with acid phosphatase shifts the multiple bands down the gel, but the pattern of multiple bands is preserved. *B.* N-deglycosylation of the dephosphorylated DPP with glycopeptidase A (lane 2) does not significantly alter the mobility of DPP or its pattern of multiple bands (lane 1). *C*. O-deglycosylation of dephosphorylated and N-deglycosylated DPP (lane 2) does not significantly alter the mobility of DPP or its pattern of multiple bands (lane 1). The three DPP bands from lane 1 in panel A were excised from the gel and characterized by N-terminal sequencing. All gave the same result: DDPNS, which is the conserved DPP amino-terminal sequence.

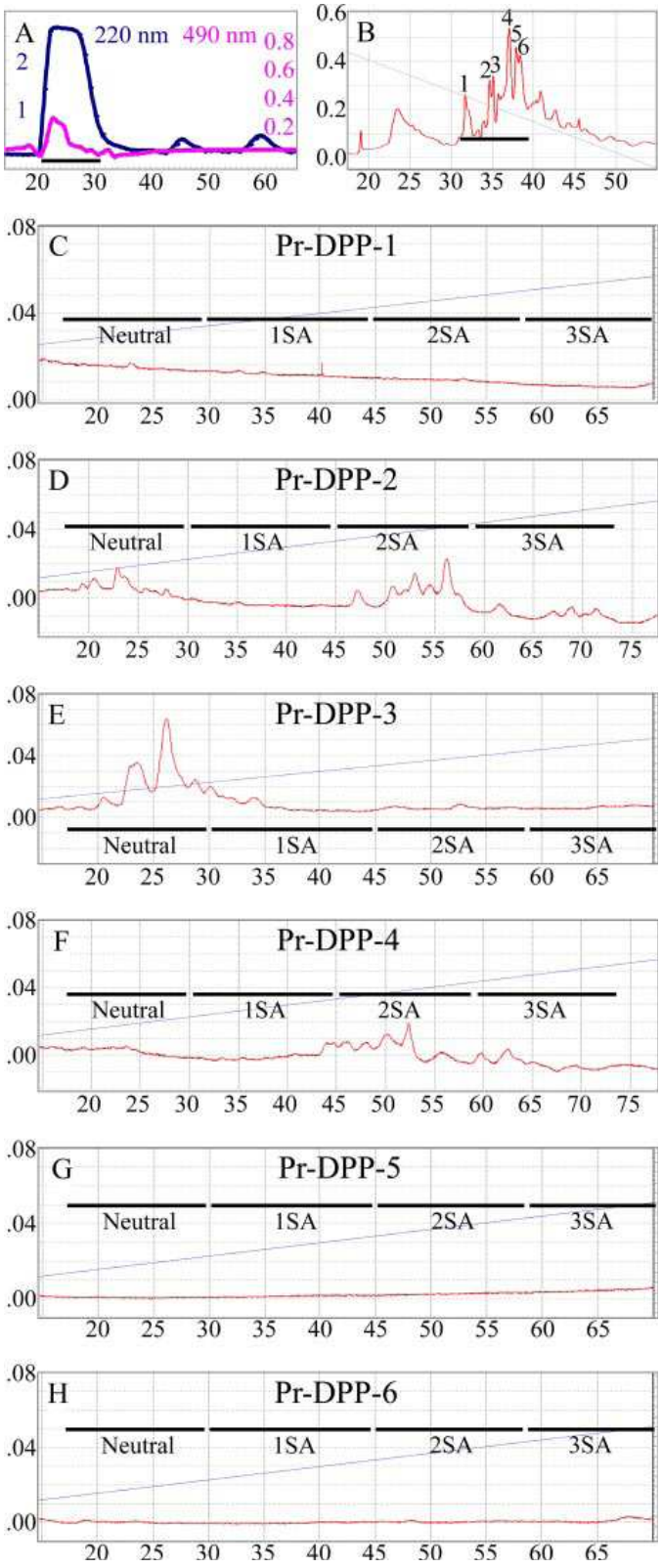

Fig A.3. Identification of two N-glycosylation sites in DPP. *A.* Size exclusion chromatogram of pronase digestion products of DPP with absorbance monitored at 220

nm (blue line). Aliquots were analyzed for glycosylations by measuring the absorbance at 490 nm (magenta) after performing the phenol-sulfuric acid assay. Fraction applied to next column is underlined. *B.* Chromatogram of glycosylation positive fraction (peak 1 in *A*) divided into 6 parts by hydrophilic interaction-HPLC. The six Pr-DPPs was digested with glycopeptidase A and the released N-glycosylations were fluorescently labeled. *C-H*. Chromatograms of labeled N-glycans on NP-HPLC and monitored with an excitation wavelength of 230 nm and an emission wavelength of 420 nm. No N-glycans were released from Pr-DPP fraction 1 (C), 5 (G), or 6 (H). N-glycans were eluted in order of the number of sialic acid (SA) indicated as Neutral, 1SA, 2SA and 3SA (Thomas et al., 2004). The N-glycan for Pr-DPP-3 (E) has no SA, while those for Pr-DPP-2 (D) and Pr-DPP-4 (F) have 2 sialic acids.

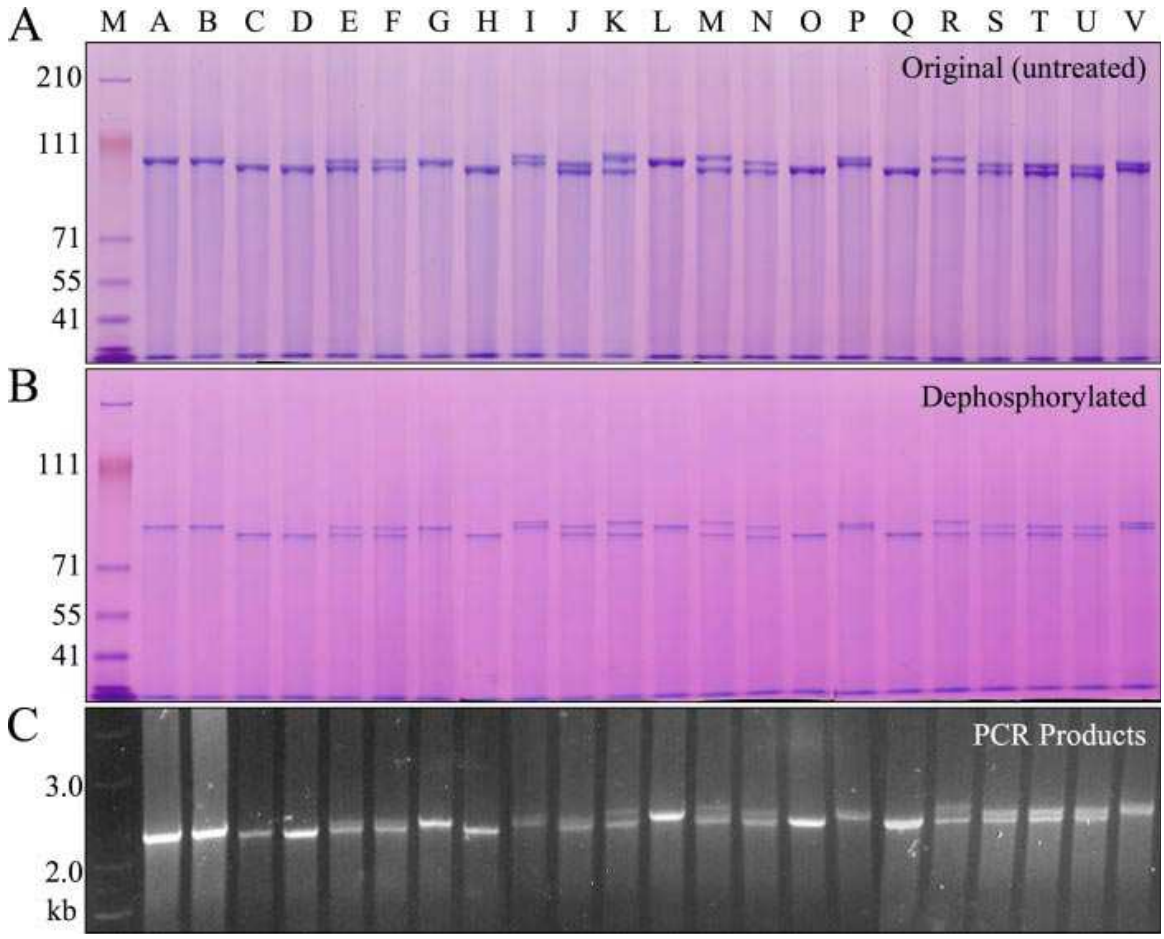

Fig A.4 Length Polymorphisms of DPP protein and coding region. *A.* SDS-PAGE showing variations in the mobility of DPP protein isolated from 22 individual pigs. Nine of the 22 pigs showed only a single band of DPP (A,B,C,D,G,H,L,O,Q). Thirteen pigs showed two DPP bands (E,F,I,J,K,M,N,P,R,S,T,U,V). Although no individual pig showed more than 2 DPP bands, six bands of non-identical size could be discerned among the 22 pigs. *B.* Dephosphorylation of DPP from the 22 pigs shifted the bands lower on the gel but did not alter the pattern of bands. *C.* DPP PCR products using genomic DNA as template generated an identical pattern of 1 or 2 bands.

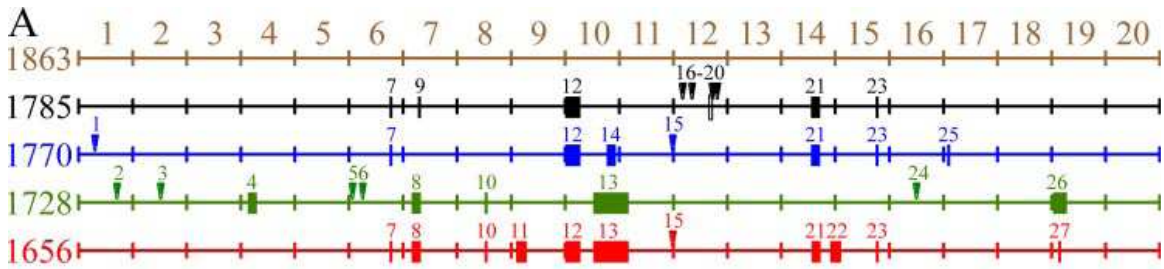

B Point Mutations and Deletions

1)	A or G	10)	9 bp	19)	A or G
2)	A or G	11)	21 bp	20)	T or C
3)	A or G	12)	30 bp	21)	18 bp
4)	18 bp	13)	63 bp	22)	21 bp
5)	A or C	14)	18 bp	23)	9 bp
6)	C or T	15)	A or G	24)	T or C
7)	9 bp	16)	T or C	25)	9 bp
8)	18 bp	17)	A or G	26)	27 bp
9)	9 bp	18)	3 bp	27)	9 bp

C Confirmed DPP alleles in 8 pigs (BHJMNPVR) tested:

Allele	Protein	Pig
1785 bp	594 aa	M & R
1770 bp	589 aa	P
1728 bp	575 aa	B, N, P & V
1656 bp	551 aa	H, J, M, N, and R

Fig A.5. DPP allelic variations. *A.* Mapping of sequence variations in the porcine DPP coding region. Point mutations are indicated by numbered arrowheads; deletions are indicated by solid rectangles. On the left is the number of basepairs in each DPP allele. The first map (1863 bp, brown) is not an allele, but a merged reference sequence that contains all of the DPP code found on the four DPP alleles characterized. The 20 divisions in the coding region correspond to rows of 93 nucleotides each in the DNA alignment of the DPP alleles (Table 1 suppl). The four DPP alleles had 1785 (black), 1770 (blue), 1728 (green) and 1656 (red) basepairs. *B.* Key to the 27 sequence variations observed in the four DPP alleles characterized. *C.* Listing of the pigs analyzed for sequence variations, the number of coding basepairs (bp) in each allele, the number of amino acids (aa) in the DPP protein, and the pigs shown to host each allele. The predominant alleles in the 22 pigs were 1656 and 1728 bp. Based upon the mobility of the proteins (Fig. 4A), and the cloning results, these alleles were likely present in 15 or 14 of the 22 pigs, respectively (1656: C_2,D_2,E,F,H_2,J,K,M,N,O_2,Q_2,R,S,T,U; 1728: A_2,B_2,E,F,G_2,I,J,L_2,N,P,S,T,U,V). Only 6 of the 22 pigs hosted other alleles (I, K,M,P,R,V). The 1770 allele in pig P also appeared to be present in pigs I and V. The 1785 allele in pigs M and R also appeared to be in pig K. The frequency of the four characterized alleles in the 22 pigs (44 alleles) were 1656: 20 alleles; 1728: 18 alleles; 1770: 3 alleles; 1785: 3 alleles.

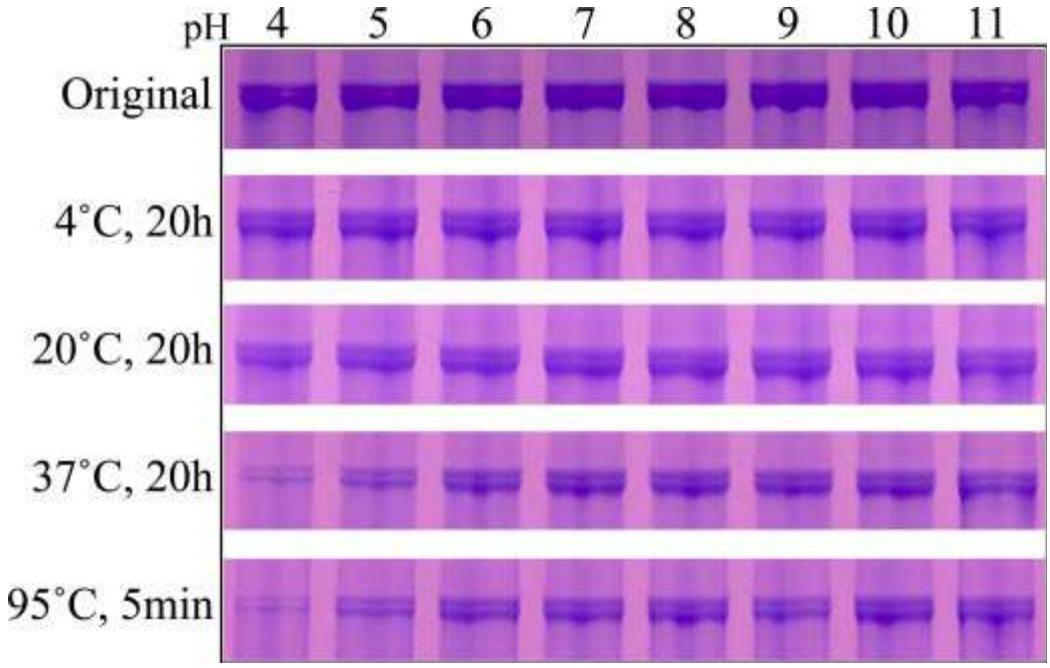

Fig A.6. Instability of DPP at low pH and high T. SDS-PAGE of DPP bands stained with Stains-all that have been incubated at the pH shown at the top and the temperature and length of time shown on the left. DPP is particularly unstable if heated at low pH.

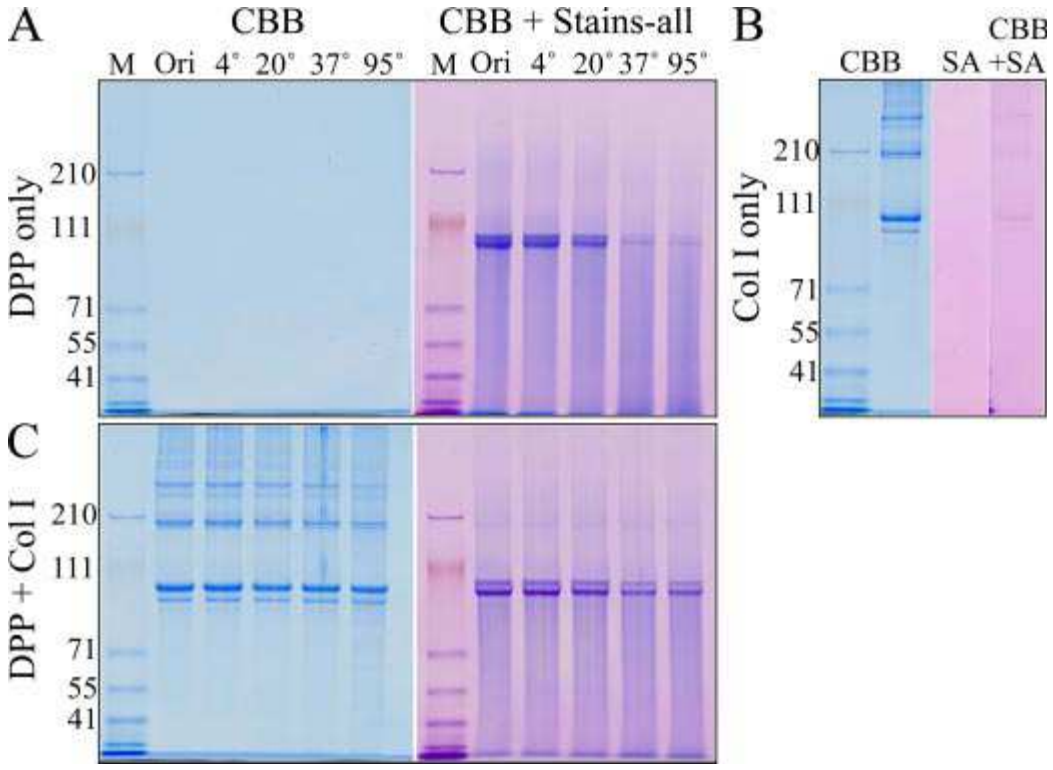

Fig A.7. Collagen-DPP interactions increase the stability of DPP and induce collagen fibril assembly. *A.* SDS-PAGE stained with CBB or CBB plus Stains-all. DPP does not stain with CBB but can be visualized with Stains-all. DPP is not stable when incubated below pH 6 at higher T. *B.* SDS-PAGE showing type I collagen (Col I). Col I stains with CBB but does not stain with Stains-all (SA) only. *C.* SDS-PAGE of Col I and DPP after being mixed together and incubated at 4˚, 20˚, 37˚, or 95 ˚C. The presence of collagen reduces the instability of DPP at 37 and 95 ˚C.

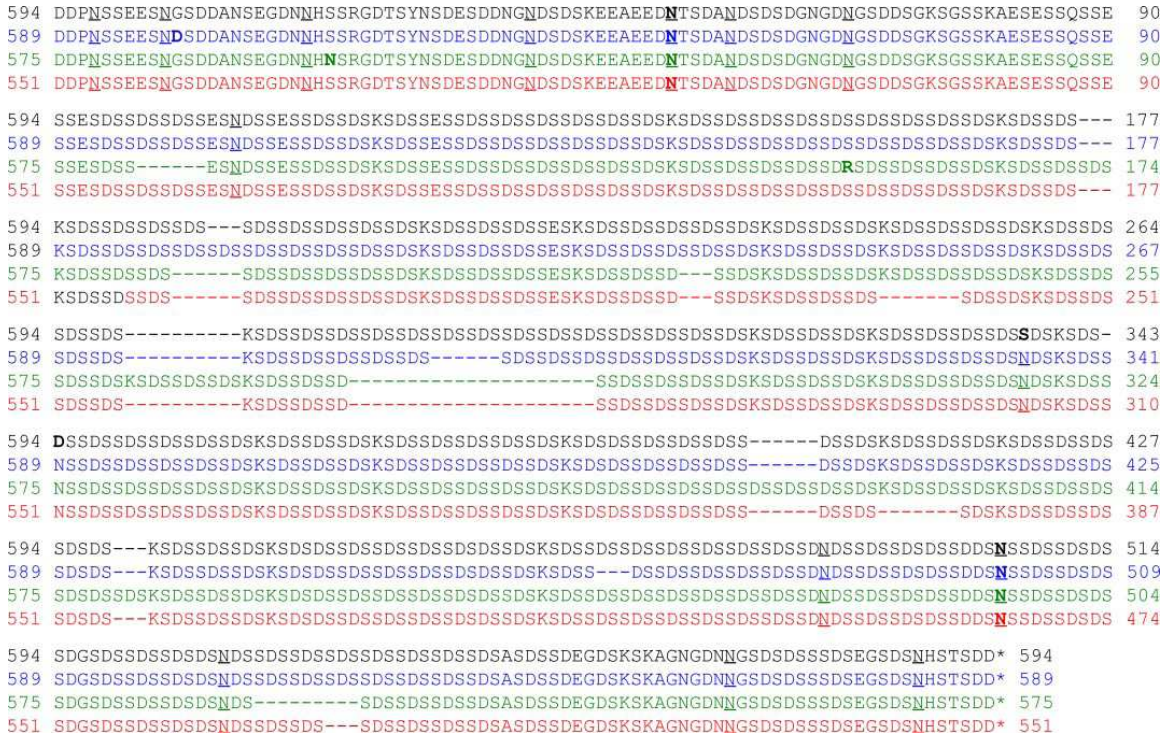

Fig. A.8. Alignment of the DPP deduced amino acid sequences of four porcine DSPP alleles. $pDSPP_{1066}/DPP_{594}$ (black), $pDSPP_{1061}/DPP_{589}$ (blue), $pDSPP_{1047}/DPP_{575}$ (green) and $pDSPP_{1023}/DPP_{551}$, (red) were aligned together. Key: The five amino acid substitutions are in bold. Asparagines (N) in the appropriate context for glycosylation are underlined. Asparagines determined to be glycosylated following pronase digestions of DPP in bold and underlined.

Table A. 1 Moles of phosphate per mole of DPP

All values based upon 100 kDa/molecule.

Pig	IP	P-Ser	Ave	Pig	IP	P-Ser	Ave
A	217	199	208	L	254	211	233
B	227	184	206	M	217	180	199
C	218	198	208	N	229	184	207
D	202	189	196	O	215	193	204
E	234	192	213	P	235	183	209
F	246	203	225	Q	206	175	191
G	255	196	226	R	262	202	232
H	203	181	192	S	252	228	240
I	272	177	225	T	251	237	244
J	231	156	194	U	216	185	201
K	249	167	208	V	221	194	208
Total	2554	2042	2298	Total	2558	2172	2365
Ave	232	186	209	Ave	233	197	215

Table A.2 N-terminal sequences of 6 pronase-generated DPP peptides

Pr-DPP	Sequence	Positions[a]	*N*-glycan
1	DDFNXXE	458–464	–
2	SKEEAE	502–508	+
3	AEEDXTSD	506–513	+
4	SDDSXS	918–924	+
5	SDES	490–494	–
6	DSASD	965–969	–

[a] Numbering for DSPP allele $pDSPP_{1025}$

References

1. Yamakoshi, Y., Hu, J. C., Fukae, M., Iwata, T., Kim, J. W., Zhang, H., and Simmer, J. P. (2005) *J Biol Chem* **280**(2), 1552-1560
2. Yamakoshi, Y., Hu, J. C., Fukae, M., Zhang, H., and Simmer, J. P. (2005) *J Biol Chem* **280**(17), 17472-17479
3. Butler, W. T., Bhown, M., DiMuzio, M. T., Cothran, W. C., and Linde, A. (1983) *Arch Biochem Biophys* **225**(1), 178-186
4. Huq, N. L., Cross, K. J., Talbo, G. H., Riley, P. F., Loganathan, A., Crossley, M. A., Perich, J. W., and Reynolds, E. C. (2000) *J Dent Res* **79**(11), 1914-1919
5. Butler, W. T., Bhown, M., Dimuzio, M. T., and Linde, A. (1981) *Coll Relat Res* **1**(2), 187-199
6. Butler, W. T. (1998) *Eur J Oral Sci* **106**(Suppl 1), 204-210
7. Patel, P. (2001) *Nat Genet* **27**(2), 129-130
8. MacDougall, M., Simmons, D., Luan, X., Nydegger, J., Feng, J., and Gu, T. T. (1997) *J Biol Chem* **272**(2), 835-842
9. Qin, C., Brunn, J. C., Baba, O., Wygant, J. N., McIntyre, B. W., and Butler, W. T. (2003) *Eur J Oral Sci* **111**(3), 235-242
10. Kim, J. W., and Simmer, J. P. (2007) *J Dent Res* **86**(5), 392-399
11. Hart, P. S., and Hart, T. C. (2007) *Cells Tissues Organs* **186**(1), 70-77
12. Sreenath, T., Thyagarajan, T., Hall, B., Longenecker, G., D'Souza, R., Hong, S., Wright, J. T., MacDougall, M., Sauk, J., and Kulkarni, A. B. (2003) *J Biol Chem* **278**(27), 24874-24880.

13. Xiao, S., Yu, C., Chou, X., Yuan, W., Wang, Y., Bu, L., Fu, G., Qian, M., Yang, J., Shi, Y., Hu, L., Han, B., Wang, Z., Huang, W., Liu, J., Chen, Z., Zhao, G., and Kong, X. (2001) *Nat Genet* **27**(2), 201-204
14. Malmgren, B., Lindskog, S., Elgadi, A., and Norgren, S. (2004) *Hum Genet* **114**(5), 491-498
15. Kim, J. W., Nam, S. H., Jang, K. T., Lee, S. H., Kim, C. C., Hahn, S. H., Hu, J. C., and Simmer, J. P. (2004) *Hum Genet* **115**(3), 248-254
16. Kim, J. W., Hu, J. C., Lee, J. I., Moon, S. K., Kim, Y. J., Jang, K. T., Lee, S. H., Kim, C. C., Hahn, S. H., and Simmer, J. P. (2005) *Hum Genet* **116**(3), 186-191
17. Holappa, H., Nieminen, P., Tolva, L., Lukinmaa, P. L., and Alaluusua, S. (2006) *Eur J Oral Sci* **114**(5), 381-384
18. Song, Y., Wang, C., Peng, B., Ye, X., Zhao, G., Fan, M., Fu, Q., and Bian, Z. (2006) *Oral Surg Oral Med Oral Pathol Oral Radiol Endod* **102**(3), 360-374
19. Zhang, X., Chen, L., Liu, J., Zhao, Z., Qu, E., Wang, X., Chang, W., Xu, C., Wang, Q. K., and Liu, M. (2007) *BMC Med Genet* **8**, 52
20. Ritchie, H. H., Hou, H., Veis, A., and Butler, W. T. (1994) *J Biol Chem* **269**(5), 3698-3702
21. Yamakoshi, Y., Hu, J. C., Liu, S., Zhang, C., Oida, S., Fukae, M., and Simmer, J. P. (2003) *Eur J Oral Sci* **111**(1), 60-67
22. Dong, J., Gu, T., Jeffords, L., and MacDougall, M. (2005) *Am J Med Genet* **132**(3), 305-309
23. Qin, C., Baba, O., and Butler, W. T. (2004) *Crit Rev Oral Biol Med* **15**(3), 126-136

24. Yamakoshi, Y., Hu, J. C., Iwata, T., Kobayashi, K., Fukae, M., and Simmer, J. P. (2006) *J Biol Chem* **281**(50), 38235-28243

25. Ibaraki, K., Shimokawa, H., and Sasaki, S. (1991) *Matrix* **11**(2), 115-124

26. Jonsson, M., and Fredriksson, S. (1978) *J Chromatogr* **157**, 234-242

27. Termine, J. D., Belcourt, A. B., Miyamoto, M. S., and Conn, K. M. (1980) *J Biol Chem* **255**(20), 9769-9772

28. Chang, S. R., Chiego, D., Jr., and Clarkson, B. H. (1996) *Calcif Tissue Int* **59**(3), 149-153

29. George, A., Bannon, L., Sabsay, B., Dillon, J. W., Malone, J., Veis, A., Jenkins, N. A., Gilbert, D. J., and Copeland, N. G. (1996) *J Biol Chem* **271**(51), 32869-32873

30. Gu, K., Chang, S., Ritchie, H. H., Clarkson, B. H., and Rutherford, R. B. (2000) *Eur J Oral Sci* **108**(1), 35-42

31. Hansen, J. C., Lu, X., Ross, E. D., and Woody, R. W. (2006) *J Biol Chem* **281**(4), 1853-1856

32. Yamakoshi, Y. (in press) *J Oral Biosciences*

33. Cross, K. J., Huq, N. L., and Reynolds, E. C. (2005) *J Pept Res* **66**(2), 59-67

34. Thomas, L. J., Panneerselvam, K., Beattie, D. T., Picard, M. D., Xu, B., Rittershaus, C. W., Marsh, H. C., Jr., Hammond, R. A., Qian, J., Stevenson, T., Zopf, D., and Bayer, R. J. (2004) *Glycobiology* **14**(10), 883-893

Appendix B

TRANGENIC RESCUE OF ENAMEL PHENOTYPE IN *AMBN* NULL MICE

Abstract

Ameloblastin null mice fail to make an enamel layer, but the defects could be due to an absence of functional ameloblastin or to the secretion of a potential toxic mutant ameloblastin. We hypothesized that the enamel phenotype could be rescued by the transgenic expression of normal ameloblastin in *Ambn*$^{-/-}$ mice. We established and analyzed five transgenic lines that expressed Ambn from the amelogenin (*AmelX*) promoter, and identified transgenic lines that express virtually no transgene, slightly less than normal (Tg+), somewhat higher than normal (Tg++), and much higher than normal (Tg+++) levels of ameloblastin. All lines expressing detectable levels of ameloblastin at least partially recovered the enamel phenotype. When ameloblastin expression was only somewhat higher than normal, the enamel covering the molars and incisors was of normal thickness, had clearly defined rod and interrod enamel, and held up well in function. We conclude that ameloblastin is essential for dental enamel formation.

Introduction

Amelogenin is a secreted enamel matrix protein that is expressed by ameloblasts starting just before the initial mineralization of dentin and terminating early in the maturation stage (Bronckers et al., 1993; Hu et al., 2001a; Inai et al., 1991; Wakida et al., 1999; Wurtz et al., 1996). Amelogenin is the most abundant protein in developing enamel (Fincham et al., 1999a), indicating that it is transcribed from a strong promoter. Amelogenin is predominantly expressed by ameloblasts, although trace expression has been reported in other tissues (Gruenbaum-Cohen et al., 2009). Mutations in *AMELX* cause X-linked amelogenesis imperfecta (AI), an inherited condition featuring "isolated" or "non-syndromic" enamel malformations, that is, having no defects outside of the dentition (Bailleul-Forestier et al., 2008; Hu et al., 2007). Vertebrates, such as birds, that have lost the ability to develop teeth during evolution, no longer encode a viable amelogenin gene (Sire et al., 2008). The strength and tissue-specificity of the amelogenin promoter make it an ideal choice to direct expression of transgenes in ameloblasts.

The mouse amelogenin (*AmelX*) 5' transcriptional regulatory region has been successfully used to drive transgenic expression specifically in ameloblasts (Paine and Snead, 2005; Snead et al., 1996; Snead et al., 1998a; Wen et al., 2008a). A 3.5 kb fragment of bovine *AmelX* 5' regulatory region up to and including part of exon 1 directed the expression of ß-galactosidase in ameloblasts, while a 5.5 kb segment of bovine *AmelX* expanded to include intron 1 and part of exon 2 directed expression of an amelogenin transgene in mouse ameloblasts (Gibson et al., 2007), which partially rescued the enamel phenotype in *AmelX* null mice (Li et al., 2008b). Transgenic expression of rat

ameloblastin by ameloblasts was successful using 2.3 kb of mouse *AmelX* promoter sequence (Paine et al., 2003) and human biglycan was expressed in ameloblasts after expanding the mouse *AmelX* promoter to include intron 1 (Wen et al., 2008a). These studies indicate that the *AmelX* promoter can direct the expression of transgenes by ameloblasts in a pattern that mimics the normal expression of enamel proteins during tooth development.

Ameloblastin (Ambn) is an enamel matrix protein that is co-secreted with amelogenin by ameloblasts during enamel formation (Zalzal et al., 2008). *AmelX* and *Ambn* are members of the secretory calcium binding phosphoprotein (SCPP) family and evolved from a common ancestral gene (Delgado et al., 2001; Kawasaki and Weiss, 2003). Ameloblastin expression is enamel-specific (Krebsbach et al., 1996; Lee et al., 1996). *Ambn* is reduced to a pseudogene in whales that evolved alternatives to teeth (Demere et al., 2008). *Ambn*$^{-/-}$ mice exhibit a non-syndromic AI phenotype (Fukumoto et al., 2004). Currently, no *AMBN* mutations have been identified in persons with amelogenesis imperfecta, although *AMBN* mutational analyses have been performed on dozens of probands from AI kindreds.

Mice normally secrete two ameloblastin isoforms, having 381 or 396 amino acids. The two isoforms differ by the alternative mRNA splicing of 15 codons at the beginning of exon 6 (Hu et al., 1997a). The best evidence that ameloblastin is essential for dental enamel formation comes from the absence of normal enamel in *Ambn*$^{-/-}$ mice (Fukumoto et al., 2004). However, the *Ambn* knockout construct deleted exons 5 and 6 and resulted in the expression of an ameloblastin protein having 279 amino acids (missing 102 or 117 amino acids depending upon the isoform) (Wazen et al., 2009). The expression of

truncated amelogenins by ameloblasts, even in the presence of normal amelogenin expression, induced enamel malformations in transgenic mice (Paine et al., 2000). Therefore, the enamel phenotype in *Ambn*$^{-/-}$ mice might be due to the absence of functional ameloblastin and/or to a negative effect caused by secretion of the mutant ameloblastin protein (Smith et al., 2009; Wazen et al., 2009). If the phenotype is caused predominantly by the lack of functional ameloblastin, we hypothesize that the enamel phenotype in *Ambn*$^{-/-}$ mice should be rescued by transgenic expression of normal ameloblastin by ameloblasts. We tested this hypothesis with a transgene that drives expression of the mouse ameloblastin 396 amino acid isoform from the mouse amelogenin promoter in *Ambn*$^{-/-}$ mice.

Material and Methods

Protocol Approval. Animal protocols were reviewed and approved by the University of Michigan Institutional Animal Care and Use Committee.

Fabricating the *Ambn* Transgene. We sacrificed C57BL/6 mice on Post-Natal day 5 (PN5) and removed the developing first molars by dissection under a stereoscopic microscope. Total RNA was extracted using Trizol (Invitrogen, Carlsbad, CA, USA) and chloroform, converted into cDNA with SuperScript II reverse transcriptase (Invitrogen), and used as template to amplify *Ambn* transcripts by polymerase chain reaction (PCR). We isolated genomic DNA from the tail tissues of C57BL/6 mice with the DNeasy Tissue kit (Qiagen, Valencia, CA) and used it as template to amplify 5' and 3' *AmelX* sequences. The amplification products were ligated into the pCR2.1-TOPO cloning vector (Invitrogen), transfected into bacteria, and selected for by ampicillin resistance. The

orientation of the inserts were determined by restriction analyses of DNA mini-preps. Clones with their 5' ends on the *NotI* side of the multiple cloning site were characterized by DNA sequencing and used to fabricate the *Ambn* transgene (see on-line appendix for details).

Generation of *Ambn* Transgenic Mice and Breeding with *Ambn*$^{-/-}$ Mice. The 7.5 kb *Ambn* transgene was excised from the vector by restriction digestion with *Not*I-*Srf*I purified with a Qiaquick gel extraction kit (Qiagen, Germantown, Md., USA) and microinjected into fertilized C57BL/6 X SJL F2 oocytes and surgically transferred to recipients at the Transgenic Animal Model Core at the University of Michigan. A total of 17 independent lines were generated and mated with C57BL/6 mice. Germline transmission was determined by PCR analysis of genomic DNA obtained from tail biopsies. Offspring carrying the *Ambn* transgene (Tg) were mated with *Ambn*$^{-/-}$ mice (Fukumoto et al., 2004). F1 offspring positive for the transgene and heterozygous for ameloblastin (*Ambn*$^{+/-}$) were mated, yielding four genotypes in the F2 generation (Suppl. Fig. B.1A). Tail biopsies were analyzed by PCR using primers specific for the *Ambn* Tg, wild-type *Ambn*, or the *Ambn* knockout gene.

Assessing *Ambn* Tg Expression Levels By Western Blotting. To obtain an antibody that would specifically recognize the ameloblastin protein expressed from the wild-type gene and the ameloblastin transgene, but not the smaller mutant ameloblastin expressed from the *Ambn* knockout gene, rabbit antibodies were raised against the KLH-conjugated peptide MRPREHETQQYEYS, which is encoded by the exon 5-6 region deleted in the ameloblastin knockout. Specific anti-peptide antibodies were purified from the final bleed

using an affinity column containing the immobilized, unconjugated ameloblastin peptide and designated Ambn-89 (YenZym, Burlingame, CA).

Tg Expression Assessment by Western Blotting. *Ambn*$^{+/+}$ mice and a litter from the F2 generation were terminated on PN5. The first molars were surgically extracted under a dissecting microscope and the soft-tissue removed. Tails were collected for PCR genotyping. The hard tissues from a maxillary and a mandibular first molars were incubated in 1 mL of 0.5% formic acid at 4 ˚C overnight, centrifuged briefly to remove residual insoluble material, and transferred to an Ultracel YM-3 filter (3 kDa cutoff, Millipore, Billerica, MA), centrifuged, and the enamel protein on the filter was raised in sample buffer, run on SDS-PAGE, transferred to a membrane, and ameloblastin bands were visualized by Western blotting.

Scanning Electron Microscopy (SEM) of Mandibular Incisors. The soft tissue was removed from left and right half-mandibles at 7 weeks. We measured the distances from the incisor tip to the labial alveolar crest and then extracted the incisors. We used a rotating diamond disc to cut through just the dentin (at the measured distance from the incisor tip) and fractured the incisor at the notch. SEM imaging of the broken surface highlights the decussating rods. The broken edge of the incisor was polished with a diamond disc and lightly etched with 0.1% nitric acid. The surface was sputter coated with gold and analyzed by SEM to determine enamel thickness.

Result

We introduced rare (8 bp) restriction sites at the edges of mouse *AmelX* 5' and 3' genomic sequences and the *Ambn* cDNA by PCR amplification, cloned the products, and fabricated an ameloblastin transgene construct. Multiple independent transgenic lines were evaluated for their levels of ameloblastin transgene expression (Fig. B.1A.) We identified transgenic lines that express virtually no transgene, slightly less than normal (Tg+), somewhat higher than normal (Tg++), and much higher than normal (Tg+++) levels of ameloblastin and then compared their gross enamel phenotypes (Fig. 1B). Whenever detectable levels of ameloblastin protein was expressed in the *Ambn*$^{-/-}$ background, the enamel phenotype was at least partially recovered. In the case where the ameloblastin transgene expression was only somewhat higher than normal (Tg++), the enamel covering the molars and incisors appeared identical to that of the wild-type. Transgenic mice with a high level of ameloblastin expression (Tg+++) displayed chalky white mandibular incisors, suggesting that there is a range of ameloblastin expression that is optimal for dental enamel formation (Fig. B.1B). The mandibular incisors were extracted and examined under a dissecting microscope. The enamel layer of the extracted mandibular incisor from the Tg++ mouse was analogous to the wild-type mouse along its entire length (Fig. B.2).

Mandibular incisors at 7 weeks were cut or fractured at the level of the labial alveolar bone crest and analyzed by scanning electron microscopy. The enamel thickness and decussating pattern of enamel rods was significantly recovered even with less than normal or much greater than normal expression of ameloblastin (Fig. B.3). Recovery was

most complete in the central region where the enamel forms earliest and reaches the greatest thickness. The area most sensitive to ameloblastin levels was the distal enamel surface, where low or high levels of ameloblastin expression resulted in reduced enamel thickness and a rough surface. The enamel thickness and rod patterns looked normal in the mouse expressing somewhat higher than normal (Tg++) levels of ameloblastin, although there seemed to be a lack of definition, which might be attributable to increased residual enamel protein.

Discussion

We designed and fabricated a plasmid construct with rare restriction enzyme sites positioned at key places to direct high levels transgenic expression of target proteins specifically in ameloblasts. This construct allows for one-step directional cloning of a desired coding sequence between the 5' and 3' sequences from *AmelX*, and is a useful vector for specifically expressing transgenic proteins in ameloblasts. Transgenic mice were generated so that ameloblasts secreted the 396 amino acid isoform of mouse ameloblastin. We characterize five transgenic lines and assessed ameloblastin protein levels in developing first molars at PN5. Two lines did not secrete detectable levels of ameloblastin. Three lines expressed progressively increasing amounts of ameloblastin, ranging from less than normal amounts to levels well above normal. The thickness of the enamel layer and the decussating pattern of enamel rod were assessed by SEM. The enamel phenotype varied in each of the transgenic lines. When no ameloblastin was expressed, there was no recovery of the enamel phenotype in *Ambn*$^{-/-}$ mice. There was partial recovery when ameloblastin expression was below normal (Tg+) or much greater

than normal (Tg+++), with the best recovery being in the central portion of the incisor enamel. Ameloblastin transgene expression at somewhat higher than normal levels (Tg++) showed full recovery of enamel thickness and rod architecture.

These results prove that the severe enamel phenotype in *Ambn*$^{-/-}$ mice is predominantly or entirely due to the absence of functional ameloblastin, and not due to toxic effects caused by secretion of the shortened 279 amino acid ameloblastin protein, which appears to be relatively inert, but might contribute to higher levels of residual protein in the rescued enamel. The recovery of the enamel phenotype in *Ambn*$^{-/-}$ by transgenic expression of functional ameloblastin confirms the previous conclusion that ameloblastin is essential for proper dental enamel formation and that *Ambn*$^{-/-}$ mice are a valid animal model to investigate the absence of functional ameloblastin on dental enamel formation.

We were surprised to observe so much variation in ameloblastin expression in the various transgenic lines. Clearly integration site and copy number have a profound effect on transgene expression levels in ameloblasts, and expression levels are a major determinant of how transgenic expression affects enamel formation. Interpretations of the affects on enamel formation of transgenic protein expression by ameloblasts are only meaningful in the context of transgenic protein expression levels in the matrix.

We used an anti-peptide antibody for this study that recognizes an epitope on the exon 5-exon 6 encoded portion of ameloblastin. This antibody specifically detected a 17-kDa ameloblastin cleavage product in mouse tooth extracts. A homologous 17-kDa ameloblastin cleavage product having this epitope was previously isolated from porcine enamel and characterized (Fukae et al., 2006). It consists of the ameloblastin N-terminal

region (Val^{1} to Arg^{170}) and is generated by Mmp-20 cleavage (Chun et al., submitted) of ameloblastin following its secretion. Despite its relatively small size, the 17-kDa ameloblastin cleavage product elutes in the first chromatographic peak on size exclusion columns, suggesting that the protein tends to aggregate (Fukae and Tanabe, 1987b). A ladder of immunopositive bands was observed on our Western blot of tooth proteins extracted from the transgenic line that over-expresses ameloblastin. These bands extend well above the apparent molecular weight of uncleaved ameloblastin (~65-kDa) and are likely to be aggregates of the 17-kDa ameloblastin cleavage product. Apparently Mmp-20 is able to process ameloblastin completely, even though significantly more ameloblastin than normal is being secreted by the ameloblastin transgene. When ameloblastin expression levels are highest, a smaller immunoreactive band appears below the 17-kDa band on the Western blot. The porcine 17-kDa ameloblastin is O-glycosylated (Kobayashi et al., 2007). We suspect that this smaller band is the unglycosylated form of the 17-kDa protein, and that excessive ameloblastin expression might allow some ameloblastin molecules to escape glycosylation.

The ameloblastin transgene was able to recover the thickness of the enamel layer as a whole, the decussating pattern enamel rods, and the overall appearance of normal enamel. SEM analysis of the incisor enamel that was fractured to highlight the decussating prism pattern, however, seemed to be less well-defined than the wild-type. This suggests that the enamel in the transgenic rescue might contain more residual protein than normal. Increased protein retention may be due to the expression of the 279 amino acid non-functional form of ameloblastin or to over-expression of the ameloblastin

transgene. Expression of the ameloblastin transgene in a total knockout might help distinguish among these explanations.

Figures and Legends

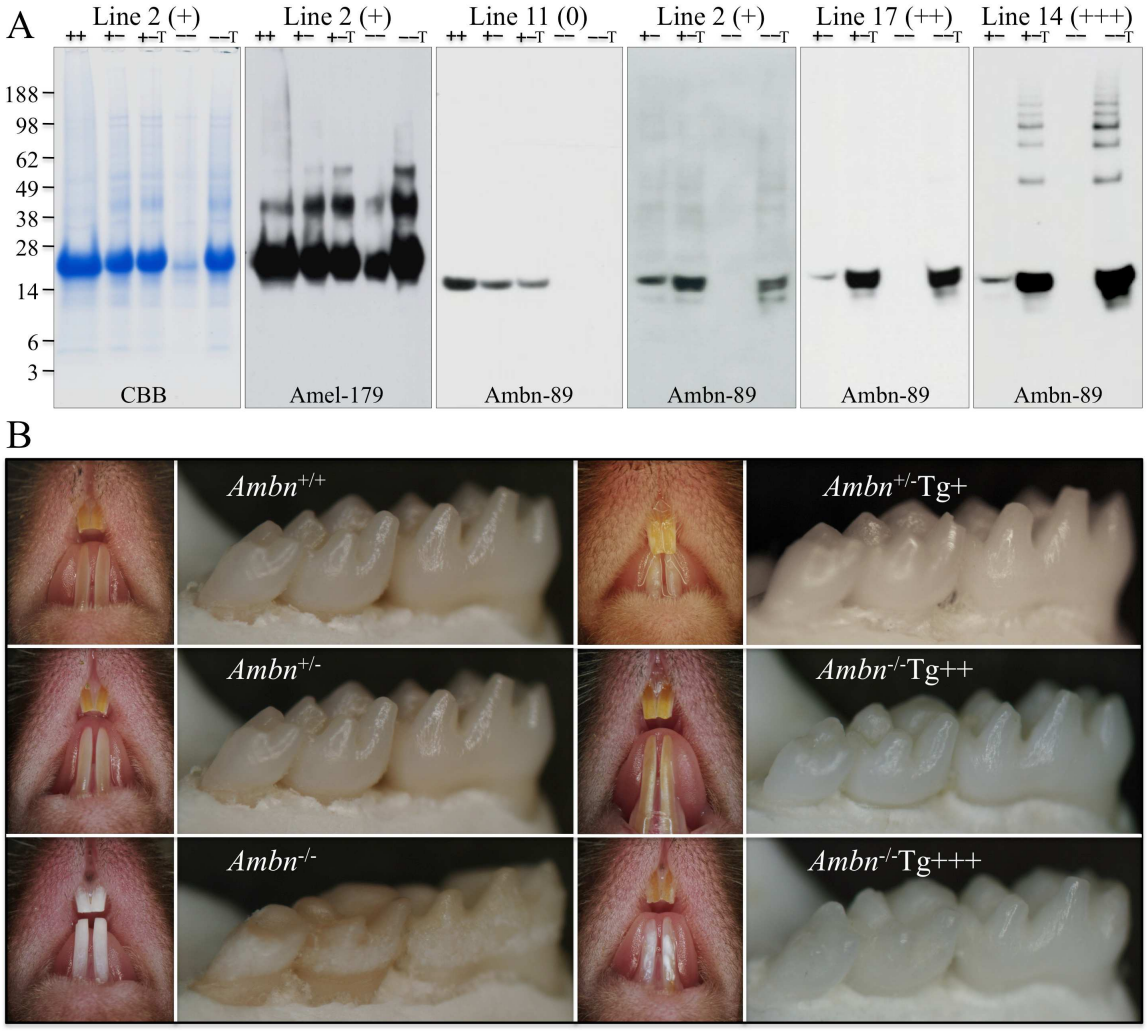

Figure B.1. Ameloblastin Expression Levels and Associated Enamel Phenotypes. ***A:*** SDS-PAGE stained with Coomassie brilliant blue (CBB), and Western blots immunostained using an antibody raised against recombinant mouse amelogenin (Amel-179), or against an ameloblastin peptide absent from the smaller ameloblastin expressed by the *Ambn* knockout (Ambn-89). The apparent molecular weights (in kDa) of protein bands in the samples are indicated on the left. Equal fractions of enamel proteins extracted from day 5 molars from *Ambn* wild-type (lanes ++), *Ambn* heterozygotes (lanes +-), *Ambn* heterozygotes expressing an ameloblastin transgene (lanes +-T), *Ambn* homozygous knockout mice (lanes --), and *Ambn* knockout mice expressing an ameloblastin transgene (lanes --T) were applied to each lane. The yield of enamel proteins from the $Ambn^{-/-}$ mice was always much lower than other samples because of the virtual absence of an enamel layer. Except for the wild-type (++) lanes, all samples on a single gel or blot are from littermates. The only ameloblastin band reacting against the Ambn-89 antibody migrates at 17-kDa. The ladder of immunopositive bands in Western for Line 14 is due to aggregation of the 17-kDa ameloblastin cleavage product when

loaded at the high concentrations expressed. ***B:*** Oral photographs at 7 weeks of the incisors *in situ* and a lingual view of molars following removal of soft tissue. The molars and incisors from the *Ambn*$^{-/-}$Tg++ mice held up to occlusal forces, did not chip or abrade, and could not be distinguished from teeth from wild-type mice. Apparent differences in the lengths of the mandibular incisors were due to variations in lip retraction.

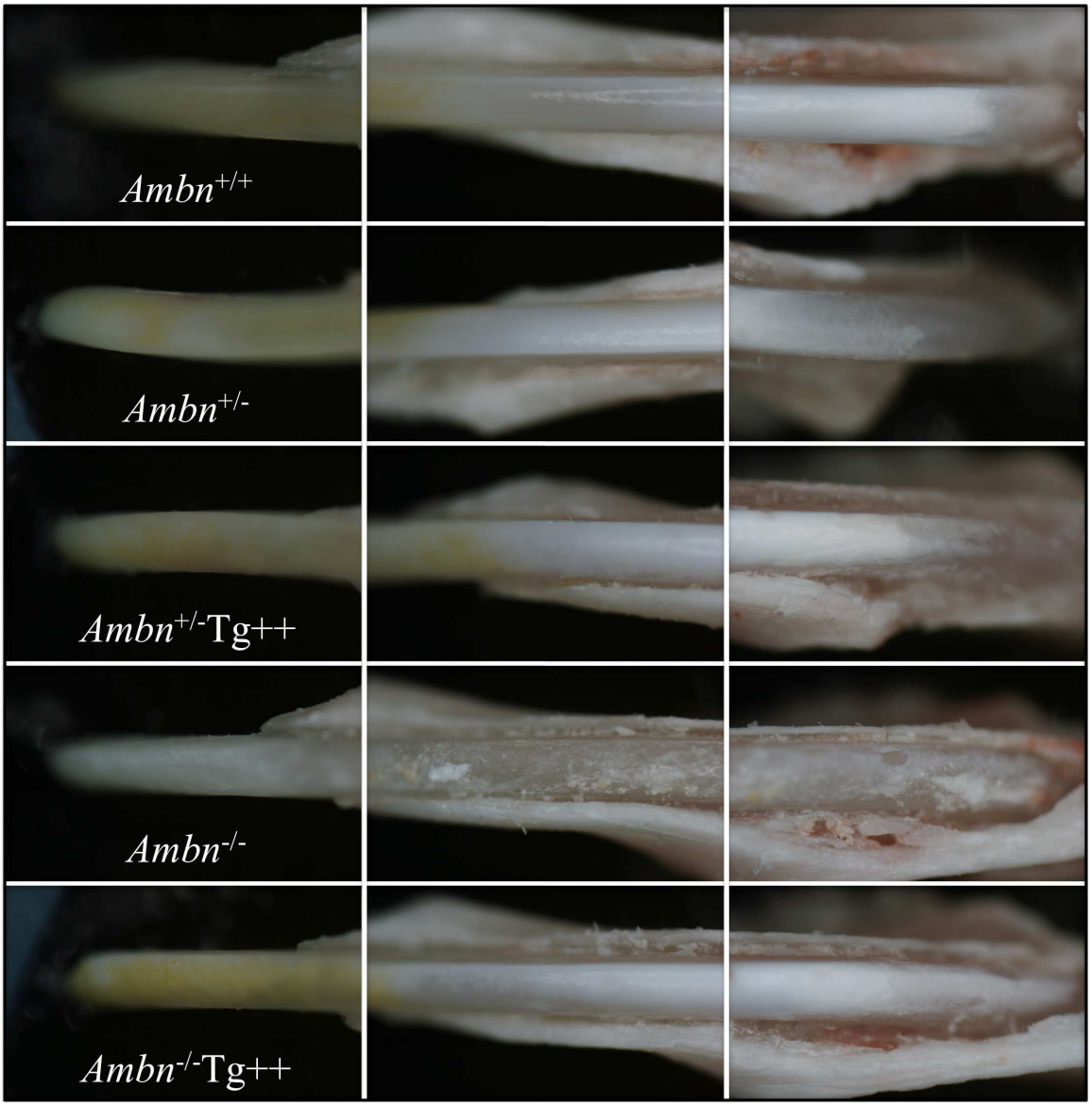

Figure B.2. Exposed Mandibular Incisors. These photos were taken through a dissecting microscope and show the labial surfaces of mandibular incisors at 7 weeks. The incisors from the transgenic line expressing somewhat higher than normal amounts of the ameloblastin transgene (Tg++) appeared similar to the wild-type when expressed in either the *Ambn* heterozygous or *Ambn* null mice.

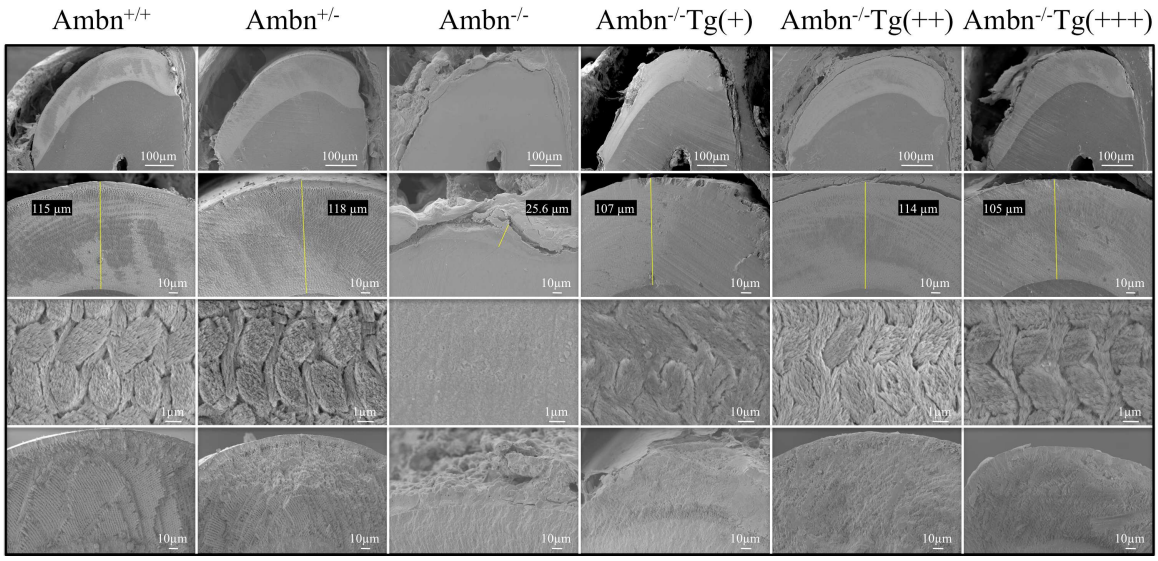

Figure B.3. Scanning Electron Micrographs of Mandibular Incisors at 9 Weeks. All images are of cross-sections obtained at the level of the buccal alveolar crest. *Row1:* Low magnification view of polished cross section showing the entire enamel layer. The *Ambn*$^{+/+}$ and *Ambn*$^{+/-}$ mice show no enamel defects. The *Ambn*$^{-/-}$ mice have no true enamel, but a thin, rough crust of mineral covers the surface of dentin. The enamel phenotype is recovered in the central region when ameloblastin transgenes provide less than (Tg+) and more than (Tg+++) optimal amounts of ameloblastin, but the distal enamel is thinner than normal and has a rough surface. *Row2:* Higher magnification view of polished enamel showing the enamel thickness in the central region. The line spanning the enamel layer is where measurements of enamel thickness were made. The enamel layer in the Tg++ mice was the same thickness as in the wild-type. *Row3:* High magnification of polished, cut, lightly etched enamel showing the underlying rod architecture. Only the *Ambn*$^{-/-}$ mice show a complete absence of enamel rods. Rod and interrod enamel are clearly distinguished in the Tg++ mice. *Row4:* The enamel layer after being fractured reveals the decussating pattern of enamel rods. Although a normal pattern of decussating enamel rods is evident in the mice expressing different levels of the ameloblastin transgene, the fractured surface of the mice expressing the smaller Ambn from the knockout gene was not as well defined as the wild-type, possibly due to an increased levels of residual enamel protein.

Reference

Aldred MJ, Crawford PJ (1995). Amelogenesis imperfecta--towards a new classification. *Oral Dis* 1(1)*:*2-5.

Aldred MJ, Savarirayan R, Crawford PJ (2003). Amelogenesis imperfecta: a classification and catalogue for the 21st century. *Oral Dis* 9(1)*:*19-23.

Bailleul-Forestier I, Molla M, Verloes A, Berdal A (2008). The genetic basis of inherited anomalies of the teeth. Part 1: clinical and molecular aspects of non-syndromic dental disorders. *Eur J Med Genet.* 51(4)*:*273-91.

Beniash E, Skobe Z, Bartlett JD (2006). Formation of the dentino-enamel interface in enamelysin (MMP-20)-deficient mouse incisors. *Eur J Oral Sci* 114 Suppl 1(24-9; discussion 39-41, 379.

Bouropoulos N, Moradian-Oldak J (2004). Induction of apatite by the cooperative effect of amelogenin and the 32-kDa enamelin. *J Dent Res* 83(4)*:*278-82.

Bronckers AL, D'Souza RN, Butler WT, Lyaruu DM, van Dijk S, Gay S, et al. (1993). Dentin sialoprotein: biosynthesis and developmental appearance in rat tooth germs in comparison with amelogenins, osteocalcin and collagen type-I. *Cell & Tissue Research* 272(2)*:*237-47.

Butler WT, Bhown M, Dimuzio MT, Linde A (1981). Nonocollagenous proteins of dentin. Isolation and partial characterization of rat dentin proteins and proteoglycans using a three-step preparative method. *Coll. Relat. Res.* 1(2)*:*187-99.

Butler WT, Bhown M, DiMuzio MT, Cothran WC, Linde A (1983). Multiple forms of rat dentin phosphoproteins. *Arch. Biochem. Biophys.* 225(1)*:*178-86.

Butler WT (1998). Dentin matrix proteins. *European Journal of Oral Sciences* 106(Suppl 1)*:*204-10.

Caterina JJ, Skobe Z, Shi J, Ding Y, Simmer JP, Birkedal-Hansen H, et al. (2002). Enamelysin (matrix metalloproteinase 20)-deficient mice display an amelogenesis imperfecta phenotype. *J Biol Chem* 277(51)*:*49598-604.

Chang SR, Chiego D, Jr., Clarkson BH (1996). Characterization and identification of a human dentin phosphophoryn. *Calcif. Tissue Int.* 59(3)*:*149-53.

Chen E, Yuan ZA, Wright JT, Hong SP, Li Y, Collier PM, et al. (2003). The small bovine amelogenin LRAP fails to rescue the amelogenin null phenotype. *Calcif Tissue Int* 73(5)*:*487-95.

Chun Y-HP, Yamakoshi Y, Yamakoshi F, Fukae M, Hu JC-C, Bartlett JD, et al. (submitted). Cleavage Site Specificity of Mmp-20 for Secretory Stage Ameloblastin. *J. Dent. Res.*

Cross KJ, Huq NL, Reynolds EC (2005). Protein dynamics of bovine dentin phosphophoryn. *J Pept Res* 66(2)*:*59-67.

Daculsi G, Kerebel B (1978). High-resolution electron microscope study of human enamel crystallites: size, shape, and growth. *J Ultrastruct Res* 65(2)*:*163-72.

Delgado S, Casane D, Bonnaud L, Laurin M, Sire JY, Girondot M (2001). Molecular evidence for precambrian origin of amelogenin, the major protein of vertebrate enamel. *Mol Biol Evol* 18(12)*:*2146-53.

Demere TA, McGowen MR, Berta A, Gatesy J (2008). Morphological and molecular evidence for a stepwise evolutionary transition from teeth to baleen in mysticete whales. *Syst Biol* 57(1)*:*15-37.

Dong J, Gu T, Jeffords L, MacDougall M (2005). Dentin phosphoprotein compound mutation in dentin sialophosphoprotein causes dentinogenesis imperfecta type III. *Am. J. Med. Genet.* 132(3)*:*305-9.

Fincham AG, Moradian-Oldak J, Simmer JP (1999a). The structural biology of the developing dental enamel matrix. *J. Struct. Biol.* 126(3)*:*270-299.

Fincham AG, Moradian-Oldak J, Simmer JP (1999b). The structural biology of the developing dental enamel matrix. *J Struct Biol* 126(3)*:*270-99.

Fukae M, Tanabe T (1987a). Nonamelogenin components of porcine enamel in the protein fraction free from the enamel crystals. *Calcif Tissue Int* 40(5)*:*286-93.

Fukae M, Tanabe T (1987b). Nonamelogenin components of porcine enamel in the protein fraction free from the enamel crystals. *Calcif. Tissue Int.* 40(5)*:*286-293.

Fukae M, Tanabe T, Murakami C, Dohi N, Uchida T, Shimizu M (1996). Primary structure of the porcine 89-kDa enamelin. *Adv Dent Res* 10(2)*:*111-8.

Fukae M, Kanazashi M, Nagano T, Tanabe T, Oida S, Gomi K (2006). Porcine sheath proteins show periodontal ligament regeneration activity. *Eur J Oral Sci* 114 Suppl 1(212-8.

Fukumoto S, Kiba T, Hall B, Iehara N, Nakamura T, Longenecker G, et al. (2004). Ameloblastin is a cell adhesion molecule required for maintaining the differentiation state of ameloblasts. *J Cell Biol* 167(5)*:*973-83.

George A, Bannon L, Sabsay B, Dillon JW, Malone J, Veis A, et al. (1996). The carboxyl-terminal domain of phosphophoryn contains unique extended triplet amino acid repeat sequences forming ordered carboxyl-phosphate interaction ridges that may be essential in the biomineralization process. *J. Biol. Chem.* 271(51)*:*32869-32873.

Gibson CW, Yuan ZA, Hall B, Longenecker G, Chen E, Thyagarajan T, et al. (2001). Amelogenin-deficient mice display an amelogenesis imperfecta phenotype. *J Biol Chem* 276(34)*:*31871-5.

Gibson CW, Yuan ZA, Li Y, Daly B, Suggs C, Aragon MA, et al. (2007). Transgenic mice that express normal and mutated amelogenins. *J Dent Res.* 86(4)*:*331-5.

Gibson CW, Li Y, Daly B, Suggs C, Yuan ZA, Fong H, et al. (2009). The leucine-rich amelogenin peptide alters the amelogenin null enamel phenotype. *Cells Tissues Organs* 189(1-4)*:*169-74.

Gruenbaum-Cohen Y, Tucker AS, Haze A, Shilo D, Taylor AL, Shay B, et al. (2009). Amelogenin in cranio-facial development: the tooth as a model to study the role of amelogenin during embryogenesis. *J Exp Zool B Mol Dev Evol.* 312B(5)*:*445-57.

Gu K, Chang S, Ritchie HH, Clarkson BH, Rutherford RB (2000). Molecular cloning of a human dentin sialophosphoprotein gene. *Eur. J. Oral Sci.* 108(1)*:*35-42.

Gutierrez SJ, Chaves M, Torres DM, Briceno I (2007). Identification of a novel mutation in the enamelin gene in a family with autosomal-dominant amelogenesis imperfecta. *Arch Oral Biol* 52(5)*:*503-6.

Hansen JC, Lu X, Ross ED, Woody RW (2006). Intrinsic protein disorder, amino acid composition, and histone terminal domains. *J Biol Chem* 281(4)*:*1853-6.

Hart PS, Michalec MD, Seow WK, Hart TC, Wright JT (2003a). Identification of the enamelin (g.8344delG) mutation in a new kindred and presentation of a standardized ENAM nomenclature. *Arch Oral Biol* 48(8)*:*589-96.

Hart PS, Hart TC (2007). Disorders of human dentin. *Cells Tissues Organs* 186(1)*:*70-7.

Hart TC, Hart PS, Gorry MC, Michalec MD, Ryu OH, Uygur C, et al. (2003b). Novel ENAM mutation responsible for autosomal recessive amelogenesis imperfecta and localised enamel defects. *J Med Genet* 40(12)*:*900-6.

Holappa H, Nieminen P, Tolva L, Lukinmaa PL, Alaluusua S (2006). Splicing site mutations in dentin sialophosphoprotein causing dentinogenesis imperfecta type II. *Eur. J. Oral Sci.* 114(5)*:*381-4.

Houzelstein D, Cohen A, Buckingham ME, Robert B (1997). Insertional mutation of the mouse Msx1 homeobox gene by an nlacZ reporter gene. *Mech Dev* 65(1-2)*:*123-33.

Hu CC, Fukae M, Uchida T, Qian Q, Zhang CH, Ryu OH, et al. (1997a). Sheathlin: cloning, cDNA/polypeptide sequences, and immunolocalization of porcine enamel sheath proteins. *J Dent Res* 76(2)*:*648-57.

Hu CC, Fukae M, Uchida T, Qian Q, Zhang CH, Ryu OH, et al. (1997b). Cloning and characterization of porcine enamelin mRNAs. *J Dent Res* 76(11)*:*1720-9.

Hu CC, Simmer JP, Bartlett JD, Qian Q, Zhang C, Ryu OH, et al. (1998). Murine enamelin: cDNA and derived protein sequences. *Connect Tissue Res* 39(1-3)*:*47-61; discussion 63-7.

Hu JC, Sun X, Zhang C, Simmer JP (2001a). A comparison of enamelin and amelogenin expression in developing mouse molars. *Eur. J. Oral Sci.* 109(2)*:*125-132.

Hu JC, Zhang CH, Yang Y, Karrman-Mardh C, Forsman-Semb K, Simmer JP (2001b). Cloning and characterization of the mouse and human enamelin genes. *J Dent Res* 80(3)*:*898-902.

Hu JC, Sun X, Zhang C, Liu S, Bartlett JD, Simmer JP (2002). Enamelysin and kallikrein-4 mRNA expression in developing mouse molars. *Eur J Oral Sci* 110(4)*:*307-15.

Hu JC, Yamakoshi Y (2003). Enamelin and autosomal-dominant amelogenesis imperfecta. *Crit Rev Oral Biol Med* 14(6)*:*387-98.

Hu JC, Yamakoshi Y, Yamakoshi F, Krebsbach PH, Simmer JP (2005). Proteomics and genetics of dental enamel. *Cells Tissues Organs* 181(3-4)*:*219-31.

Hu JC, Chun YH, Al Hazzazzi T, Simmer JP (2007). Enamel formation and amelogenesis imperfecta. *Cells Tissues Organs* 186(1)*:*78-85.

Hu JC, Hu Y, Smith CE, McKee MD, Wright JT, Yamakoshi Y, et al. (2008). Enamel defects and ameloblast-specific expression in Enam knock-out/lacz knock-in mice. *J Biol Chem* 283(16)*:*10858-71.

Huq NL, Cross KJ, Talbo GH, Riley PF, Loganathan A, Crossley MA, et al. (2000). N-terminal sequence analysis of bovine dentin phosphophoryn after conversion of phosphoseryl to S-propylcysteinyl residues. *J. Dent. Res.* 79(11)*:*1914-1919.

Ibaraki K, Shimokawa H, Sasaki S (1991). An analysis of the biochemical and biosynthetic properties of dentin phosphoprotein. *Matrix* 11(2)*:*115-24.

ibarPatel P (2001). Soundbites. *Nat Genet* 27(2)*:*129-30.

Inai T, Kukita T, Ohsaki Y, Nagata K, Kukita A, Kurisu K (1991). Immunohistochemical demonstration of amelogenin penetration toward the dental pulp in the early stages of ameloblast development in rat molar tooth germs. *Anat. Rec.* 229(259-270.

Jonsson M, Fredriksson S (1978). Isoelectric focusing of the phosphoprotein of rat-incisor dentin in ampholine and acid pH gradients. Evidence for carrier ampholyte-protein complexes. *J Chromatogr* 157(234-42.

Kang HY, Seymen F, Lee SK, Yildirim M, Tuna EB, Patir A, et al. (2009). Candidate gene strategy reveals ENAM mutations. *J Dent Res* 88(3)*:*266-9.

Karrman C, Backman B, Dixon M, Holmgren G, Forsman K (1997). Mapping of the locus for autosomal dominant amelogenesis imperfecta (AIH2) to a 4-Mb YAC contig on chromosome 4q11-q21. *Genomics* 39(2)*:*164-70.

Kawasaki K, Weiss KM (2003). Mineralized tissue and vertebrate evolution: the secretory calcium-binding phosphoprotein gene cluster. *Proc Natl Acad Sci U S A* 100(7)*:*4060-5.

Kida M, Ariga T, Shirakawa T, Oguchi H, Sakiyama Y (2002). Autosomal-dominant hypoplastic form of amelogenesis imperfecta caused by an enamelin gene mutation at the exon-intron boundary. *J Dent Res* 81(11)*:*738-42.

Kim JW, Nam SH, Jang KT, Lee SH, Kim CC, Hahn SH, et al. (2004). A novel splice acceptor mutation in the DSPP gene causing dentinogenesis imperfecta type II. *Hum. Genet.* 115(3)*:*248-54.

Kim JW, Hu JC, Lee JI, Moon SK, Kim YJ, Jang KT, et al. (2005a). Mutational hot spot in the DSPP gene causing dentinogenesis imperfecta type II. *Hum. Genet.* 116(3)*:*186-91.

Kim JW, Seymen F, Lin BP, Kiziltan B, Gencay K, Simmer JP, et al. (2005b). ENAM mutations in autosomal-dominant amelogenesis imperfecta. *J Dent Res* 84(3)*:*278-82.

Kim JW, Simmer JP (2007). Hereditary dentin defects. *J. Dent. Res.* 86(5)*:*392-9.

Kobayashi K, Yamakoshi Y, Hu JC, Gomi K, Arai T, Fukae M, et al. (2007). Splicing determines the glycosylation state of ameloblastin. *J Dent Res* 86(10)*:*962-7.

Krebsbach PH, Lee SK, Matsuki Y, Kozak CA, Yamada K, Yamada Y (1996). Full-length sequence, localization, and chromosomal mapping of ameloblastin: a novel tooth-specific gene. *J. Biol. Chem.* 271(8)*:*4431-4435.

Lee SK, Krebsbach PH, Matsuki Y, Nanci A, Yamada KM, Yamada Y (1996). Ameloblastin expression in rat incisors and human tooth germs. *Int. J. Dev. Biol.* 40(6)*:*1141-1150.

Li Y, Suggs C, Wright JT, Yuan ZA, Aragon M, Fong H, et al. (2008a). Partial rescue of the amelogenin null dental enamel phenotype. *J Biol Chem* 283(22)*:*15056-62.

Li Y, Suggs C, Wright JT, Yuan ZA, Aragon M, Fong H, et al. (2008b). Partial rescue of the amelogenin null dental enamel phenotype. *J Biol Chem.* 283(22)*:*15056-62. Epub 2008 Apr 3.

Lu Y, Ye L, Yu S, Zhang S, Xie Y, McKee MD, et al. (2007). Rescue of odontogenesis in Dmp1-deficient mice by targeted re-expression of DMP1 reveals roles for DMP1 in early odontogenesis and dentin apposition in vivo. *Dev Biol* 303(1)*:*191-201.

MacDougall M, Simmons D, Luan X, Nydegger J, Feng J, Gu TT (1997). Dentin phosphoprotein and dentin sialoprotein are cleavage products expressed from a single transcript coded by a gene on human chromosome 4. Dentin phosphoprotein DNA sequence determination. *J. Biol. Chem.* 272(2)*:*835-42.

Malmgren B, Lindskog S, Elgadi A, Norgren S (2004). Clinical, histopathologic, and genetic investigation in two large families with dentinogenesis imperfecta type II. *Hum. Genet.* 114(5)*:*491-8.

Mardh CK, Backman B, Holmgren G, Hu JC, Simmer JP, Forsman-Semb K (2002). A nonsense mutation in the enamelin gene causes local hypoplastic autosomal dominant amelogenesis imperfecta (AIH2). *Hum Mol Genet* 11(9)*:*1069-74.

Margolis HC, Beniash E, Fowler CE (2006). Role of macromolecular assembly of enamel matrix proteins in enamel formation. *J Dent Res* 85(9)*:*775-93.

Nagano T, Oida S, Ando H, Gomi K, Arai T, Fukae M (2003). Relative levels of mRNA encoding enamel proteins in enamel organ epithelia and odontoblasts. *J Dent Res* 82(12)*:*982-6.

Nanci N (2003). Ten Cate's Oral Histology: Development, Structure, and Function. 6th edition).

Ozdemir D, Hart PS, Firatli E, Aren G, Ryu OH, Hart TC (2005). Phenotype of ENAM mutations is dosage-dependent. *J Dent Res* 84(11)*:*1036-41.

Paine ML, Zhu DH, Luo W, Bringas P, Jr., Goldberg M, White SN, et al. (2000). Enamel biomineralization defects result from alterations to amelogenin self-assembly. *J Struct Biol* 132(3)*:*191-200.

Paine ML, Wang HJ, Luo W, Krebsbach PH, Snead ML (2003). A transgenic animal model resembling amelogenesis imperfecta related to ameloblastin overexpression. *J Biol Chem* 278(21)*:*19447-52.

Paine ML, Snead ML (2005). Tooth developmental biology: disruptions to enamel-matrix assembly and its impact on biomineralization. *Orthod Craniofac Res* 8(4)*:*239-51.

Park CH, Abramson ZR, Taba M, Jr., Jin Q, Chang J, Kreider JM, et al. (2007). Three-dimensional micro-computed tomographic imaging of alveolar bone in experimental bone loss or repair. *J Periodontol* 78(2)*:*273-81.

Pavlic A, Petelin M, Battelino T (2007). Phenotype and enamel ultrastructure characteristics in patients with ENAM gene mutations g.13185-13186insAG and 8344delG. *Arch Oral Biol* 52(3)*:*209-17.

Pispa J, Jung HS, Jernvall J, Kettunen P, Mustonen T, Tabata MJ, et al. (1999). Cusp patterning defect in Tabby mouse teeth and its partial rescue by FGF. *Dev Biol* 216(2)*:*521-34.

Qin C, Brunn JC, Baba O, Wygant JN, McIntyre BW, Butler WT (2003). Dentin sialoprotein isoforms: detection and characterization of a high molecular weight dentin sialoprotein. *Eur. J. Oral Sci.* 111(3)*:*235-42.

Qin C, Baba O, Butler WT (2004). Post-translational modifications of sibling proteins and their roles in osteogenesis and dentinogenesis. *Crit. Rev. Oral Biol. Med.* 15(3)*:*126-36.

Rajpar MH, Harley K, Laing C, Davies RM, Dixon MJ (2001). Mutation of the gene encoding the enamel-specific protein, enamelin, causes autosomal-dominant amelogenesis imperfecta. *Hum Mol Genet* 10(16)*:*1673-7.

Ritchie HH, Hou H, Veis A, Butler WT (1994). Cloning and sequence determination of rat dentin sialoprotein, a novel dentin protein. *J. Biol. Chem.* 269(5)*:*3698-702.

Satokata I, Maas R (1994). Msx1 deficient mice exhibit cleft palate and abnormalities of craniofacial and tooth development. *Nat Genet* 6(4)*:*348-56.

Simmer JP, Fukae M, Tanabe T, Yamakoshi Y, Uchida T, Xue J, et al. (1998). Purification, characterization, and cloning of enamel matrix serine proteinase 1. *J Dent Res* 77(2)*:*377-86.

Simmer JP, Hu JC (2002). Expression, structure, and function of enamel proteinases. *Connect Tissue Res* 43(2-3)*:*441-9.

Simmer JP, Hu Y, Lertlam R, Yamakoshi Y, Hu JC (2009). Hypomaturation enamel defects in Klk4 knockout/LacZ knockin mice. *J Biol Chem* 284(28)*:*19110-21.

Sire JY, Delgado SC, Girondot M (2008). Hen's teeth with enamel cap: from dream to impossibility. *BMC Evol Biol* 8(246.

Smith CE, Wazen R, Hu Y, Zalzal SF, Nanci A, Simmer JP, et al. (2009). Consequences for enamel development and mineralization resulting from loss of function of ameloblastin or enamelin. *Eur J Oral Sci.* 117(5)*:*485-97.

Snead ML, Paine ML, Chen LS, Luo BY, Zhou DH, Lei YP, et al. (1996). The murine amelogenin promoter: developmentally regulated expression in transgenic animals. *Connect Tissue Res* 35(1-4)*:*41-7.

Snead ML, Paine ML, Luo W, Zhu DH, Yoshida B, Lei YP, et al. (1998a). Transgene animal model for protein expression and accumulation into forming enamel. *Connect Tissue Res* 38(1-4)*:*279-86; discussion 295-303.

Snead ML, Paine ML, Luo W, Zhu DH, Yoshida B, Lei YP, et al. (1998b). Transgene animal model for protein expression and accumulation into forming enamel. *Connect Tissue Res* 38(1-4)*:*279-86; discussion 295-303.

Song Y, Wang C, Peng B, Ye X, Zhao G, Fan M, et al. (2006). Phenotypes and genotypes in 2 DGI families with different DSPP mutations. *Oral Surg Oral Med Oral Pathol Oral Radiol Endod* 102(3)*:*360-74.

Sreenath T, Thyagarajan T, Hall B, Longenecker G, D'Souza R, Hong S, et al. (2003). Dentin sialophosphoprotein knockout mouse teeth display widened predentin zone and develop defective dentin mineralization similar to human dentinogenesis imperfecta type III. *J. Biol. Chem.* 278(27)*:*24874-80.

Stephanopoulos G, Garefalaki ME, Lyroudia K (2005). Genes and related proteins involved in amelogenesis imperfecta. *J Dent Res* 84(12)*:*1117-26.

Termine JD, Belcourt AB, Miyamoto MS, Conn KM (1980). Properties of dissociatively extracted fetal tooth matrix proteins. II. Separation and purification of fetal bovine dentin phosphoprotein. *J Biol Chem* 255(20)*:*9769-72.

Thomas LJ, Panneerselvam K, Beattie DT, Picard MD, Xu B, Rittershaus CW, et al. (2004). Production of a complement inhibitor possessing sialyl Lewis X moieties by in vitro glycosylation technology. *Glycobiology* 14(10)*:*883-93.

Tucker AS, Headon DJ, Courtney JM, Overbeek P, Sharpe PT (2004). The activation level of the TNF family receptor, Edar, determines cusp number and tooth number during tooth development. *Dev Biol* 268(1)*:*185-94.

Uchida T, Tanabe T, Fukae M, Shimizu M (1991a). Immunocytochemical and immunochemical detection of a 32 kDa nonamelogenin and related proteins in porcine tooth germs. *Arch Histol Cytol* 54(5)*:*527-38.

Uchida T, Tanabe T, Fukae M, Shimizu M, Yamada M, Miake K, et al. (1991b). Immunochemical and immunohistochemical studies, using antisera against porcine 25

kDa amelogenin, 89 kDa enamelin and the 13-17 kDa nonamelogenins, on immature enamel of the pig and rat. *Histochemistry* 96(2)*:*129-38.

Wakida K, Amizuka N, Murakami C, Satoda T, Fukae M, Simmer JP, et al. (1999). Maturation ameloblasts of the porcine tooth germ do not express amelogenin. *Histochem Cell Biol* 111(4)*:*297-303.

Wazen RM, Moffatt P, Zalzal SF, Yamada Y, Nanci A (2009). A mouse model expressing a truncated form of ameloblastin exhibits dental and junctional epithelium defects. *Matrix Biol.* 28(5)*:*292-303.

Wen X, Zou Y, Luo W, Goldberg M, Moats R, Conti PS, et al. (2008a). Biglycan overexpression on tooth enamel formation in transgenic mice. *Anat Rec (Hoboken).* 291(10)*:*1246-53.

Wen X, Zou Y, Luo W, Goldberg M, Moats R, Conti PS, et al. (2008b). Biglycan overexpression on tooth enamel formation in transgenic mice. *Anat Rec (Hoboken)* 291(10)*:*1246-53.

Witkop CJ, Jr. (1988). Amelogenesis imperfecta, dentinogenesis imperfecta and dentin dysplasia revisited: problems in classification. *J Oral Pathol* 17(9-10)*:*547-53.

Wurtz T, Lundmark C, Christersson C, Bawden JW, Slaby I, Hammarstrom L (1996). Expression of amelogenin mRNA sequences during development of rat molars. *J Bone Miner Res* 11(1)*:*125-31.

Xiao S, Yu C, Chou X, Yuan W, Wang Y, Bu L, et al. (2001). Dentinogenesis imperfecta 1 with or without progressive hearing loss is associated with distinct mutations in DSPP. *Nat. Genet.* 27(2)*:*201-4.

Yamakoshi Y (1995). Carbohydrate moieties of porcine 32 kDa enamelin. *Calcif Tissue Int* 56(4)*:*323-30.

Yamakoshi Y, Hu JC, Liu S, Zhang C, Oida S, Fukae M, et al. (2003). Characterization of porcine dentin sialoprotein (DSP) and dentin sialophosphoprotein (DSPP) cDNA clones. *Eur. J. Oral Sci.* 111(1)*:*60-7.

Yamakoshi Y, Hu JC, Fukae M, Iwata T, Kim JW, Zhang H, et al. (2005a). Porcine dentin sialoprotein is a proteoglycan with glycosaminoglycan chains containing chondroitin 6-sulfate. *J. Biol. Chem.* 280(2)*:*1552-60.

Yamakoshi Y, Hu JC, Fukae M, Zhang H, Simmer JP (2005b). Dentin glycoprotein: the protein in the middle of the dentin sialophosphoprotein chimera. *J. Biol. Chem.* 280(17)*:*17472-9.

Yamakoshi Y, Hu JC, Iwata T, Kobayashi K, Fukae M, Simmer JP (2006). Dentin sialophosphoprotein is processed by MMP-2 and MMP-20 in vitro and in vivo. *J. Biol. Chem.* 281(50)*:*38235-28243.

Yamakoshi Y (in press). Dentin Sialophophoprotein (DSPP) and Dentin. *J. Oral Biosciences*.

Ye L, MacDougall M, Zhang S, Xie Y, Zhang J, Li Z, et al. (2004). Deletion of dentin matrix protein-1 leads to a partial failure of maturation of predentin into dentin, hypomineralization, and expanded cavities of pulp and root canal during postnatal tooth development. *J Biol Chem* 279(18)*:*19141-8.

Yoshizaki K, Yamamoto S, Yamada A, Yuasa K, Iwamoto T, Fukumoto E, et al. (2008). Neurotrophic factor neurotrophin-4 regulates ameloblastin expression via full-length TrkB. *J Biol Chem* 283(6)*:*3385-91.

Zalzal SF, Smith CE, Nanci A (2008). Ameloblastin and amelogenin share a common secretory pathway and are co-secreted during enamel formation. *Matrix Biol* 27(352–9.

Zhang X, Chen L, Liu J, Zhao Z, Qu E, Wang X, et al. (2007). A novel DSPP mutation is associated with type II dentinogenesis imperfecta in a Chinese family. *BMC Med Genet* 8(52.

Zhao X, Zhang Z, Song Y, Zhang X, Zhang Y, Hu Y, et al. (2000). Transgenically ectopic expression of Bmp4 to the Msx1 mutant dental mesenchyme restores downstream gene expression but represses Shh and Bmp2 in the enamel knot of wild type tooth germ. *Mech Dev* 99(1-2)*:*29-38.